DOKUZ EYLÜL UNIVERSITY
GRADUATE SCHOOL OF NATURAL AND APPLIED SCIENCES

PHYSICAL OCEANOGRAPHY OF THE KEKOVA BAY

by
Filiz EREK

April, 2013
İZMİR

PHYSICAL OCEANOGRAPHY OF THE KEKOVA BAY

A Thesis Submitted to the
Graduate School of Natural and Applied Sciences of Dokuz Eylül University
In Partial Fulfillment of the Requirements for the Degree of Master of Science
in Marine Sciences and Technology, Physical Oceanography

by
Filiz EREK

April, 2013
İZMİR

M.Sc THESIS EXAMINATION RESULT FORM

We have read the thesis entitled **"PHYSICAL OCEANOGRAPHY OF THE KEKOVA BAY"** completed by **FİLİZ EREK** under supervision of **PROF. DR. ŞÜKRÜ BEŞİKTEPE** and we certify that in our opinion it is fully adequate, in scope and quality, as a thesis for the degree of Master of Science.

Prof. Dr. Şükrü BEŞİKTEPE

Supervisor

Doç.Dr. Erdem SAYIN

(Jury Member)

Yrd. Doç.Dr. Can Özgür ÇOLPAN

(Jury Member)

Prof.Dr. Ayşe OKUR

Director

Graduate School of Natural and Applied Sciences

ACKNOWLEDGEMENTS

I wish to express my sincere gratitude to my advisor, Ass. Prof. Dr. Şükrü BEŞİKTEPE, for providing excellent guidance and constant encouragement throughout the preparation of this work. His contribution to the achievements of this work is significant.

I would also like to thank the Asisst.Prof. Dr. ERDEM SAYIN providing his expertise for this thesis.

I also wish to express to thank the Mustafa Kemal CAMBAZOĞLU at Research Scientist - University of Southern Mississippi and the Asisst.Prof. Dr. Çınar YENİ at the Dept. of Mechanical Engineering for their endless patience, help and support.

Finally, I would like to thank my daughter for their encouragements, especially my husband Asisst.Prof. Dr. Aytunç EREK.

Filiz EREK

PHYSICAL OCEANOGRAPHY OF THE KEKOVA BAY

ABSTRACT

In this study, flow analysis of Kekova Bay is performed under initial and boundary condition derived experimental measurement by using SMS / ADCIRC commercial code. Here, The most important force in the determining of initial and boundary conditions is Tidal ones. The flow analysis is performed by consideration of this Tidal force. The numerical results are then verified by testing the resulting predictions for independence of the grid size, time-step and other parameters. The grid size used for the solution was 3 m with a time step $\Delta t = 0.5$ s.

As future work, further numerical studies will be conducted to investigate more accurate solution.

Keywords: Basin scale, coastal, estuarine, general circulation model, geophysical fluid dynamics, global, hydrodynamic model, ocean model, three-dimensional model, ADCIRC

KEKOVA KÖRFEZİNİN FİZİKSEL OŞİNOGRAFİSİ

ÖZ

Bu çalışmada deneysel ölçümlerle elde edilen başlangıç ve sınır koşulları altında Kekova Körfezinin akış analizi SMS/ADCIRC (Coastal Circulation and Storm Surge Model) yardımı ile elde edilmiştir.Burada sınır ve başlangıç koşullarının belirlenmesindeki en önemli kuvvetlerden birisi Med-Cezir'dir.Bunun için bu durumda dikkate alınarak Analiz gerçekleştirilmiş, grid ve zaman adımından bağımsız çözüm elde edilmiştir.

Gelecekteki çalışmalarda, daha doğru bir çözüm araştırmak için daha fazla sayısal çalışma yapılacaktır.

Anahtar kelimeler: Havza ölçeği, kıyı, haliç, genel dolaşım modeli, jeofizik akışkan dinamiği, küresel, hidrodinamik modeli, okyanus modeli, üç boyutlu model, ADCIRC

CONTENTS

Page

LIST OF FIGURES

Page

LIST OF TABLES

Page

CHAPTER ONE
INTRODUCTION

1.1 Introduction

The Mediterranean Sea is a semi-enclosed marginal sea. The negative freshwater and heat budgets of the basin drive its lagoonal (anti-estuarine) thermohaline circulation and determines its hydrological characteristics. Low salinity Atlantic water (AW) that enters in the upper layer of the Gibraltar Strait is transformed to saline Mediterranean water that subsequently exits into the Atlantic via the lower layer. The salty water of Mediterranean origin may affect water formation processes and variabilities and even the stability of the global thermohaline equilibrium state (Allan, Leslie, Alexander, & Alex, 2011). Mediterranean sea circulation Although the surface AW progressively loses its characteristics through mixing and evaporation during its travel to the east, (salinity rising from 36.15 at Gibraltar Strait, to 38.6 in the eastern Levantine Basin according to Lacombe & Tchernia (1972) and (Ozsoy, Hecht, & Unluata, 1989), the transformation to intermediate and deep water occurs in selected areas within the basin (Wüst, 1961). In these areas, favorable oceanic conditions and extreme air–sea interaction processes lead to the downward mixing extending deep into the water column.

This process of dense water formation is as important for the Mediterranean Sea as it is for the world ocean. First of all, it allows the exchange of physical and biochemical properties (e.g. oxygen, nutrients) between the surface and deep layers. On a larger scale, this process maintains the permanent thermocline at low and mid latitudes. Once the dense water leaves the surface and sinks to deep layers, it maintains its characteristics that were determined by the prevailing atmospheric conditions at its site of formation. Therefore, the study of deep water characteristics gives us access to past climatic variations at time scales depending on the renewal time scales of the basin (for the Mediterranean: decades to centuries).

The most recent observational efforts have revealed that significant changes have taken place during the past few years in the intermediate and deep thermohaline circulation of the Eastern Mediterranean (Roether, Manca, Klein, Bregant, Georgopoulos, Beitzel, Kovacevic, & Luchetta, 1996). As a result of these changes within a few years a totally new pattern of thermohaline circulation has developed in the basin.

The principal cell describes the transformation of the surface Atlantic Water (AW) to the Levantine Intermediate Water (LIW), which is the main contributor to the Mediterranean outflow into the Atlantic.The Levantine Basin is one of the major basins of the Mediterranean Sea and occupies the easternmost part of the Mediterranean Sea. The LB is bounded by the Cretean Atchipelago and The Asia Minor to the north,the Middle East to the cast, and the north-eastern Africa to the south. The Levantin Basin (LB), which is the saltiest water mass that forms in the eastern Mediterranean Sea, is considered one of the drivers of the thermohaline circulation in the Mediterranean Sea, owing to the Levantine Intermedite Water (LIW) formation by the loss of water due to intense surface evaporation (Lacombe & Tchernia, 1972; Tchernia, 1980). The actual circulation picture of the Levantine Basin is rather complex, consisting of basin- scale, sub-basin-scale and mesoscale structures. Permanent, recurrent and transient cyclonic and anticyclonic eddies are interconnected by jets and currents (Ayoub, Traon, & De Mey, 1998). Mesoscale process play an important role in the formation and spreading of Levantine Intermediate Water.

1.1.1 Hydrographic Characteristic and Water Mases of the Levantin Basin

Hydrographic measurements shows three permanent water masses (Lacombe & Tchernia, 1972; Zavatarelli & Mellor, 1995) which are schematized in Figure 1.1. The most imporatant water mass in the Eastern Mediterranean is the Levantine Intermediate Water, which affects not only the entire MED, but the Atlantic Ocean as well. A homogenous water mass occupies the intermediate depth between 300 and 700 m, below the AW. İt is Known that this water mass is formed in the winter in the LB by the transformation of AW. LB forms a layer identified by a salinity maximum between the overlying Modified Atlantic Water (MAW) and the underlying Eastern Mediterranean Deep Water (EMDW).The core depth fluctustes from 50 to 600 m. While the characteristics of The LIW is characterized by the highest sub-surface salinity and temperature at different regions vary (14.70-16.95 oC, 38.85-39.15) in the LB, mixing results in homogeneity and the loss of heat and salt as the LIW spread westward. Its salinity decreases due to the mixing with adjacent water masses (Tchernia, 1980; Özsoy et al.,1989; Ozsoy, Ünlüata & Top, 1993b)

The abbysal layers below 800 m depth are occupied by a colder, less saline and dense water mass, the Eastern Mediterranean Deep Water (EMDW;~13.6 oC, 38.7 and > 29.05), which is formed by strong cooling in the northern part of the eastern basin (i.e., in the Adriatic and the the Aegan Seas), The winter properties of LIW as it leaves the Levantine Sea are 15 oC ≤ ϴ ≤ 16 oC ,39.0 ≤ S ≤ 39.2. In summer the LB surface is entirely covered by a thin, warm and saline layer that overlies the AW, the so-called the Levantine Surface Water (LSW).This water mass plays an important role in the formation of the LIW (see Malanotte-Rizoli & Hetcht, 1988; Özsoy et al., 1991; Malanotte-Rizoli, 1994; Robinson & Golnaraghi, 1994; Robinson, Theocharis, Lascaratos, & Leslie , 2001 for a review).

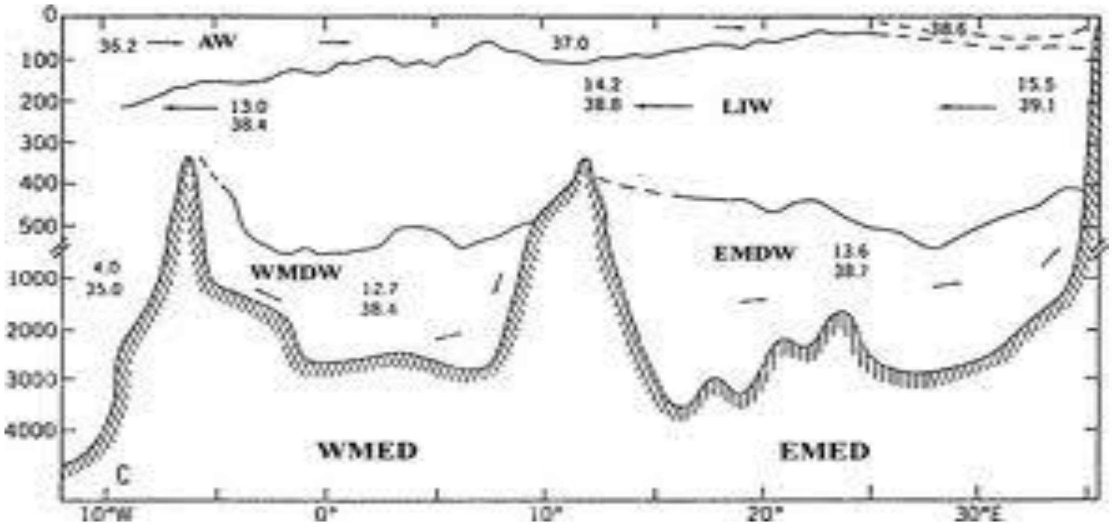

Figure 1.1 Vertical distribution of the major Mediterranean sea water masses,adapted (Zavaterelli & Mellor. 1995)

1.1.2 Circulation Of the Levantin Basin

The general circulation of water mases in the MED has been studied since the beginning of the 20th century. In East Mediterranean, deep waters _EMDW. are formed on the shallow shelf of north Adriatic and eventually slide down to South Adriatic and through Otranto to the deepest areas of Ionian and Levantine. The surface currents entering Strait of Gibraltar and brancing in the Balgearic basin and Tyrrenian Sea, and flows the through the strait of Siciliy into the Eastern Basin.They form a meandering current along the Libyan coast and progress up to the Levantin Basin.Thus, Previous studies of general circulation showed that the presence of numerous cyclonic and anticyclonic sub-basin gyres in the general circulation. Moreover, Ovchinikov et al. (1987), observed that during that particular winter, EMDW is formed in the center of the cylonic gyre in south Adriatic and eventually slide to settle in the deepest areas of the Ionian and Levantine basins.

In the LB, Nielsen described the circulation as a simple basin-wide cyclonic force effect which maintains the current along the basin coast in the LB . Also Ovchinnikov indicated that AW flows through southern part of the Cretan and appears in the eastern coast of LB. Then AW bifurcates near the Egyptian. The first branch follows the cyclonic coastal circulation across the Egyptian continental shelf then it turns northward along the Middle-East coasts generating many anticyclonic eddies along its path. The second branch re-circulates in the periphery of a complex anticyclonic system of eddies in the southern part of the LB (Mersa-Matruh and Shikmona areas). Then it turns westward again south of Cyprus to feed the AMC. The Central Levantine Basin Current by Özsoy et al. (1989) or The Mid Mediterranean Jet (MMJ) by Robinson et al. (1991), which is associated with the AW, enters the LB by way of Cretan and move around eastward between the RG and MMA. In the South of Cyprus is separated two branches , one of them is SMA and the other turns to the north then westward to reach and feed the Asia Minor current (AMC). AMC carries LCW, which is marked by its high salinity and temperature, flows to the westward carrying LSW into the Aegean Sea. It has been well documented by Malanotte-Rizzoli & Hecht (1989); Malanotte-Rizzoli (1994); and Robinson & Golnaraghi (1999).

1.1.3 Study Area

Kekova, also named Caravola (Lycian: Dolichiste), is a small Turkish island near Demre (Demre is the Lycian town of Myra) district of Antalya province which faces the villages of Kaleköy (ancient Simena) and Üçağız (ancient Teimioussa). Kekova has an area of 4.5 km^2 and is uninhabited.SEPA covers an area of approximately 260 km2. Kekova Island, the biggest island in the region. This island lies the Anatolian side forming an adjacent passage. Inner Islands, Earth Island, Aşırlı Kişnali Ada Ada and other major islands. Peninsula, which stretches parallel to the coast and the island of Kekova is Oludeniz serve as an inland sea. Heights in the region dates back to the north. Now beginning to rise from the shore slopes, narrow plains rising 550 m over the mountains and then all of a sudden turn into steep hillsides. The coasts are indented bays shows the topography occurring. Region is dominated by Mediterranean vegetation, the climate is suitable for the type of scrub and pine trees are always green. The area is also, in terms of bulbous plants with medicinal and aromatic plants, there is a considerable degree of wealth.

Kekova Island and the town are among the region’s most idyllic spots. There is a marina and a marinette in the region. Provisional facilities are well developed. Transport facilities to major cities are regularly available.There are several options to enter into the bay. When entering from the west to Ölüdeniz, care is required for sea-level rocks on the southeast of Kekova Island.Mediterranean weather conditions are predominant in the region. Prevailing wind blow from the southwest – west. The prevailing westerlies build by noon, but die off by late afternoon. July and august are real warm and sea-water temperature also reaches to the maximum (Kumlutaş, Durmuş, & Ilgaz, 2011)

A general consideration of the batimetric structure of the area indicates that the maximum depth reaches about 109 m (Figure 1.2), as a continuation of the step rocky shore line the grift model consists of elevations and pits at the see base. The upwards-downwards structure which is more obvious along a depth band between 0-50 m, also exists at the deepest base along the central axis of Üçağız and Ölüdeniz that is lying on east-west line. The closed structure of Üçağız and it being subjected to land based fresh water and sediment entrances, especially during rainy seasons, there is no elevation named as sil (=threshold) at the clearance of Ölüdeniz to Akdeniz, it having a contact with Üçağız by a strait having a greater average depth than Üçağız, although they contain between Ölüdeniz's Sıçak peninsula and Kekova island opening to Akdeniz by relatively deep two straits in South direction come out as distinct batimetric features in the generaton of the ecosystem. This subject will be handled in detail below. However, due to the geomorphological characteristics of the area it will be more useful to evaluate as two subareas since this will allow better understanding of the flow and water regime in the area. These subareas are determined as,

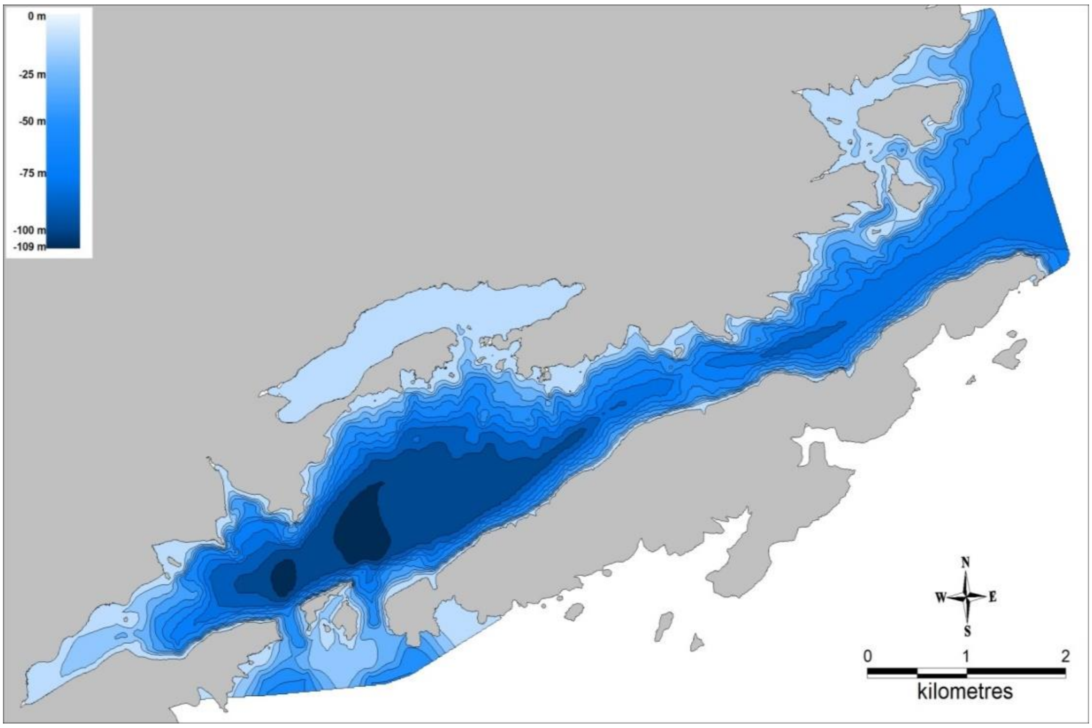

(a)

Figure 1.2 Bathymetric structure of the area (a); sea floor relief (b) (Google Earth, n.d.)

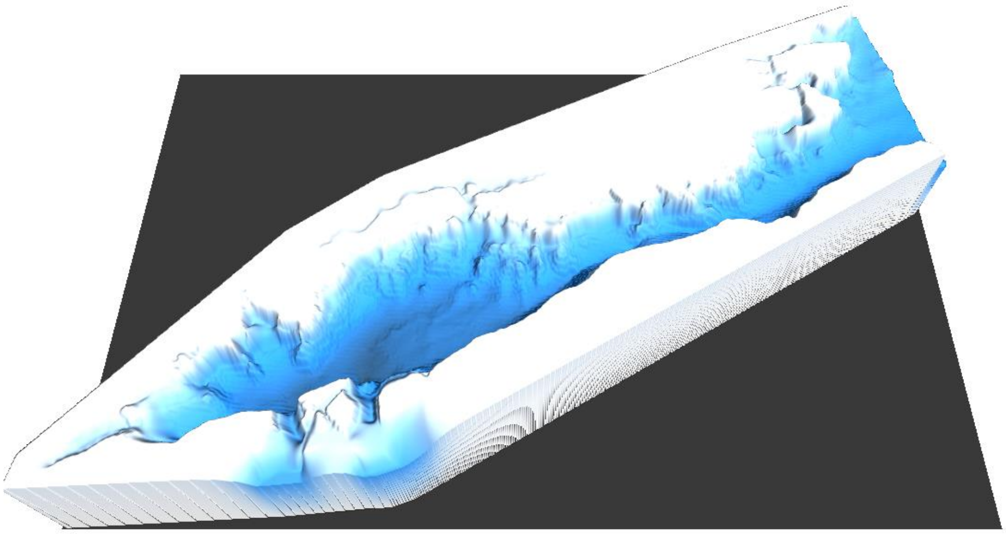

(b)

Figure 1.2 continues

In the evaluation of the batimetric properties of the defined subareas, it will be helpful to make use of the section informations gathered at certain intervals (Figure 1.3). As seen in the figure, Üçağız subarea is investigated with sections 9-12 and 18, and Ölüdeniz with 1-8, 13-17 and 19. Paying attention to the sections, it will be understood that numbers 1, 2, 3 and 9 represent the straits or openings of water exchange points, numbers 18 and 19 represent batimetric varations Üçağız and Ölüdeniz show along the specifed line which have, respectively, two dihes in east-west directions. Other sections are the lines intersecting north-south dishes in transverse direction.

1.1.3.1 Ölüdeniz

Ölüdeniz surrounding areas with an average depth of 50.36 meters, Inner Islands, Hot Peninsula and north of the island of Kekova Cevreli the overall structure of the village of Upper Cretaceous limestone Ulu Burun dispersion and low-lying areas towards the shore and shallow sea areas is dominated by the spread of quaternary alluvium have been reported (http://kaskekovabiyocesitlilik.com/jeoloji.php). Ölüdeniz, hot and delete located between the peninsula and the island of Kekova if you sink relatively deep (~ 50 m) in the direction of the southern Mediterranean, the opening of two strait (Figur 1.4 a), the opening in the east end of the Mediterranean Sea Clear (= threshold) an elevation of the so-called is not (Figure 1.4 b)

Ölüdeniz is that the relationship between the depth of the Mediterranean straits Ölüdeniz its east and south of the main determining factor in the quality characteristics of the water is remarkable. Üçağız containing suspended solids quite high due to the terrestrial effects, and that the relationship between Ölüdeniz and üçağız about 2-3 times deeper than Üçağız also have a determining effect in the throat.

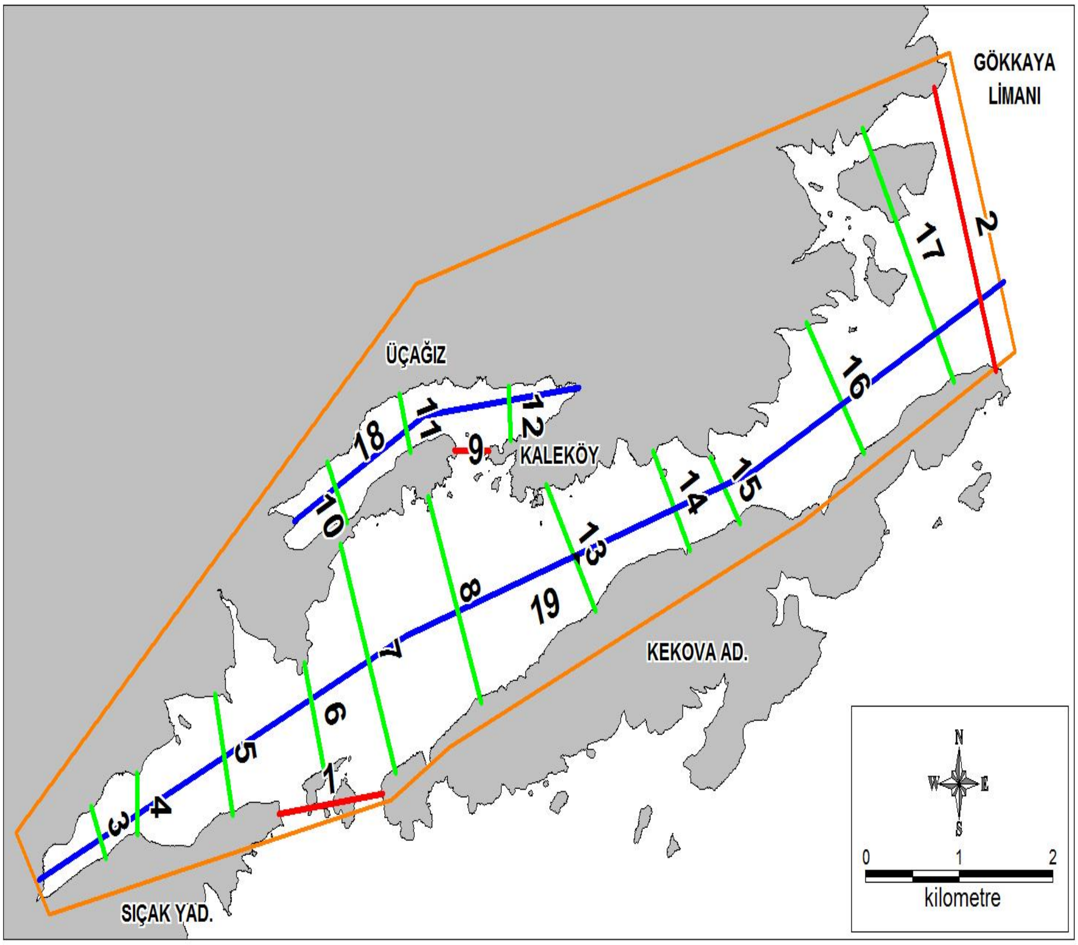

Figure 1.3 Bathymetric sections utilized in the study area locations (Google Earth, n.d.)

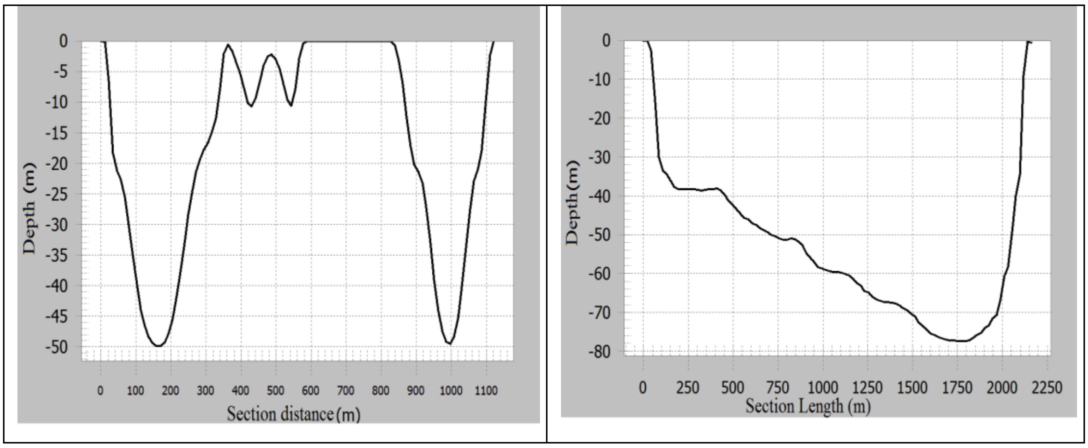

(a) Cross-section of number 1 (b) Cross-section of number 2

Figure 1.4 Öludeniz dish bathymetric sections of (a) and (b)

1.1.3.2 Üçağız

A shallow patch extends out for about 200 meters to the north from the western point of Kekova Island. This patch is around 20 m in diameter. Extreme care is required if you are routing to Kaleköy from the western side of Ölüdeniz. When you use the passage from Ölüdeniz to Üçağız. Pay attention for the sea-level rocks.The western and the eastern shores of Kaleköy is shallow.Üçağız has an E/W orientation – 1.5 miles long. On approaching from the South, two islets in the middle are conspicuous. Care is needed for the reefs extending from the islets. The shallow areas can clearly be seen. There is 5 meter depth in the fairway. There is 7 – 8 meters depth in the inlet. The bottom is mud and provides excellent holding.

1.1.4 Objective of the Present Study

Gulf and coastal waters and marine life more unique in terms of the biological cycle provide hydro-ecological environment. Common characteristics of these waters are a complex geometry, shallow and high degree of mobility that they are bio-chemically. These waters with suspended sediment carry a significant amount of water with many features.These important roles in the cycle, the nutrients and other water features. Fluid flow in this aspect, the movement of sediment and find out more at the base exchange relations. The primary purpose of the modeling system is to study potential structural and non-structural alternatives with the goal of providing improved circulation and water quality characteristics within Gulf and Estuary. The numerical modeling study will provide decision makers with modeling results that could be used to evaluate the proposed alternatives and identify priority items for implementation.What are the patterns of circulation and water mass properties in seasons where field data are lacking. For model purposes, a high horizontal as well as vertical resolution of model grid is required to resolve the mesocyle dynamics as well as the basin structured bottom topography and the complicated costline. By modelling of the Kekova bay is able to simulate most of the characteristic flow features.

Sometimes,a numerical simulation of differential equations that cannot be solved analytically, theories that involve continuous systems such as phenomena in physical cosmology, fluid dynamics (e.g. climate models, roadway noise models,roadway air dispersion models,ocean models), continuum mechanics and chemical kinetics fall into this category. Computational fluid dynamics simulations are used to simulate the behaviour of flowing air, water and other fluids. Modelling of ocean focuses on motions of incompressible fluids of a freely moving surfacebeing influenced by both the Earth's rotation and density stratification. Adcirc,Nemo and Hydrotam etc., are numerical model studies, which are highly developed computer program for solving the equations of motion for a moving fluid on a rotating earth.

CHAPTER TWO
MATERIAL AND METHODS

2.1 Material and Methods

In order to understand the flow characteristic and water budget of the region, within the framework of 1. and 2. stage studies, every day for a week, flow measurements are carried out at 6 stations taht are shown in Figure 2.1 and whose coordinates are given in Table 2.1. Flow measurements have been recorded every minute during a period of one hour, every 2 meters from surface to ground using a 300 kHz RDI Acoustic Flow Profile Measurement apparatus. But due to the shallowness of Üçağız, where station A4 is located, flow profile could not be obtained.

2.2 Current Measurements

WH 150 kHz RDI ADCP current measurements in this study were made using Mariner. WH150 rented unit on the side of a boat, so that the transducers are placed within one meter of water. Ship reference system, which is needed to convert the coordinates of the measurements in the magnetic compass heading information provided within WM150. The data collected by WH150 transferred to a PC via the RS-232 channel, and the computer çalışanVM-DAS (input) and WinADCP (for display and data conversion) software is transferred to the computer with the measurements. ADCP collected simultaneously with the very DGPS and DGPS data is also transferred to another computer with the RS232 channel ADCP measurements matched. Given the speed of the boat with DGPS to find the absolute value of the calculated and the discharge current velocities were measured by the speed of the ADCP. ADCP water in the study area could see the base of the ship's speed is constantly comparing these two methods yollada hesaplanabilmiş and made the necessary corrections.

WM150, can be selected depending on the application, including broadband and narrowband works in two modes. Up to approximately 80 m from the surface when the water column Darbantta be measured currents, Broadband Kaynak surface current measurements can be up to 50m. On the other hand, increasing measurement accuracy broadband mode. Maximum depth is around 50 to 60 m measured discharge areas in order to increase the sensitivity of the measurements used in this study WH150 broadband mode. WH150 within the limits of the technique, the bottom of the sea surface to the bottom between 2m and 4m were measured every second. Each subsequent stage of data processing flows per second by taking the mean of the distribution of the collected data was 120 sec.

Figure 2.1 Flow measurement stations locations (Google Earth, n.d.)

Table 2.1 The current coordinates of the measuring stations

STATION	LATITUDE	LONGITUDE
A1	36° 10' 15.4"	29° 49' 08.4"
A2	36° 10' 03.6"	29° 49' 51.9"
A3	36° 10' 08.8"	29° 50' 23.3"
A4	36° 11' 40.3"	29° 50' 42.3"
A5	36° 11' 27.1"	29° 51' 04.3"
A6	36° 12' 03.9"	29° 54' 26.4"

2.3 Hydrographic Measurements

See water physical characteristics have been realized in 11 stations which have been thought to represent the area of study and have an importance in terms of hidrography (Figure 2.2, Table 2.2). Salinity-density*, temperature (CTD) measurements are carried out simultaneously with flow measurements once a day using the Sea-Bird CTD probe. In addition, see water muddiness/lucidity values have been measured in 8 stations (Figure 2.3, Table 2.3).

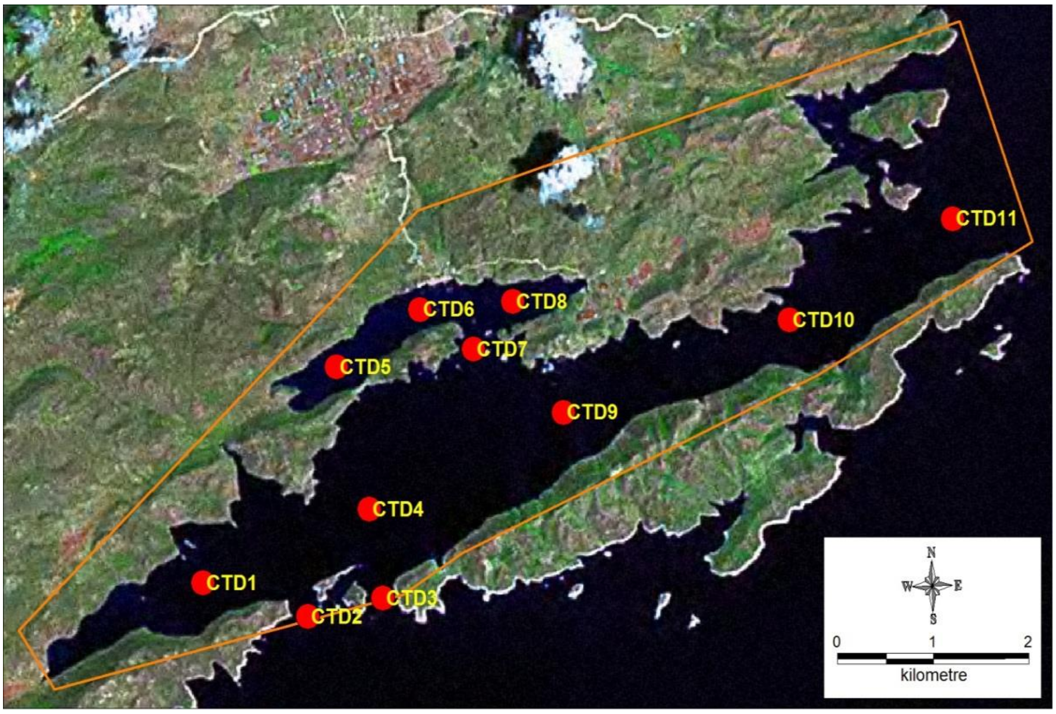

Figure 2.2 CTD measurement stations locations (Google Earth, n.d.)

Table 2.2 The coordinates of the CTD measuring stations

STATIO N	LATITUDE	LONGITUDE	STATION	LATITUDE	LONGITUDE
1*	36° 10' 15.4"	29° 49' 08.4"	7*	36° 11' 27.1"	29° 51' 04.3"
2*	36° 10' 03.6"	29° 49' 51.9"	8	36° 11' 41.9"	29° 51' 21.3"
3*	36° 10' 08.8"	29° 50' 23.3"	9	36° 11' 06.1"	29° 51' 41.2"
4	36° 10' 37.2"	29° 50' 18.9"	10	36° 11' 33.2"	29° 53' 16.7"
5	36° 11' 22.9"	29° 50' 06.7"	11*	36° 12' 03.9"	29° 54' 26.4"
6*	36° 11' 40.3"	29° 50' 42.3"			

*Yellow filling stations is common with current stations

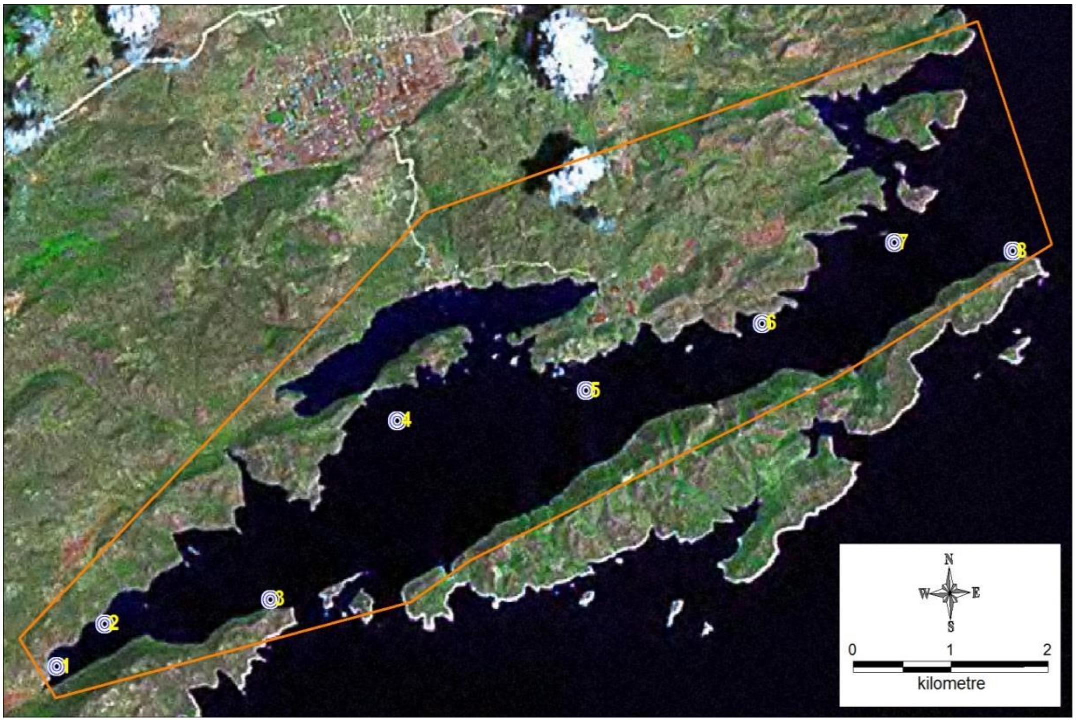

Figure 2.3 Secchi disk measurement stations locations (Google Earth, n.d.)

Table 2.3 Secchi disk measurement stations coordinates

STATION	LATITUDE	LONGITUDE
1	36° 09' 53"	29° 48' 06"
2	36° 10' 06"	29° 48' 26"
3	36° 10' 12"	29° 49' 34"
4	36° 11' 07"	29° 50' 29"
5	36° 11' 15"	29° 51' 46"
6	36° 11' 34"	29° 53' 00"
7	36° 11' 58"	29° 53' 55"
8	36° 11' 54"	29° 54' 43"

2.4 Hydrodynamic Modeling

The purpose of a barotropic hydrodynamic model is to characterize the important flow features of surface waters driven by tides, wind, and atmospheric pressure gradients. The complexity of circulation patterns in coastal and continental shelf margin waters necessitates use of a numerical hydrodynamic model. Such models compute spatial and temporal distributions of velocity and sea surface elevation from which circulation patterns can be inferred. Success of the computed tidal response in resembling the actual coastal ocean depends in part on selection of an appropriate hydrodynamic model. An optimal model is one that captures tidal-induced dynamics, yet remains computationally feasible.

Numerical modeling has become an essential tool for assessing the hydrodynamics of continental margin waters. It is important to recognize that the computed response of these waters is controlled by the various components that make up the model, including the governing equations, boundary conditions, forcing functions, discrete equations, grid structure, and the computational domain itself. The more that is understood about a numerical model, how its various components influence computations and is put into practice, the more successful the model will be in representing hydrodynamic processes within shallow waters.

The theoretical basis of a hydrodynamic model is found in the principles of mass and momentum conservation. For vertically well-mixed surface waters experiencing tidal and atmospheric forcing, the flow physics are described by the shallow-water equations, a depth-integrated form of the conservation laws (Le Mehaute 1976). The shallow-water equations have been used successfully by engineers and researchers for many years to predict tidal circulation (e.g., Reid & Whitaker, 1981; Gray & Kinnmark, 1983; LeProvost & Vincent, 1986; Flather, 1988; Al-Rabeh et al., 1990; Westerink et al., 1989, 1992a, 1994a, 1995; Luettich & Westerink, 1995).

A second consideration in selection of a model is efficiency of the numerical solution algorithm. Meaningful boundary forcing can necessitate the use of large model domains that cover the continental shelf, coastal regions, and include portions of the deep ocean (Blain et al., 1994). Furthermore, the time frame for typical simulations ranges from hours to months. The feasibility of a model that utilizes large domains and extended simulation periods depends upon the efficiency of the numerical solution algorithm. Efficiency is achieved by minimizing the number of degrees of freedom and the number of operations per degree of freedom at each computational timestep.

The search for accurate and efficient solution algorithms for the shallow-water equations has led to a variety of equation formulations and the use of several numerical solution techniques. Two prevalent numerical discretization strategies utilize the finite difference and FE approaches. Finite difference methods discretize derivative operators contained in the model equations using point difference expressions (Lapidus & Pinder 1982), while FE techniques approximate the solution to the model equations through the use of interpolation functions (Celia & Gray, 1992).

A review of several FE solution techniques for the shallow-water equations is given by Lee & Froehlich (1986). Westerink & Gray (1991), in their recent review, note increasing similarities between finite difference- and FE-based models, especially with regard to the accurate propagation of short wavelengths, grid flexibility, and complex boundary representation. Further comparison and discussion of these methods is given by Blain & McManus (1998).

Early finite difference solutions of the shallow-water equations were quite accurate, owing in part to implementation of a staggered grid approach, which successfully avoided the introduction of artificial short waves . In contrast, early FE schemes were plagued by spurious oscillations or numerical noise due to the introduction of 2 -Ax wavelengths, a consequence of folded dispersion characteristics (Lynch, 1983; Kolar et al. ,1994b). Note that 2 – Ax wavelengths are the smallest wavelengths captured by a mesh having a minimum spacing Ax. Early FE algorithms included excessive damping mechanisms to counter the generation of spurious modes and, as a result, yielded inaccurate solutions. It wasn't until Lynch and Gray (1979) introduced the wave-continuity equation (WCE) formulation for the shallow-water equations that the viability of FE approaches improved.

The WCE formulation simply involves a rearrangement of the shallow-water equations prior to spatial discretization. Solutions using the WCE successfully suppress short wavelengths without resorting to nonphysical dissipation. Understanding the origin and behavior of spurious oscillations within FE formulations (Walters & Carey,1983), together with extensive numerical testing of the WCE formulation (Kinnmark & Gray, 1984, 1985; Luettich et al. 1992; Westerink et al. 1992b; Kolar et al., 1994 a,b) has resulted in very accurate WCE-based FE solutions (Lynch & Gray 1979; Foreman 1983).

In contrast to an application of FEs to the primitive shallow-water equation, a WCE-based FE formulation leads to decoupled elevation and velocity solutions and sparse, symmetric matrices (Lynch & Gray, 1979). Solutions for elevation are time independent due to a reformulation of the WCE by Kinnmark (1984) into a GWCE. Matrices resulting from an application of the FE method to the momentum equations remain time dependent, but this time dependence is overcome by lumping these matrices (that is, summing off-diagonal terms and adding the sum to the diagonal term), which causes only a slight degradation in accuracy. As a consequence, velocities are computed by solving a trivial tridiagonal system of equations (Lynch & Gray, 1979).

A numerical solution algorithm is grid flexibility. To date, the finite difference method is not readily amenable to providing high levels of refinement in localized areas. Restrictions on acceptable grid skewness and maximum cell-to-cell size ratios (i.e.,Heath et al.,1990; Celia & Gray, 1992) often result in finite difference.

2.4.1 Description of the model (Advanced Circulation Model For Oceanic, Coastal and Estuarine Waters (ADCIRC)

Adcirc is a highly developed computer program for solving the equation of motion for a moving fluid on a rotating earth. These equations have been formulated using the traditional hydrostatic pressure and Boussinesq approximations and have been discretized in space using the finite element (FE) method and in time using the finite difference (FD) method.

ADCİRC can be run either as a two- dimensional depth intedrated (2DDI) model or as a three-dimensional (3D) model, in either case, elevation is obtained from the solution of the depth-integrated continuity equation in Generalized Wave-Continuity Equation (GWCE) form. Velocity is obtained from the solution of either the 2DDI and 3D momentum equations. All nonlinear terms have been retained in these equations. The GWCE can be solved using either a consistent or a lumped mass matrix and an implicit or explicit time stepping scheme. If a lumped, fully explicit formulation is specified, no matrix solver is necessary. In all other cases the GWCE is solved using the Jacobi preconditioned iterative solver from the ITPACKV 2D package. The 2DDI momentum equations are lumped and therefore require no matrix solver,In 3D, vertical diffusion is treated implicitly and the vertical mass matrix is not lumped, thereby requiring the solution of a complex, tri-diagonal matrix problem over the vertical at every horizontal node. Adcirc can be forced with elevation boundary, tidal potential, normal flow boundary conditions and earth load/self attraction tide. Adcirc includes a least squares analysis routine that computes harmonic constituents for elevation and depth averaged velocity during the course of the run thereby avoiding the need to write out long time series for post processing.

The generalized wave-continuity equation formulation in ADCIRC-2DDI is based on the well-known, shallow-water equations (Le Mehaute, 1976; Kinnmark, 1984). The primitive form of the shallow-water equations is derived by averaging conservation laws of mass and momentum over the timescale of turbulent fluctuations and ocean depth. Turbulent fluctuations at the microscale present in all hydrodynamic flows are characterized by spatial and temporal variations in velocity and pressure fields and are a mechanism for momentum transfer. Time averaging the conservation laws generates macroscale quantities representing microscale fluctuations that must be parameterized. The scale for time averaging is selected to be long enough to span a statistically significant sample of turbulent fluctuations, and yet short enough so that macroscopic variations of the averaged quantity are not included (Gray et al., 1993).

Depth averaging the conservation laws reduces a 3D problem to 2D, leaving as unknowns the surface water elevation and the depth-averaged lateral velocities U and

V. For flows having small, vertical velocity gradients or environments where lateral flows are quite large in comparison to vertical velocities, application of the shallowwater equations is accepted practice. Derivation of the shallow-water equations from the time- and depth-averaged conservation laws involves the Boussinesq approximation in addition to hydrostatic and incompressibility assumptions.

In practice, incompressibility of a fluid implies that density variations seen while moving with the fluid are negligible (i.e., DP = 0). Furthermore, the Boussinesq approximation specifies density as a constant value, p = po, except when gradients of density are considered. In flows appropriate for 2D, depth-averaged equations, vertical acceleration is assumed negligible. Consequently, the momentum equation over the vertical reduces to a balance between pressure and gravitational forces. This is commonly referred to as the hydrostatic assumption. Other simplifications implicit within the shallow-water equations include neglecting changes in the position of the ocean floor with respect to time and excluding mass exchanges with the environment (i.e., evaporation, precipitation, overland flow, and groundwater interactions).

For a Cartesian coordinate system, the conservative form of the shallow-water equations are written:

$$\frac{\partial \zeta}{\partial t} + \frac{\partial UH}{\partial x} + \frac{\partial VH}{\partial y} = 0 \tag{2.1}$$

$$\frac{\partial UH}{\partial t} + \frac{\partial UUH}{\partial x} + \frac{\partial UVH}{\partial y} - fVH = -H\frac{\partial}{\partial x}\left[\frac{p_s}{\rho_o} + g(\zeta - \alpha\eta)\right] + M_x + D_x + B_x + \frac{\tau_{sx}}{\rho_o} - \frac{\tau_{bx}}{\rho_o} \tag{2.2}$$

$$\frac{\partial VH}{\partial t} + \frac{\partial VUH}{\partial x} + \frac{\partial VVH}{\partial y} + fUH = -H\frac{\partial}{\partial y}\left[\frac{p_s}{\rho_o} + g(\zeta - \alpha\eta)\right] + M_y + D_y + B_y + \frac{\tau_{sy}}{\rho_o} - \frac{\tau_{by}}{\rho_o}\ , \tag{2.3}$$

where t represents time, x, y are the Cartesian coordinate directions, ζ is the free surface elevation relative to the geoid, U, V are the depth-averaged horizontal velocities, H = ζ + h is the total water column depth, h is the bathymetric depth relative to the geoid, *f* is the Coriolis parameter, ps is the atmospheric pressure at the free surface, g is the acceleration due to gravity, α is the Earth elasticity factor,η is the Newtonian equilibrium tide potential, ρo is the reference density of water, Mx, My represents the depth-integrated horizontal momentum diffusion, Dx, Dy are the depth-integrated horizontal momentum dispersion terms, Bx, By are the depth-integrated baroclinic forcings, and τsx ,τsy are the applied free surface stresses. Further justification regarding the appropriateness of these equations in modeling tidal and atmospheric forces flows is provided by Blumberg & Mellor (1987), Westerink et al. (1989), Luettich et al. (1992).

In operator notation, a relationship between the conservative and nonconservative momentum equations is given (Kolar, 1992):

$$M^{NC} = \frac{1}{H}(M^{C} - v\,C)\,, \tag{2.4}$$

where MNC are the nonconservative momentum equations, MC represents the conservative momentum Eqs. (2.2) and (2.3), v is the horizontal velocity vector, and C is the primitive continuity Eq. (2.1). Substituting Eqs. (2.1)-(2.3) into Eq. (2.4) leads to a reformulation of the momentum equations into primitive, nonconservative

$$\frac{\partial U}{\partial t} + U\frac{\partial U}{\partial x} + V\frac{\partial U}{\partial y} - fV = -\frac{\partial}{\partial x}\left[\frac{p_s}{\rho_o} + g(\zeta - \alpha\eta)\right] + \frac{1}{H}\left[M_x + D_x + B_x + \frac{\tau_{sx}}{\rho_o} - \frac{\tau_{bx}}{\rho_o}\right] \tag{2.5}$$

$$\frac{\partial V}{\partial t} + U\frac{\partial V}{\partial x} + V\frac{\partial V}{\partial y} + fU = -\frac{\partial}{\partial y}\left[\frac{p_s}{\rho_o} + g(\zeta - \alpha\eta)\right] + \frac{1}{H}\left[M_y + D_y + B_y + \frac{\tau_{sy}}{\rho_o} - \frac{\tau_{by}}{\rho_o}\right] \tag{2.6}$$

Implementation of a standard quadratic parameterization for bottom stress and the neglect of baroclinic and lateral diffusion/dispersion terms leads to a modified form of the primitive, nonconservative, shallow-water equations:

$$\frac{\partial \zeta}{\partial t} + \frac{\partial UH}{\partial x} + \frac{\partial VH}{\partial y} = 0 \tag{2.7}$$

$$\frac{\partial U}{\partial t} + U\frac{\partial U}{\partial x} + V\frac{\partial U}{\partial y} - fV = -\frac{\partial}{\partial x}\left[\frac{p_s}{\rho_o} + g(\zeta - \alpha\eta)\right] + \frac{\tau_{sx}}{\rho_o H} - \tau_* U \tag{2.8}$$

$$\frac{\partial V}{\partial t} + U\frac{\partial V}{\partial x} + V\frac{\partial V}{\partial y} + fU = -\frac{\partial}{\partial y}\left[\frac{p_s}{\rho_o} + g(\zeta - \alpha\eta)\right] + \frac{\tau_{sy}}{\rho_o H} - \tau_* V \tag{2.9}$$

with T. given by the expression Cy (U2 + V2)1/ 2/H, for C_f equal to the bottom friction coefficient.

Recall that one objective of the ADCIRC-2DDI hydrodynamic model is to be able to consider very large domain problems. The use of large domains coupled with a recognition that tidal forcing is a global phenomena necessitates the inclusion of effects caused by curvature of the Earth's surface. Thus, shallow-water Eqs. (2.7)-(2.9) are recast into spherical coordinates (Flather ,1988; Kolar et al., 1994a):

$$\frac{\partial \zeta}{\partial t} + \frac{1}{R\cos\phi}\left[\frac{\partial u_\lambda H}{\partial \lambda} + \frac{\partial (v_\phi H \cos\phi)}{\partial \phi}\right] = 0 \tag{2.10}$$

$$\frac{\partial u_\lambda}{\partial t} + \frac{u_\lambda}{R\cos\phi}\frac{\partial u_\lambda}{\partial \lambda} + \frac{v_\phi}{R}\frac{\partial u_\lambda}{\partial \phi} - \left[\frac{\tan\phi u_\lambda}{R} + f\right] v_\phi = -\frac{1}{R\cos\phi}\frac{\partial}{\partial \lambda}\left[\frac{p_s}{\rho_o} + g(\zeta - \eta)\right] + \frac{\tau_{s\lambda}}{\rho_o H} - \tau_* u_\lambda \tag{2.11}$$

$$\frac{\partial v_\phi}{\partial t} + \frac{u_\lambda}{R\cos\phi}\frac{\partial v_\phi}{\partial \lambda} + \frac{v_\phi}{R}\frac{\partial v_\phi}{\partial \phi} + \left[\frac{\tan\phi u_\lambda}{R} + f\right] u_\lambda = -\frac{1}{R}\frac{\partial}{\partial \phi}\left[\frac{p_s}{\rho_o} + g(\zeta - \eta)\right] + \frac{\tau_{s\phi}}{\rho_o H} - \tau_* v_\phi\ , \tag{2.12}$$

where X, are degrees longitude (east of Greenwich positive) and degrees latitude (north of the equator positive), u, v are depth - averaged velocities in spherical coordinates, R is the radius of the Earth, f is given by 2 sin Ω , Q is the angular speed of the Earth, and $\tau_{s\lambda}$, $\tau_{s\Phi}$ are the applied free surface stresses.

A practical expression for the Newtonian equilibrium tide potential is given by Reid (1990) as:

$$\eta(\lambda, \phi, t) = \sum C_{jn}\ f_{jn}\ (t_0)\ L_j(\phi) \cos\left[2\pi(t - t_0)/T_{jn} + j\lambda + \nu_{jn}(t_0)\right], \tag{2.13}$$

where t is time relative to the reference time, to, Cjn is a constant characterizing the amplitude of tidal constituent n of species j, f is a time-dependent nodal factor, vj is the time-dependent astronomical argument, j = 0, 1, 2 are the tidal species (j = 0 declinational; j = 1 diurnal, j = 2 semidiurnal), $L_o = 3\sin^2\Phi - 1$, $L_1 = \sin(2\Phi)$, $L_2 = \cos^2(\Phi)$, and Tj, is the period of constituent n for species j. Values for C_{jn} are presented by Reid (1990) and the Earth elasticity factor is often taken as 0.69 for all tidal constituents (Schwiderski, 1980; Hendershott, 1981), although its value has been shown to be slightly constituent-dependent, ranging between 0.693 and 0.736 (Wahr, 1981; Woodworth ,1990).

The Earth's curvature must be accounted for, not only in the governing equations, but also in the FE discretization (Kolar et al., 1994a). In the FE method, the solution to the governing equations is approximated using interpolating functions. These interpolating functions are defined over elements and these elements are most often cast within the framework of a Cartesian coordinate system. To conveniently implement the FE method, governing equations in spherical coordinates are projected onto a planar surface using cartographic projection techniques. Mapping spherical Eqs. (2.10)-(2.12) to a rectilinear coordinate system is accomplished using a Carte Parallelogramatique Projection (CP)

$$x' = R(\lambda - \lambda_o) \cos \phi_o \tag{2.14}$$

$$y' = R\phi , \tag{2.15}$$

where (40) is the center point of the projection. An application of the CP projection to Eqs. (2.10)-(2.12) yields shallow-water equations in primitive, nonconservative form expressed in the CP coordinate system:

$$\frac{\partial \zeta}{\partial t} + \frac{\cos \phi_0}{\cos \phi} \frac{\partial (UH)}{\partial x'} + \frac{1}{\cos \phi} \frac{\partial (VH \cos \phi)}{\partial y'} = 0 \tag{2.16}$$

$$\frac{\partial U}{\partial t} + \frac{\cos \phi_0}{\cos \phi} U \frac{\partial U}{\partial x'} + V \frac{\partial U}{\partial y'} - \left[\frac{\tan \phi}{R} U + f \right] V = - \frac{\cos \phi_0}{\cos \phi} \frac{\partial}{\partial x'} \left[\frac{p_s}{\rho_0} + g(\zeta - \eta) \right] + \frac{\tau_{s\lambda}}{\rho_0 H} - \tau_* U \tag{2.17}$$

$$\frac{\partial V}{\partial t} + \frac{\cos \phi_0}{\cos \phi} U \frac{\partial V}{\partial x'} + V \frac{\partial V}{\partial y'} + \left[\frac{\tan \phi}{R} U + f \right] U = - \frac{\partial}{\partial y'} \left[\frac{p_s}{\rho_0} + g(\zeta - \eta) \right] + \frac{\tau_{s\phi}}{\rho_0 H} - \tau_* V . \tag{2.18}$$

As discussed in Sec. 2.2, utilizing the FE method to resolve spatial dependencies in the primitive shallow-water equations leads to inaccurate solutions with severe artificial, near 2 - Ax modes (Gray,1982; Lynch, 1983; Westerink et al., 1989).

Reformulation of the primitive equations into a GWCE gives highly accurate, noise-free, FE-based solutions to the shallow-water equations (Lynch & Gray, 1979; Kinnmark, 1984). The high accuracy of GWCE-based FE solutions is a result of their excellent numerical amplitude and phase propagation characteristics. In fact, Fourier analysis indicates that for constant-depth water using linear interpolation, a linear tidal wave resolved with 25 nodes per wavelength is more than adequately represented over the range of Courant numbers, C = $\sqrt{gh}$ At/Ax, less than or equal to one (Luettich et al., 1992). Furthermore, the monotonic dispersion behavior of GWCE-based FE solutions avoids generating artificial, near 2 -Ax modes that have plagued the primitive FE-based solutions on the interior and at the boundary (Platzman, 1981; Foreman, 1983; Westerink et al., 1994b). Note that the monotonic dispersion behavior of GWCEbased FE solutions is very similar to that associated with staggered finite difference solutions to the primitive shallow-water equations (Westerink & Gray, 1991). GWCE-based FE solutions to the shallow-water equations allow extremely flexible spatial discretizations that effectively minimize the discrete size of any problem (LeProvost & Vincent, 1986; Foreman, 1988; Vincent & LeProvost, 1988; Westerink et al., 1994a, 1995; Luettich & Westerink, 1995). Derivation of the GWCE is presented concisely using the operator notation invoked by Kinnmark (1984) and Kolar (1992):

$$GWCE = \frac{dC}{dt} + \tau_o C - \nabla \cdot \boldsymbol{M}^c, \qquad (2.19)$$

where GWCE is the generalized wave-continuity equation and T is a nonphysical constant in time and space that controls the balance between primitive and wave equation formulations (Lynch & Gray, 1979; Kinnmark, 1984; Luettich et al., 1992; Kolar et al., 1994b). Substituting continuity Eq. (2.16) and the conservative form of momentum Eqs. (2.17) and (2.18) into Eq. (2.19), the GWCE in the CP coordinate system is:

$$\frac{\partial^2 \zeta}{\partial t^2} + \tau_0 \frac{\partial \zeta}{\partial t} + \frac{\cos \phi_0}{\cos \phi} \frac{\partial}{\partial x'} \left[U \frac{\partial \zeta}{\partial t} - \frac{\cos \phi_0}{\cos \phi} UH \frac{\partial U}{\partial x'} - VH \frac{\partial U}{\partial y'} + \left[\frac{\tan \phi}{R} U + f \right] VH \right.$$

$$
-H\frac{\cos\phi_0}{\cos\phi}\frac{\partial}{\partial x'}\left(\frac{p_s}{\rho_0}+g(\zeta-\alpha\eta)\right)-(\tau_*-\tau_0)\,UH+\frac{\tau_{s\lambda}}{\rho_0}\Bigg]
$$

$$
+\frac{\partial}{\partial y'}\left[V\frac{\partial\zeta}{\partial t}-\frac{\cos\phi_0}{\cos\phi}UH\frac{\partial V}{\partial x'}-VH\frac{\partial V}{\partial y'}-\left[\frac{\tan\phi}{R}U-f\right]UH\right.
$$

$$
\left.-H\frac{\partial}{\partial y'}\left(\frac{p_s}{\rho_0}+g(\zeta-\alpha\eta)\right)-(\tau_*-\tau_0)\,VH+\frac{\tau_{s\phi}}{\rho_0}\right]
$$

$$
-\frac{\partial}{\partial t}\left[\frac{\tan\phi}{R}VH\right]-\tau_0\left[\frac{\tan\phi}{R}VH\right]=0\,. \qquad (2.20)
$$

Advective terms in the GWCE, written in nonconservative form, improve global and local mass conservation (Kolar et al., 1994b), as well as numerical stability, especially for advection dominant flows (Westerink et al., 1992b). The ADCIRC-2DDI hydrodynamic model solves the GWCE, Eq. (2.20), in conjunction with the primitive momentum equations in nonconservative form, Eqs. (2.17) and (2.18).

Numerical discretization of GWCE Eq. (2.20) and momentum Eqs. (2.17) and (2.18) is implemented in three stages. First, the symmetrical weak weighted residual (SWWR) statements for Eqs. (2.17), (2.18), and (2.20) are developed. This procedure is based on a standard Galerkin FE formulation (Becker et al., 1981; Celia & Gray, 1992). One consequence of the SWWR is that the order of the derivatives in the governing equations is reduced, leading to a requirement of only CO functional continuity (i.e., only the interpolating functions themselves and not their derivatives need be continuous between discrete points). Next, the stable and accurate time discretization strategies of Kinnmark (1984) and Werner & Lynch (1989) are implemented. A variably weighted three-time-level implicit scheme is applied to linear terms in the GWCE. The nonlinear Coriolis, atmospheric pressure, and tidal potential terms are all treated explicitly. Alternatively, advective terms within the GWCE are evaluated at two known time levels. This time discretization results in a system of linear algebraic equations associated with the GWCE, which is solved for unknown elevations. In the momentum equations, a Crank-Nicolson two-time-level implicit scheme is applied to all terms except the bottom friction and advective terms, which are treated explicitly.

The final step in the numerical discretization scheme is approximation of the spatial domain using the FE method. Variables are expanded using a C0 interpolation basis over three-node, linear triangular elements. Elemental equations are summed over the global domain and inter-element CO functional continuity is enforced. Details of the FE implementation on a term-by-term basis is presented by Luettich et al. (1992) and Westerink et al. (1992b).

The fully discretized model equations are written in matrix notation (Luettich et al. 1992):

$$M^{GWCE}\zeta^{k+1} = P^{GWCE} \quad (2.21)$$

$$M^{\lambda\lambda ME}U^{k+1} + M^{\lambda\phi ME}V^{k+1} + P^{\lambda ME} \quad (2.22)$$

$$M^{\phi\lambda ME}U^{k+1} + M^{\phi\phi ME}V^{k+1} + P^{\phi ME}, \quad (2.23)$$

where MGWCE is the banded, time-independent mass matrix in the GWCE equation, k + 1 is the vector of unknown surface elevations at time level k + 1, pGWCE is the load vector of known forcings in the GWCE equation, MAMMEXk,M E, M+XME, and MOME are the time-dependent, lumped mass matrices in the X,¢ directions, Uk+1, V*+1 are the vectors of unknown velocity components at the k + 1 time level, and PX-ME, pWME are the load vectors of known forcings for the momentum equations.

Elevation boundary conditions are enforced within the load vector pGWCE of the GWCE Eq. (2.21) and zero normal velocity boundary conditions are enforced in the momentum Eqs. (2.22) and (2.23). Westerink et al. (1994b) have shown that solutions to the GWCE equation are insensitive to this standard boundary condition formulation. The decoupled discrete GWCE and momentum Eqs. (2.21)-(2.23) lead to a sequential solution procedure. GWCE Eq. (2.21) is solved at each timestep for the surface water elevations k+ 1 The GWCE mass matrix MGWCE is time-independent, so it is assembled and decomposed only once. The banded structure of this matrix is not utilized by the iterative preconditioned conjugate gradient matrix solver used for computations performed in this work (Kincaid & Cheney, 1991). A preconditioned conjugate gradient solver is implemented because of its efficiency at minimizing memory requirements within ADCIRC-2DDI for larger problems. The load vector PGWCE is updated at each timestep with newly computed surface water elevations and velocities from the previous timestep.

After solving the GWCE for surface water elevations, these computed elevations are substituted into momentum Eqs. (2.22) and (2.23) prior to solution for the velocity components and Uk + and Vk + 1. The time-dependent mass matrices in the momentum equations MXXME, M PE, MOXME,and MEGME are lumped to yield diagonal matrices that require trivial solution. The lumping procedure applied here does not introduce significant errors as shown by Lynch & Gray (1979). The numerical solution algorithm just described for the ADCIRC-2DDI model is implemented in fully vectorized form. A consequence of this solution procedure is a highly efficient code in terms of central processing unit (CPU) requirements per node. This efficiency is largely due to the fact that GWCE-based FE solutions to the shallow-water equations allow for extremely flexible spatial discretizations that result in minimization of the discrete size of any problem (LeProvost & Vincent, 1986; Foreman, 1988; Vincent & LeProvost, 1988; Westerink et al., 1992 a,b, 1994a, 1995) .

CHAPTER THREE
RESULTS

3.1 Wind Properties

Wind and tide climate spesific to the area of study have been investigated using data on daily wind direction and blow intensity and blow frequency of the last 28 years. The data have been gathered from Turkish State Meteorological Service of T.R. Environmental and Forestry Ministry, Demre Meteorological Station (Figure 3.1) east of the study area and Kaş Meteorological Station (Figure 3.2) west of the study area.

Demre Meteorological Station, located east of the study area, shows that the widns in the region it representshas a speed of 5 km/h or less in south and south east directions (Figure 3.1a). In the same way, although seen rarely, wind speeds of 5-10 km/hour and 10-20 km/hours can be observed frm the same directions. Figure 3.1b which shows the major wind directions, clearly establishes the dominance of south winds. It can be understood that winds more strong than these and which may be considered as storms are met rarely. These storm winds blow from south and south west directions (Figure 3.1c).

The data from the Kaş Meteorological Station, at the west of the study area, different from the situation monitored in Demre, as recorded that the dominant wind speed around Kaş is 5-10 km/h and the dominant directions are southwest and northeast, and it has also been understood that wind speeds of 10-20 km/h and 5 km/h or less are blowing from the same dominant directions but in a secondary frequency (Figure 3.2a, 3.2b and 3.2c). Stronger winds that may be accepted as storm, though rare, are met more often comared to Demre. It has ben seen that these storm winds also blow from the same dominant directions and also from west. Winds speeds in excess of 40 km/h or more are seen to blow that may be considered exceptional, nevertheless, these winds blow from northeast and/or west directions.

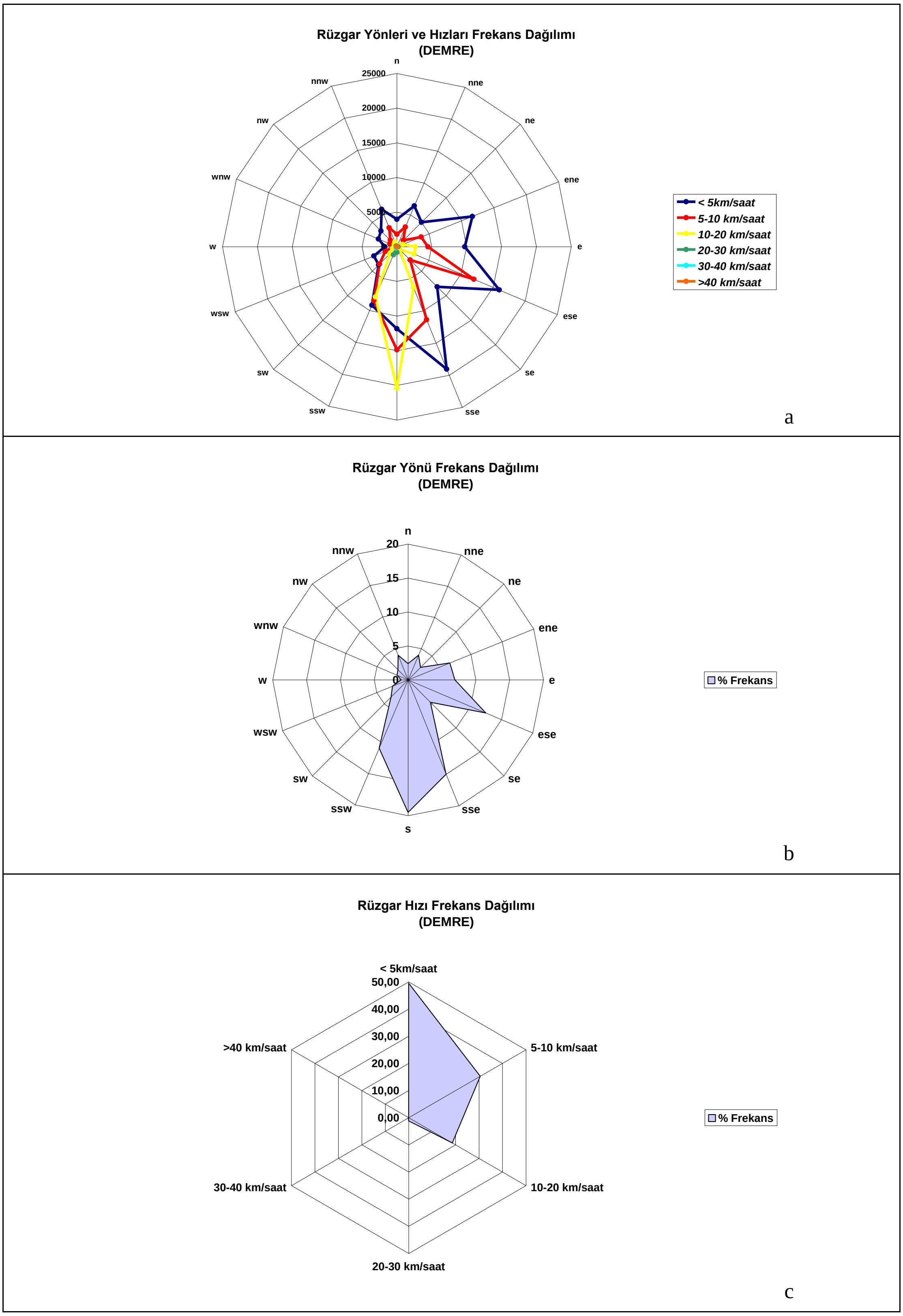

Figure 3.1 Demre weather station data: (a) wind direction and speed, (b) Wind direction frequency, (c) wind speed frequency

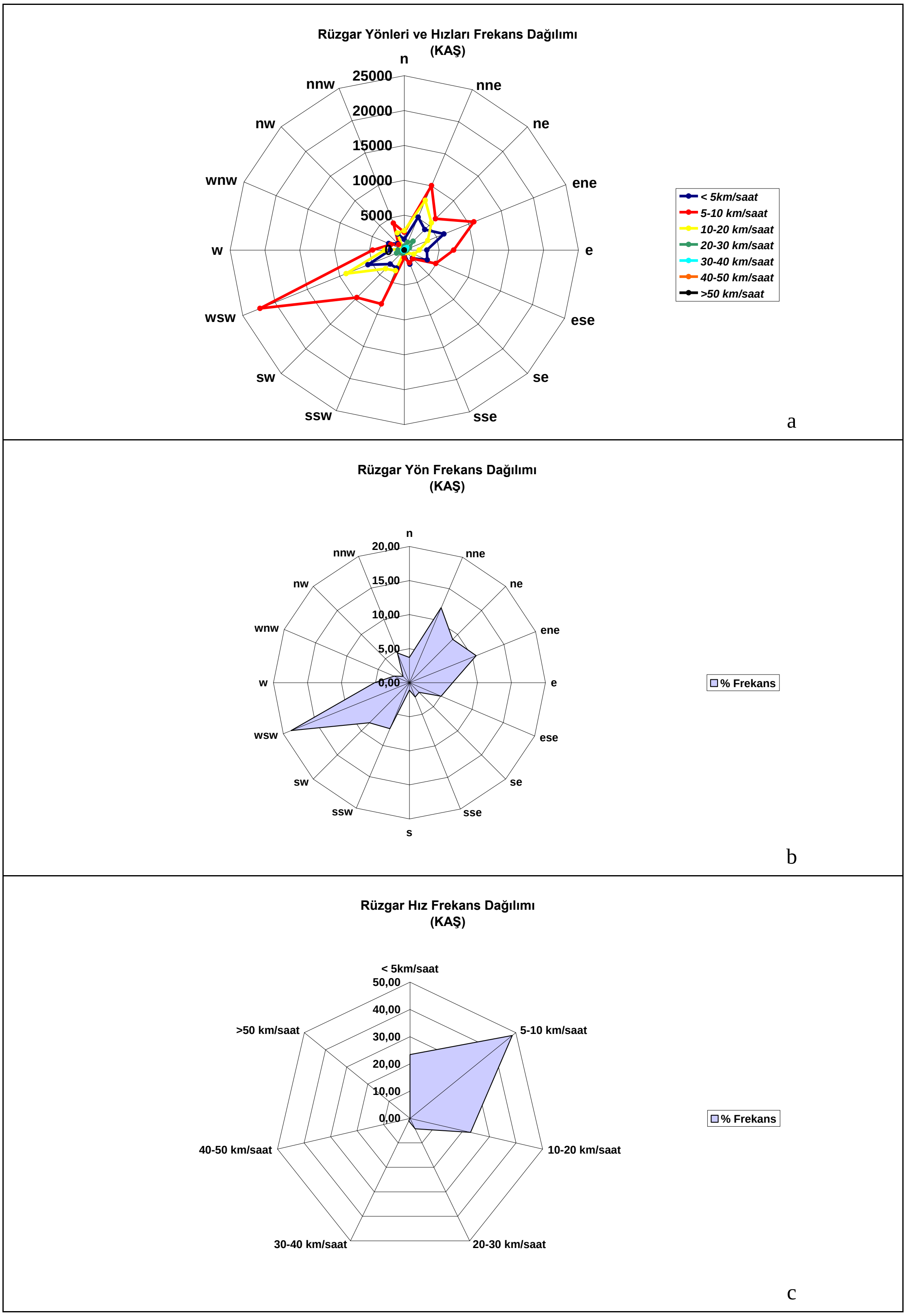

Figure 3.2 Demre weather station data: (a) wind direction and speed, (b) Wind direction frequency, (c) wind speed frequency

Within the frame of the data gathered from both meteorology stations, when the waves generated by the winds of dominant magnitude and directions along the shores facing the open see are taken into consideration, it can be calculated that the wave heights may vary between 1 and 3 m deending on the duration of wind blow. On the other hand, since the study area Ölüdeniz has a rather closed harbour structure, it is clear that the only wind directions that may be effective can be those blowing from east and west. Therefore, the relative short fetch distances show that, 15 km from East (Demre), 5 km from West (Sıçak bay shore) when the wave height in Ölüdeniz for a wind speed of 50 km/h from east or west direction can be only about 1-1,5 m.

It should be noted that the approximate information given above is calculated by limiting the wind blow duration to 12 hours. Unfortunately, the meteorological data does not include the duration of wind blow to be evaluated together with the wind speed and direction data.

3.2 Flow Structure

The resultant speeds and their dominant directions, obtained from the measurements in 6 stations where flow measurements had been carried out in both time periods are given in Table 3.1. It can be understood that the stations A2 and A3, which enable Ölüdeniz's connection with open see between the Kekova Island and Sıçak peninsula, are the points having the greatest average speeds. Station A6, located at the open area where the connection of the east end Ölüdeniz with the open see is situated, follows these stations. Stations at the strait connecting Sıçak bay (A1) and Üçağız to Ölüdeniz have almost the same flow rates. At station A4 in Üçağız, no flow profile have been obtained due to shallow depth of about 5 m.

It should be mentioned that the speed data in the table are the resultant speed and directions gathered from speed data in all depths. The high values of the speed ranges indicating the differences between the maximum and minimum resultant speeds reflect the variability of flow rates in the study area.

Although the dominant direction represents the direction of motion of the water column, it can be understood from the flow vector profiles that the flow directions are highly variable in terms of both measurement days and hours and depth. With regards to the dominant directions given in the table, it can be seen that from station A6, there is incoming water into Ölüdeniz. Similarly, from both straits where stations A2 and A3 are locted, although effective much less, it is understood that there is incomng water to Ölüdeniz. The flow direction in station A1 located in Sıçak Bay show an east directed motion along Ölüdeniz.The dominant direction of A5 station located on the strait combinng Üçağız and Ölüdeniz indicate a flow from Üçağız to Ölüdeniz.

Table 3.1 Current measurements obtained by the end of the speed and direction of currents

Station	The resultant velocity (cm/sn)			The resultant Speed Value Range	Dominance Orientation Degree
	Average	Highest	Lowest		
A1	1.03	12.52	0.57	11.94	(SSW) 200
A2	14.12	48.78	0.25	48.53	(WNW) 294
A3	5.28	48.07	0.14	47.93	(W) 269
A4	--	--	--	--	--
A5	1.37	11.84	0.17	11.67	(ESE) 109
A6	4.02	28.89	0.75	28.14	(SW) 252

These data on speed and directions and the study area volume calculated as a result of batimetric study, in calculations carried out using batimetrc cross-sections at points where the study area exchanges water, it is determined that the water renewal rate in the study area varies between 6 days and 23 days.

It is important to realize that the information and data explained above on flow regime reflect the wind and see conditions at the data the measurements are done. Because this situation in flow motion clearly varying day by day and hour by hour based on both speed and direction, is an indicator that under different conditions a different regime can be created. When the wind, rain and also the closedness of the study area is taken into consideration, in types of areas where the tide movements may also have a potential to be effective, estimate capabilities close to real life situations are being restricted without continuous measurements of anuual periods.

A1- 29/09/2010	A2- 29/09/2010	A3- 29/09/2010	A5-29/09/2010
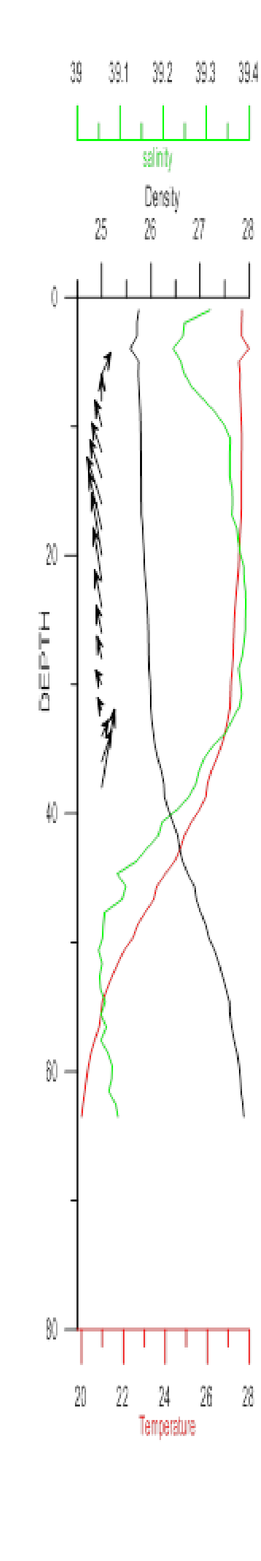	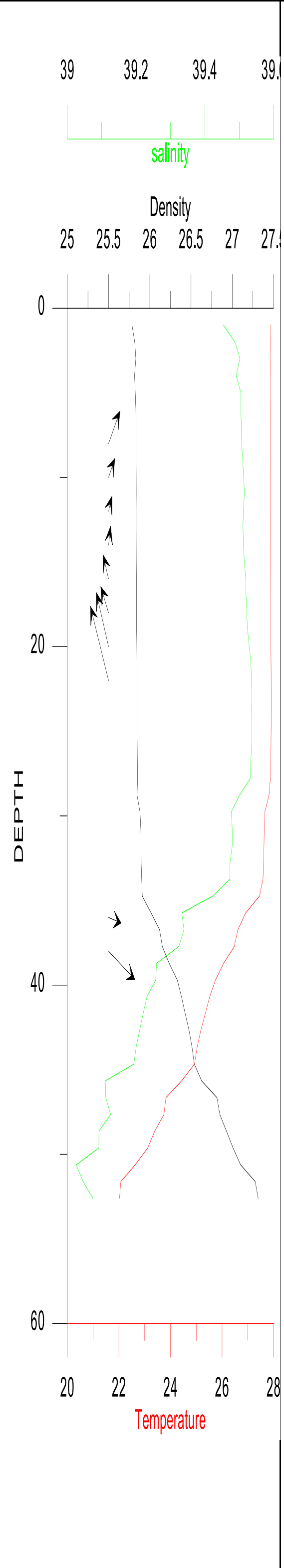	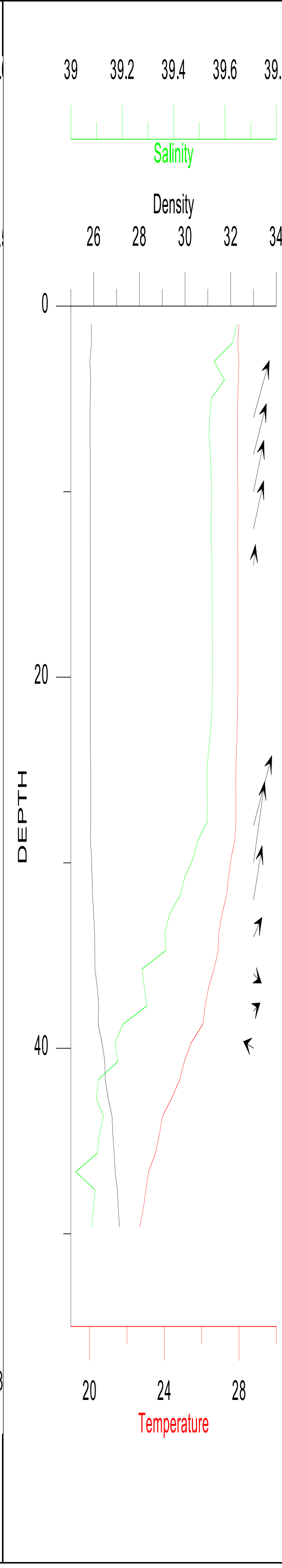	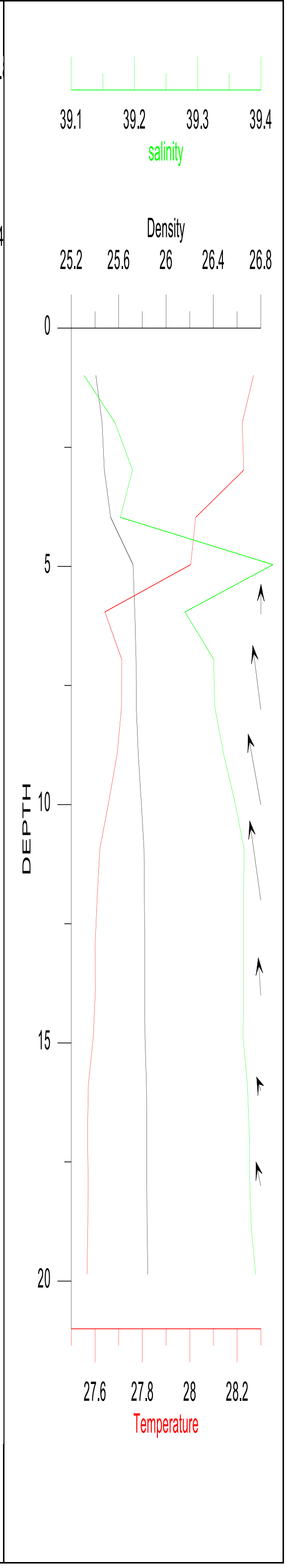

Figure 3.3 The salinity, density, temperature and velocity vector variations with water depth for different stations and different days in September and October

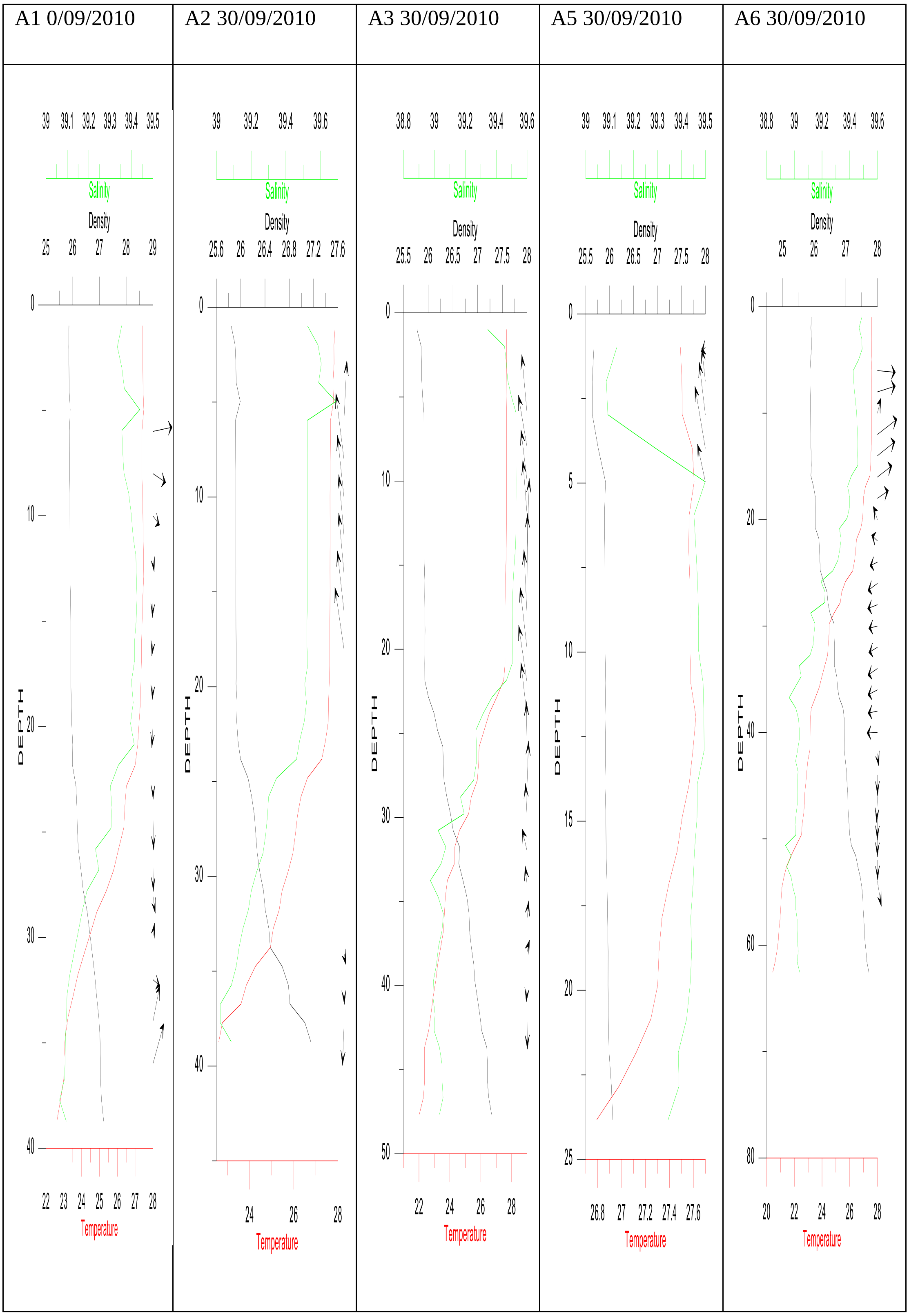

Figure 3.3 continues

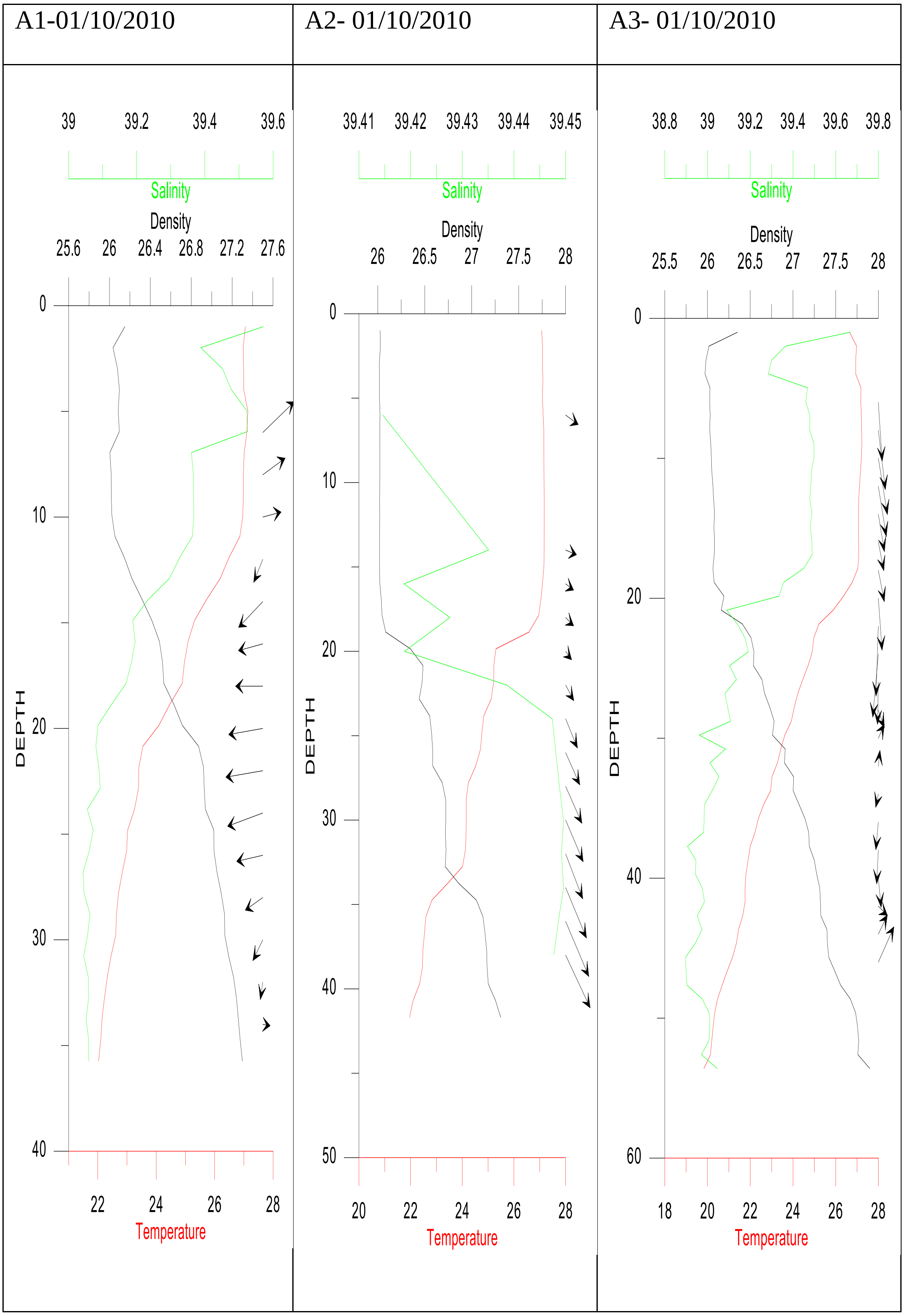

Figure 3.3 continues

A1-02/10/2010	A2-02/10/2010	A3-02/10/2010	A5-2/10/2010	A6-2/10/2010
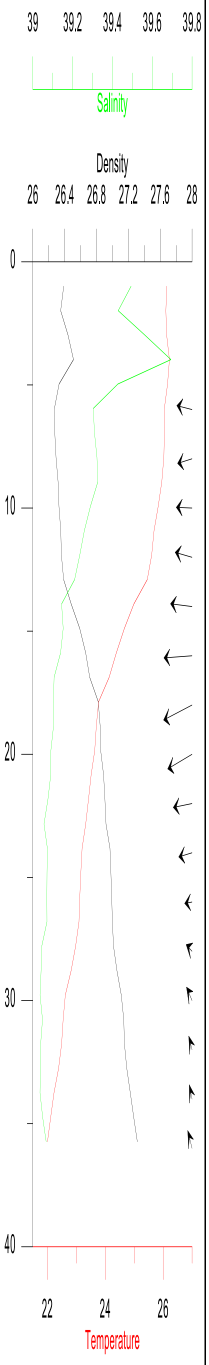	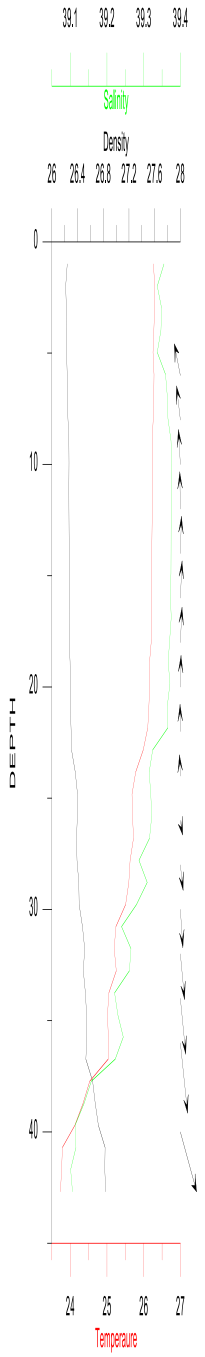	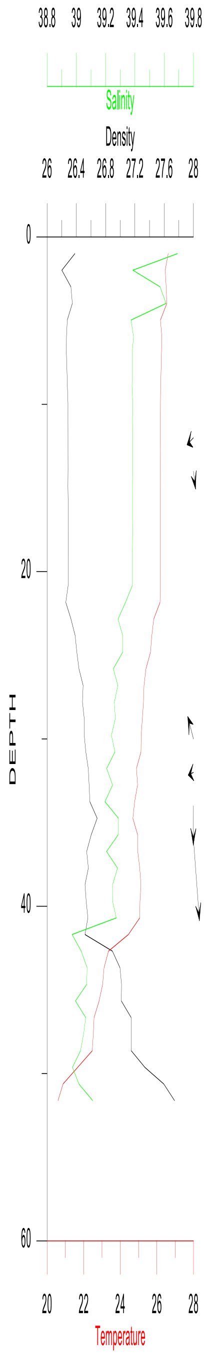	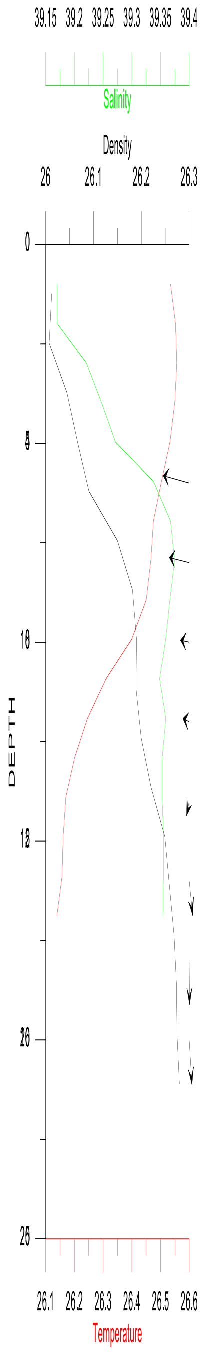	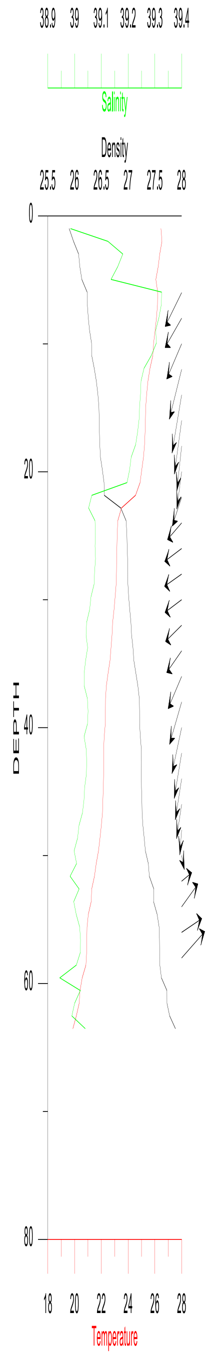

Figure 3.3 continues

A1-03/10/2010	A2-03/10/2010	A3-3/10/2010	A5-03/10/2010	A6-03/10/2010
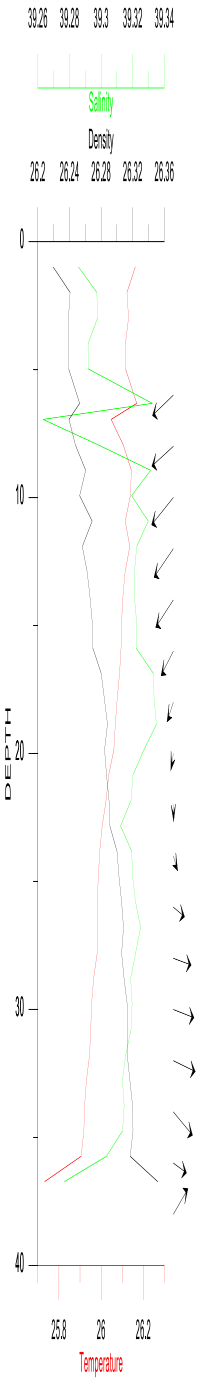	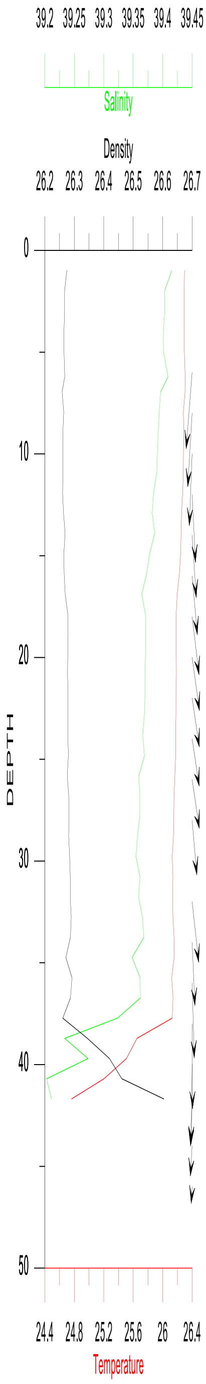	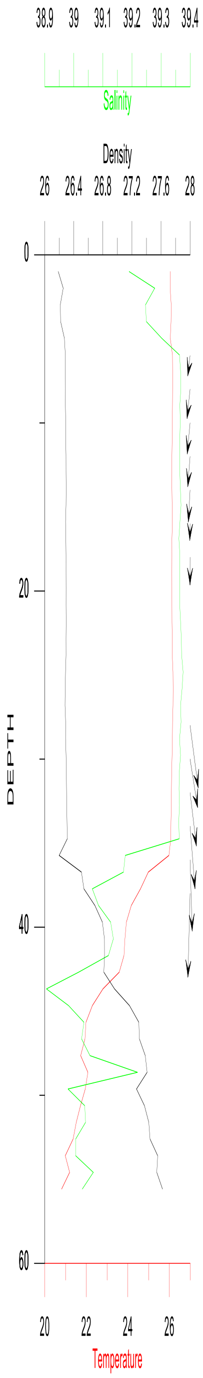	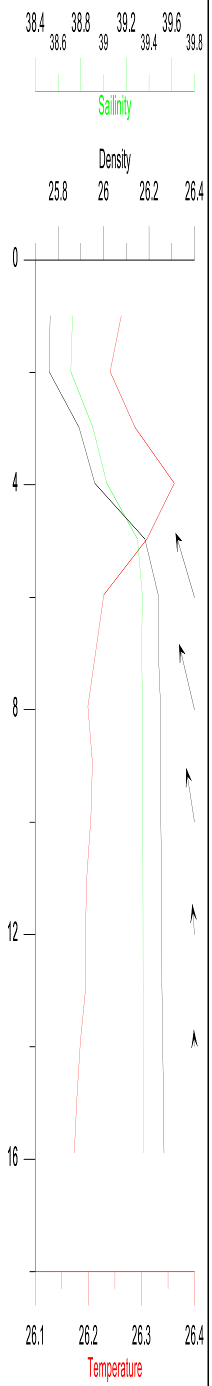	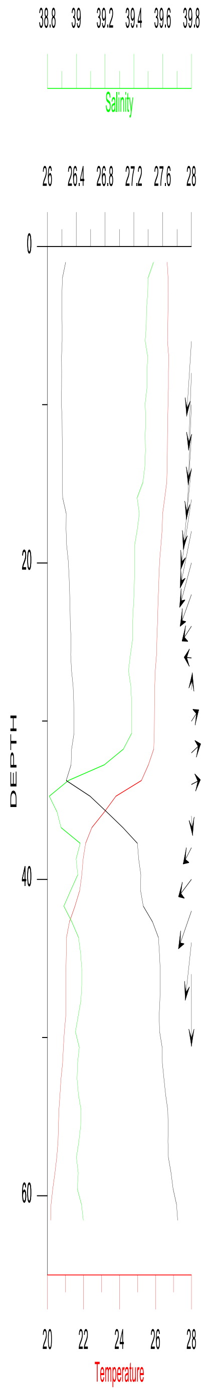

Figure 3.3 continues

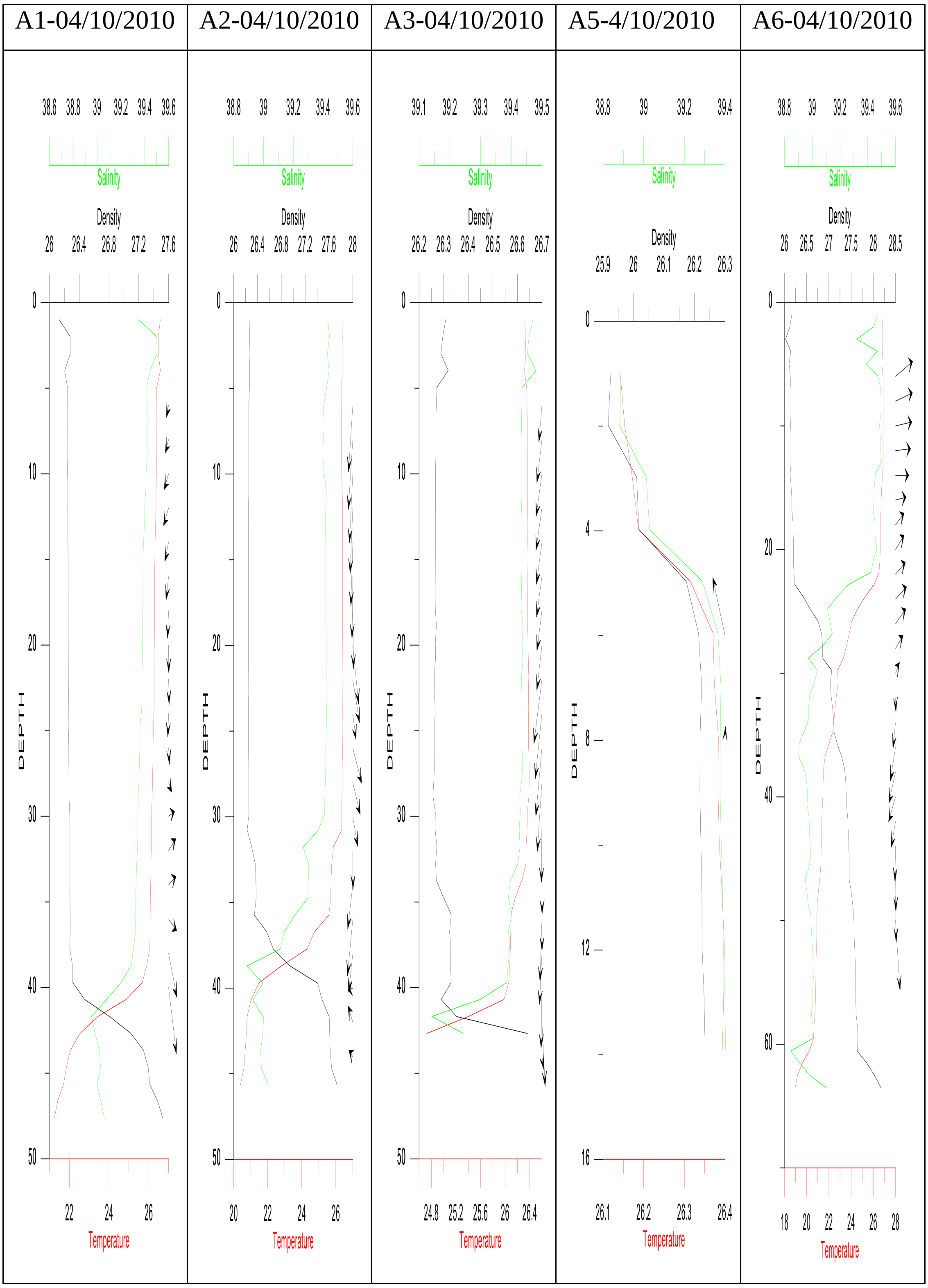

Figure 3.3 continues

A1-5/10/2010	A2- 05/10/2010	A3- 05/10/2010	A5- 05/10/2010	A6- 05/10/2010
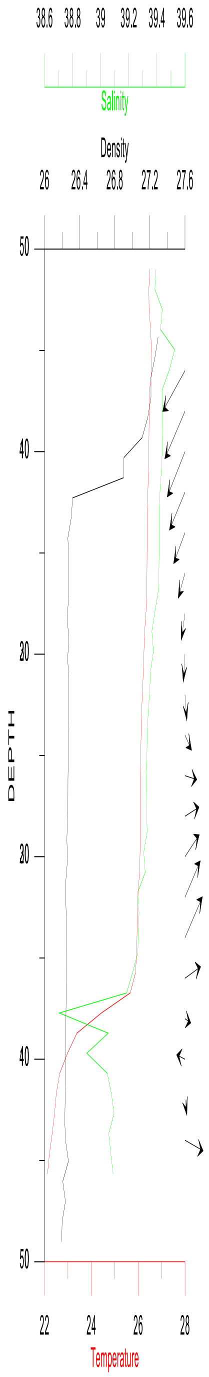	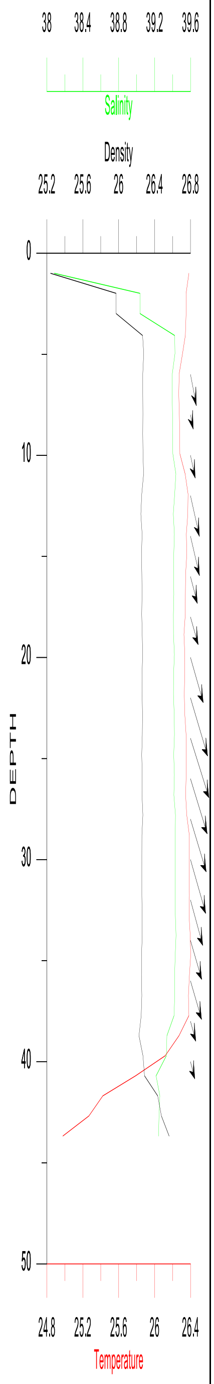	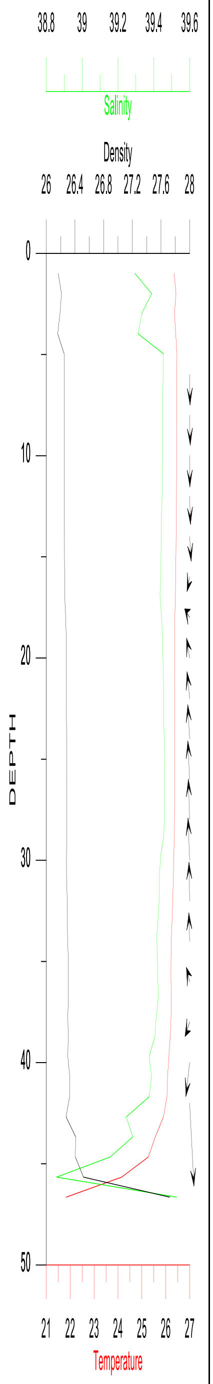	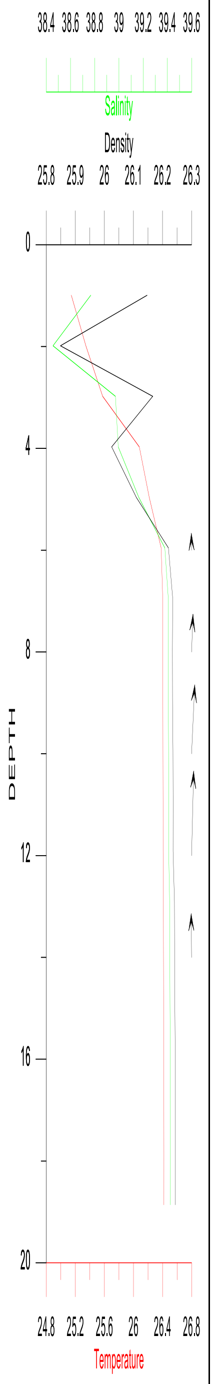	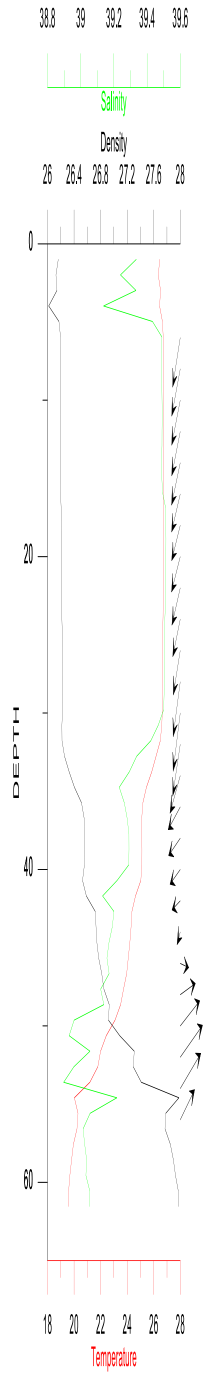

Figure 3.3 continues

Nevertheless, based on the oshinographic and batimetric data gathered in the following section, modelling studes are carried out investigating various condition scenarios.

3.3 Hydrographic Structure

Within the framework of oshinographic properties the stations in the study area, the measurements of temperature, salinity and density values of seewater physical properties, the profiles showing the vertical variation from see surface to see base, are obtained synchronised with the flow measurements. In Figure 3.4, measurements made at different times for each three parameter measured at eleven stations are presented by synchronizing.

When the figures 3.4 are examined, it is seen that during the period of September-October 2010, the temperature at the surface reaches maximum values of 26 - 29 ^{o}C, at the see base of depth 70 - 100 m, even to values of 19 - 20 ^{o}C. But especially at stations with depths more than 50 m, the depth range where the termoklin layer is effective, it is a noteworthy detection that may change showing a vertical mobility in levels of time to time of 20 - 30 m at several measurment days. This situation reflects the dynamism of the flow system at Ölüdeniz during the study. As will be explained in greater detail at the section on flow system, the variations on dominant wind direction and magnitude may affect the water movements directly and very fast. The rate of this effect may be understood from the fact that water, in both horizontal and vertical planes, may move so fast as to create a temperature difference of about 3 - 4 oC day by day on surface waters. This situation may clearly be monitored at shallow stations despite the relative decreasing trend from surface to base. The same varation patterns are also observed in salinity and densty profiles.

However, the salinity variations at the surface (0 - 1 m) the effects of underground and overground fresh land water entrance can observe in Figures 3.5(2b), 3.5(4b-8b) and 3.5(2c), 3.5(4-8c). This effect may decrease up to 2 - 3 m at shallow stations.

On the other hand, it will be useful to emphasize that the study area carries strand characteristics in accordance with the Mediterranean region oshinographic character. However, during winter and spring seasons, subjected to heavy rain, it is clear that the salinity ratio mentioned above may create obvous effects on whole Ölüdeniz system, especially at Üçağız and Gökkaya. When the data of 80 years and 9 months, starting from 1929 to February 2011 at which data the measurementd have been terminated are examined , it is seen that Kaş-Kekova region gets a daily average of 13.4 (±22.1) mm/m^2 rain in rainy days (a total of 14186 days), the maximum amount may reach 331.5 mm/m^2. When a categorization is made with respect to rain intensity, the most frequently observed rain intensity frequences over the long time period are measured as those above 10%, as >1 mm, 1-5 mm, 5-10 mm, 10-25 mm ve 25-50 mm. But if it is considered that the daily vaporization amount in the open weather at the region is 4.8 (±3.2) mm, it is not very likely to accept the rain magnitude categories >1 mm, 1-5 mm, 5-10 mm as rain. The rain magnitude categories 10-25 mm and 25-50 mm besides the other categories have a total frequency of about 30%. It has been calculated that these two rain magnitude categories are seen at about 14.3 % of total annual rainy days and enable a total of 9018 mm/m^2 rain fall.

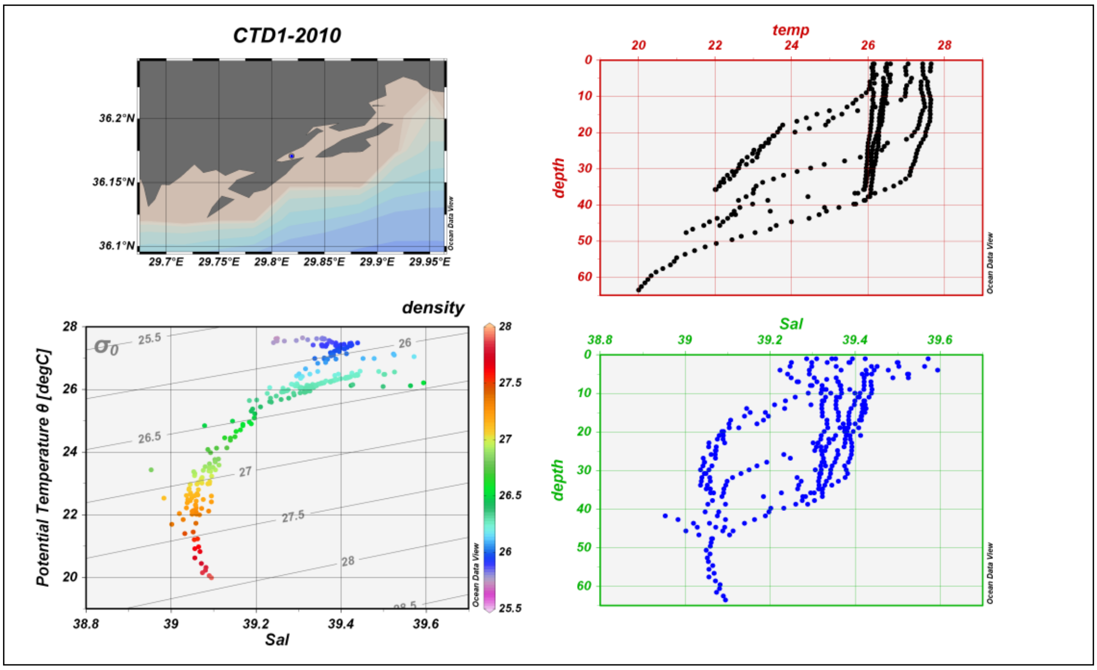

Figure 3.4 Temperature, density and salinity station's vertical CTD profile in September and October 2010

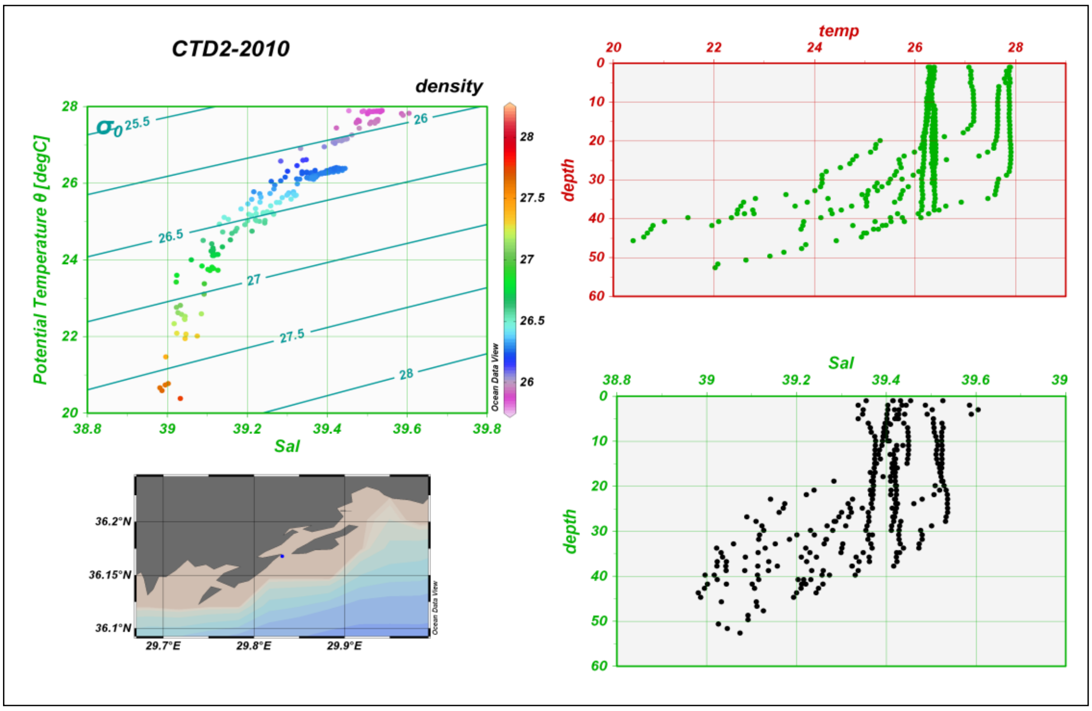

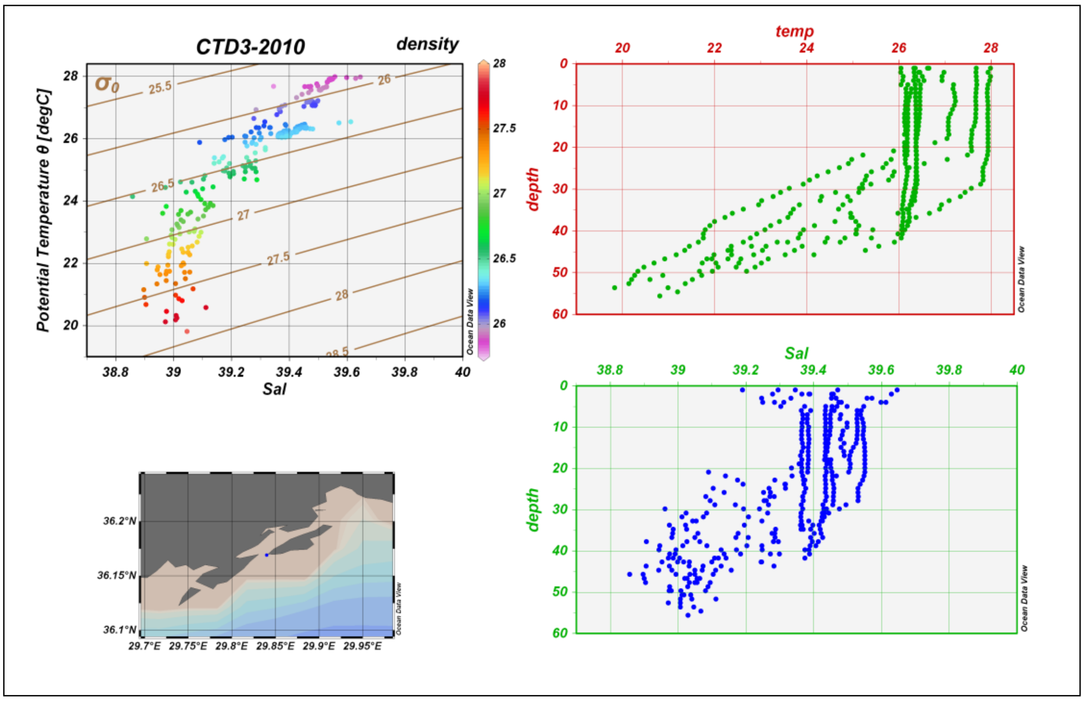

Figure 3.4 continues

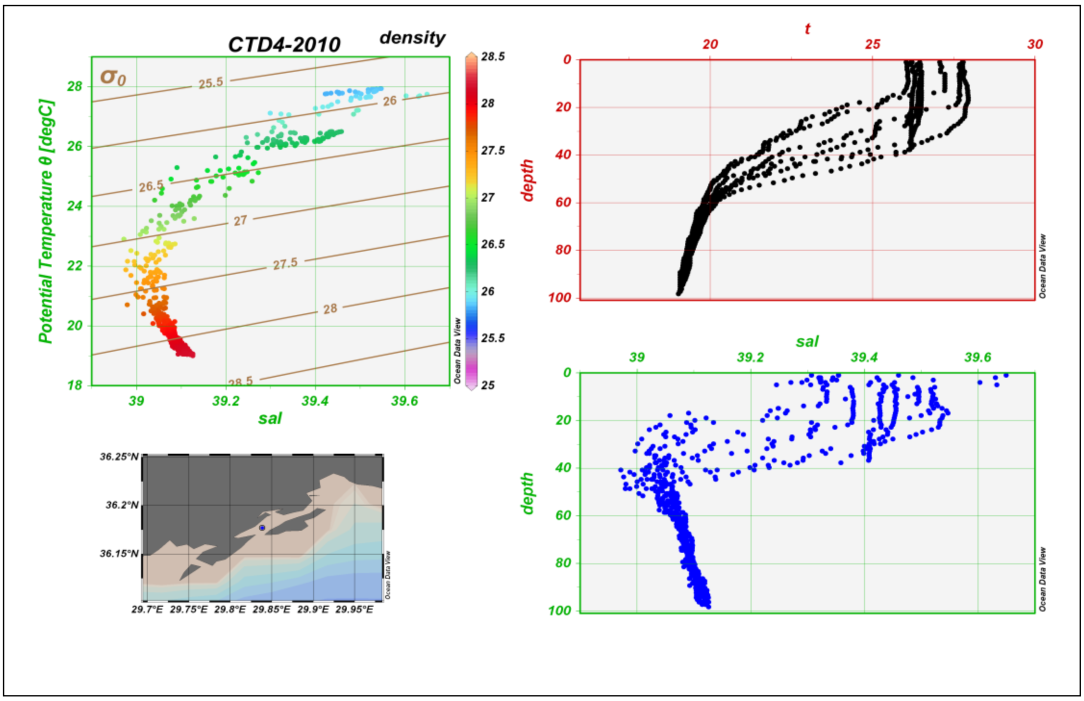

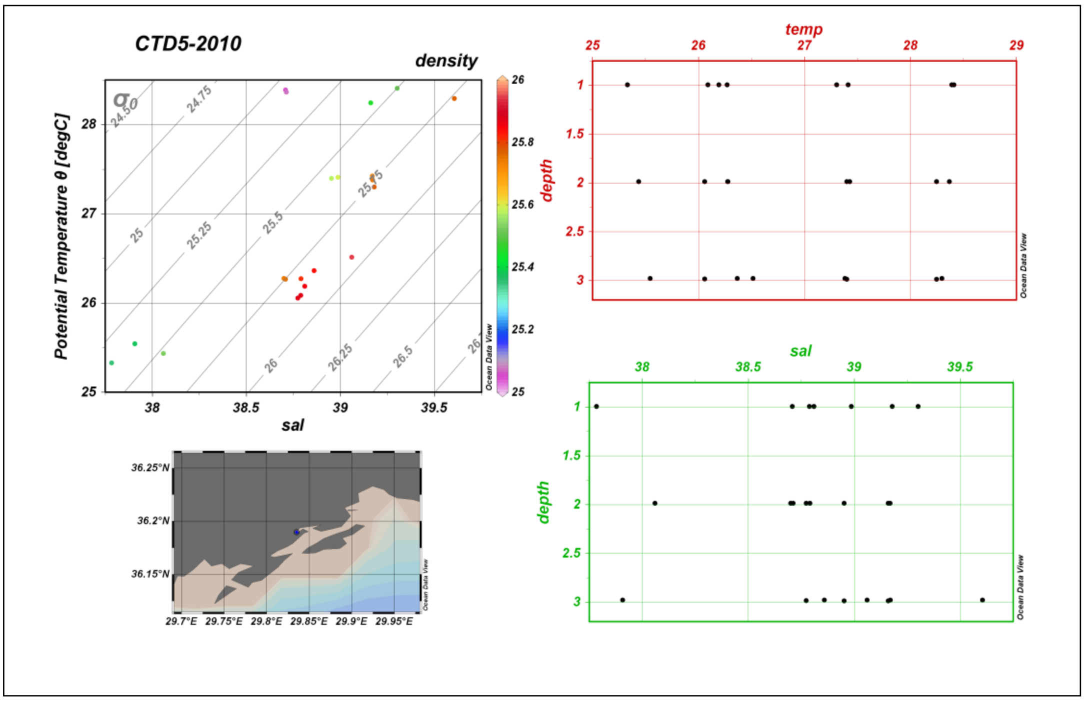

Figure 3.4 continues

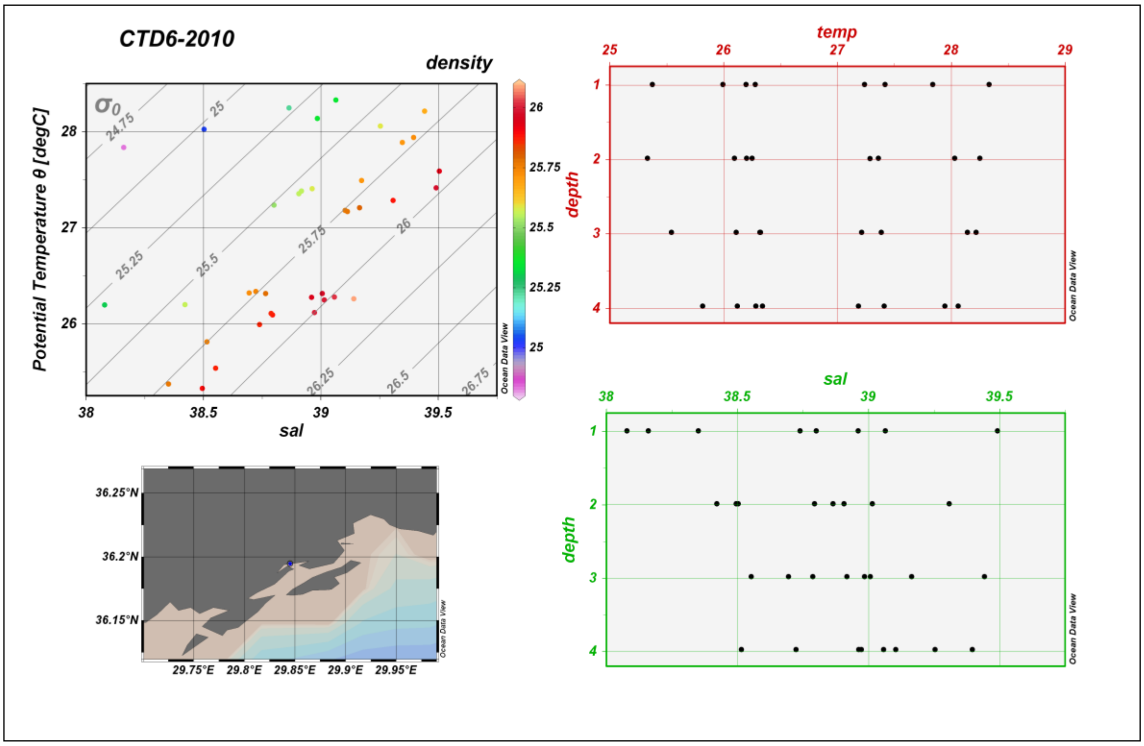

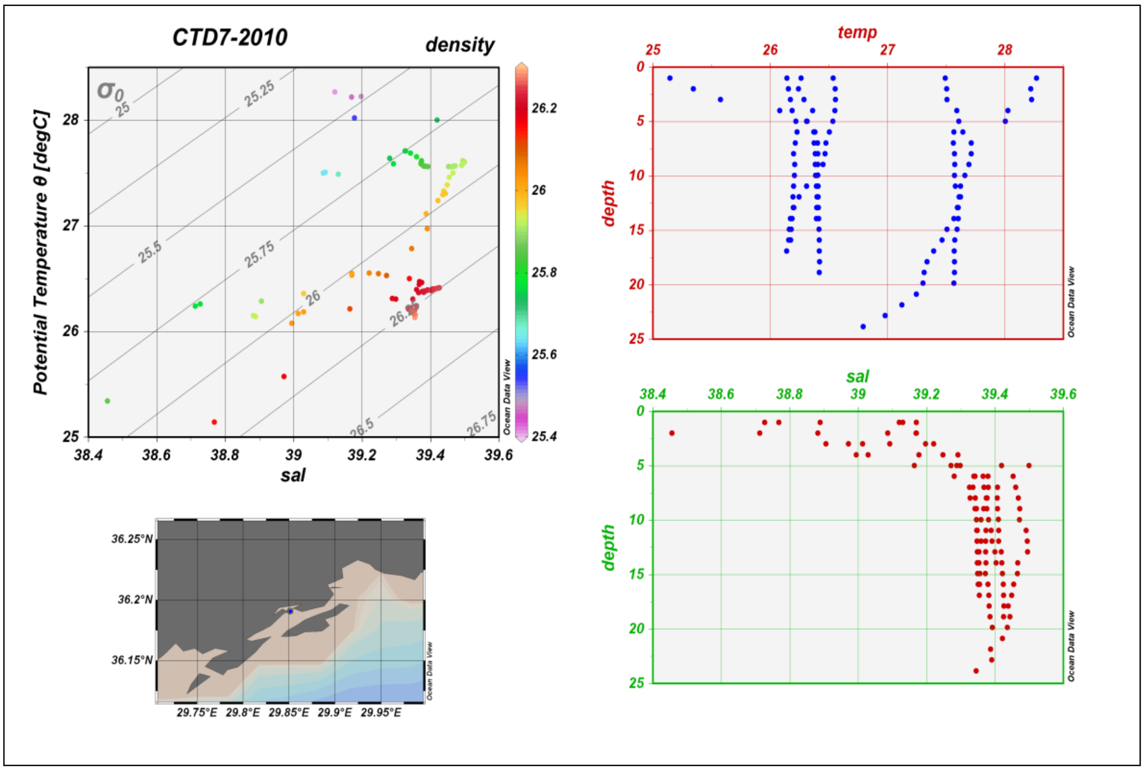

Figure 3.4 continues

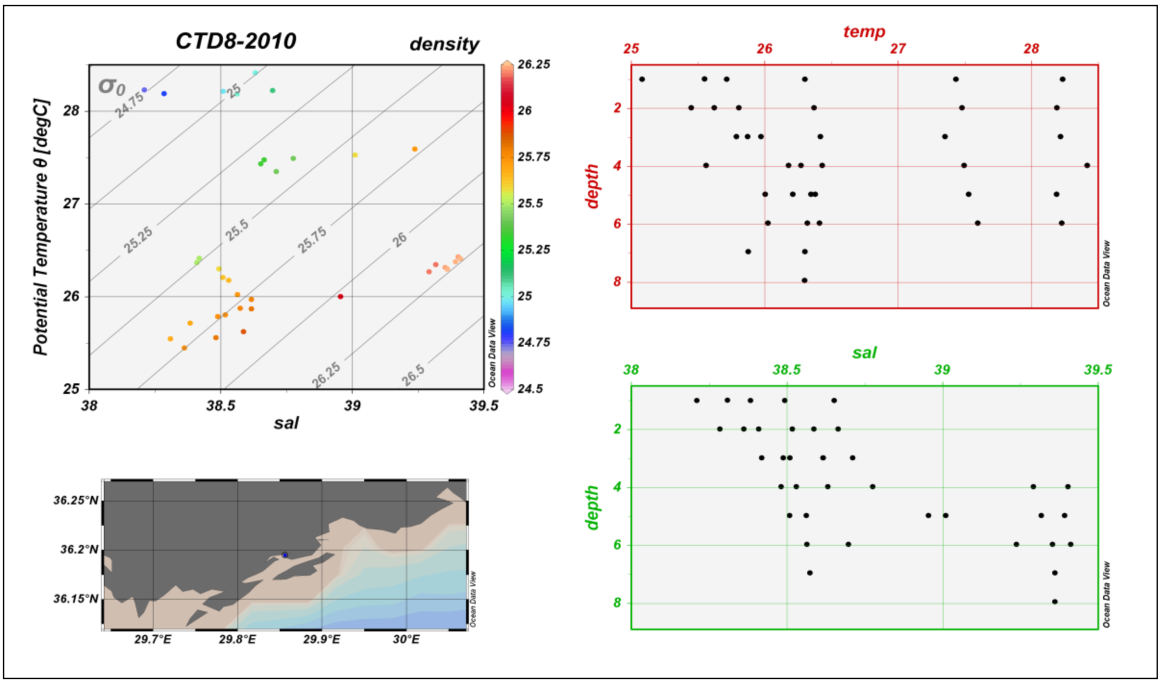

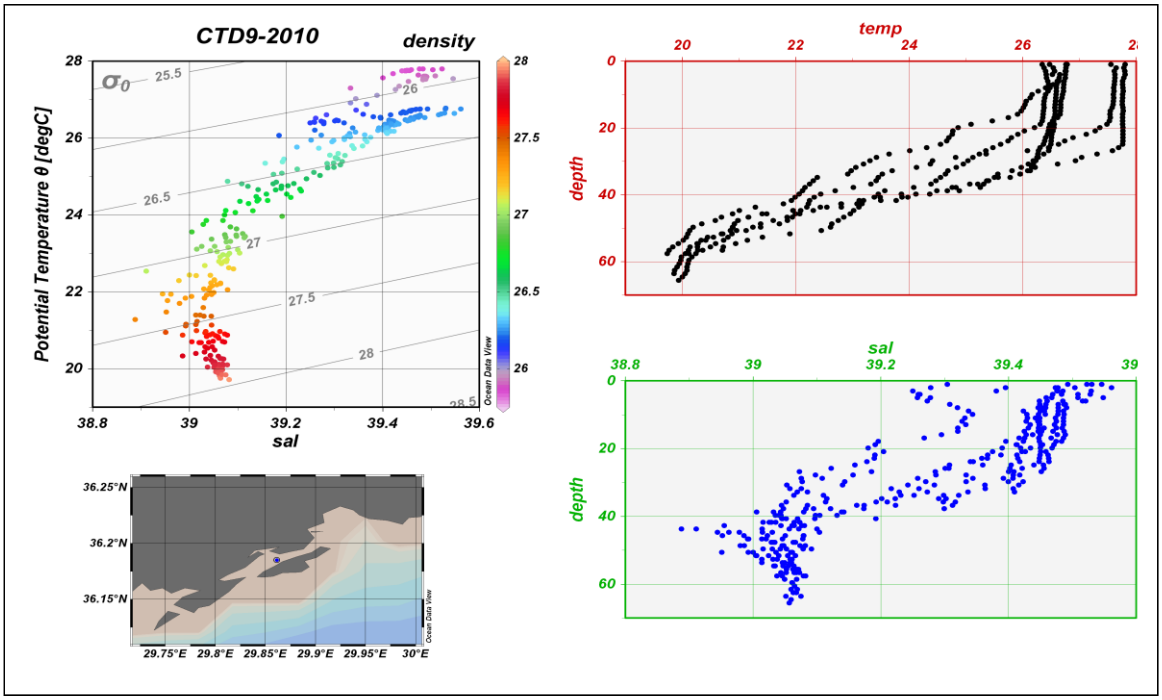

Figure 3.4 continues

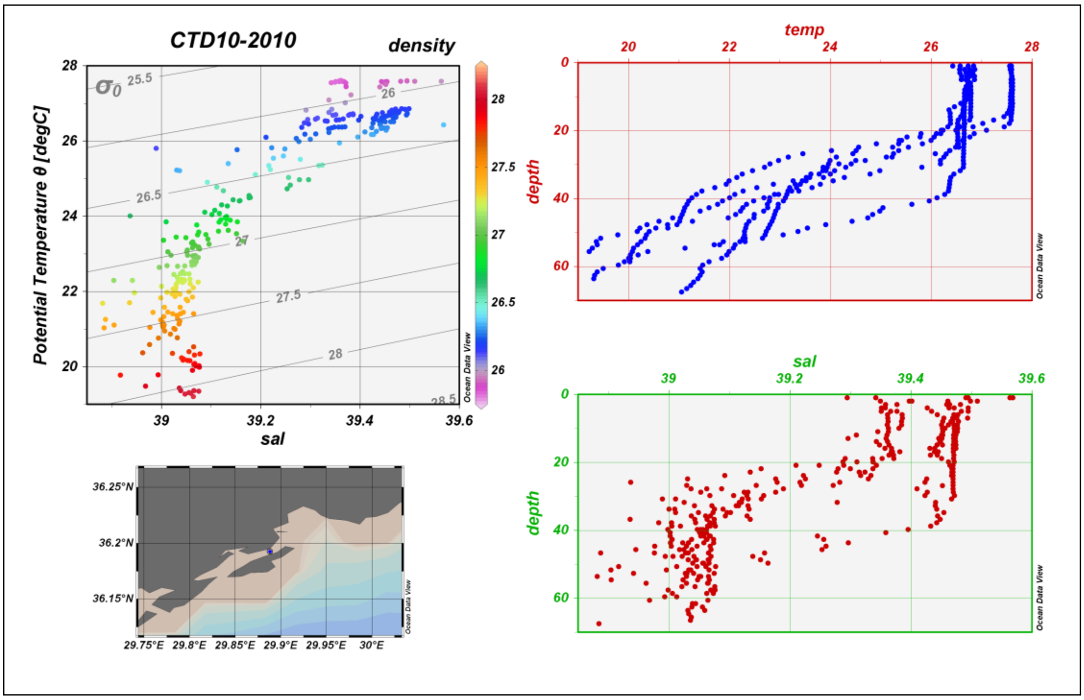

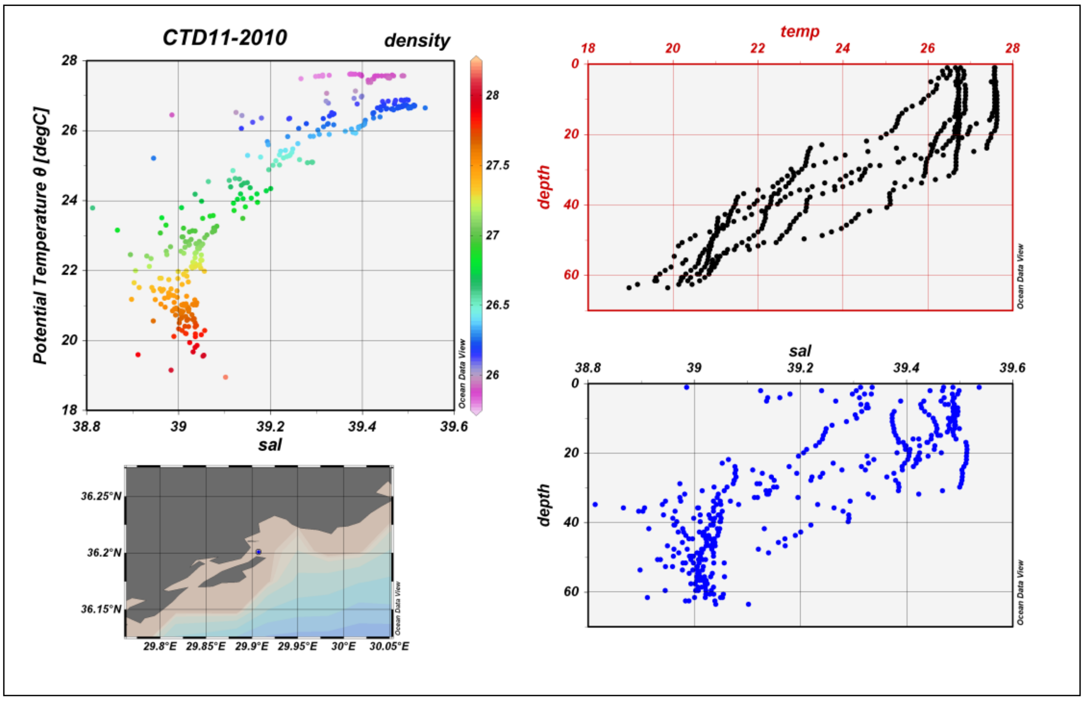

Figure 3.4 continues

Temperature (°C)	Salinity (psu)	Density (kg/m³)
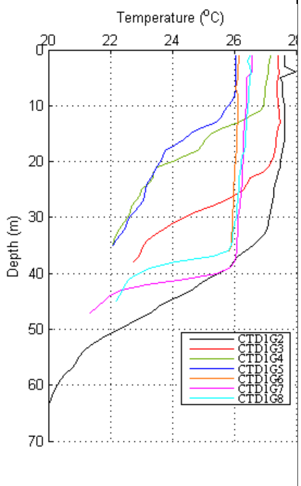 1a	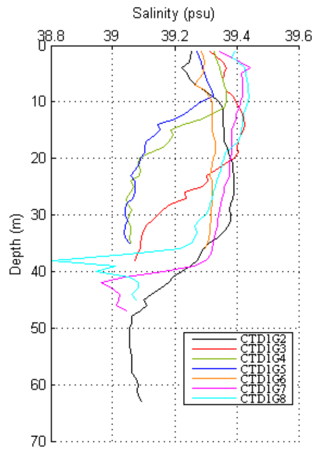 1b	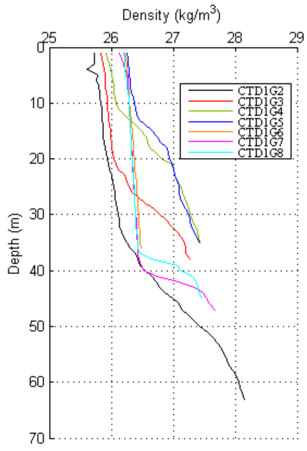 1c
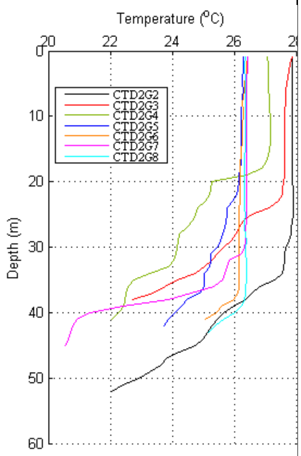 2a	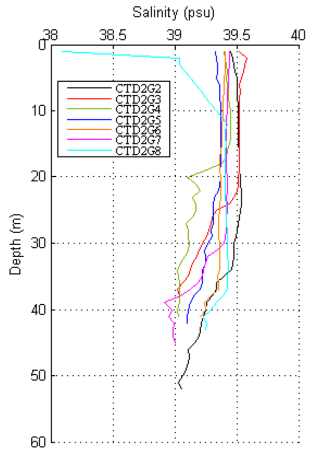 2b	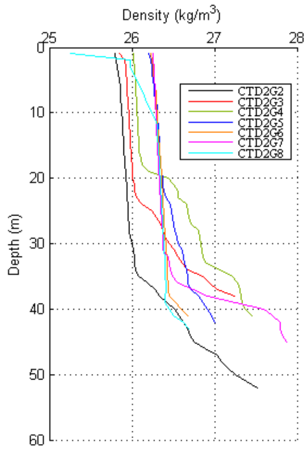 2c
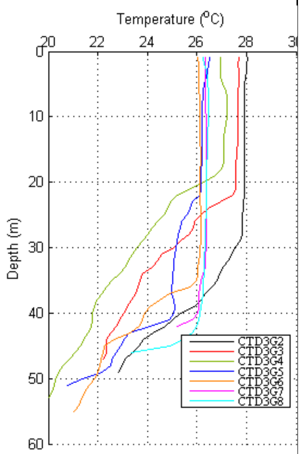 3a	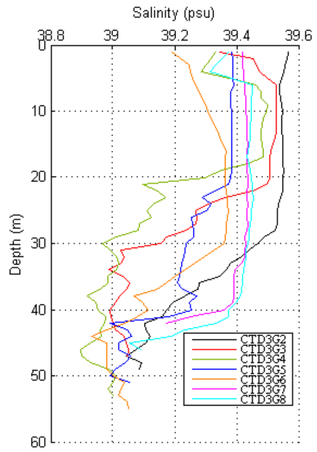 3b	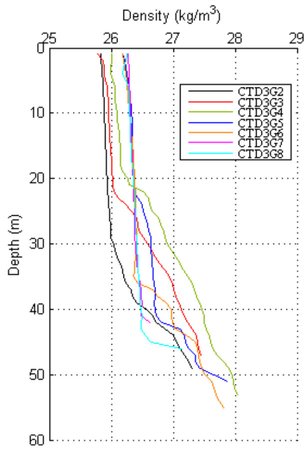 3c

Figure 3.5 Station's vertical CTD profile in September and October in 2010.Numbers show station's numbers.Letters indicate measurement parameters (a) Temperature, (b) Salinity and (c) Density

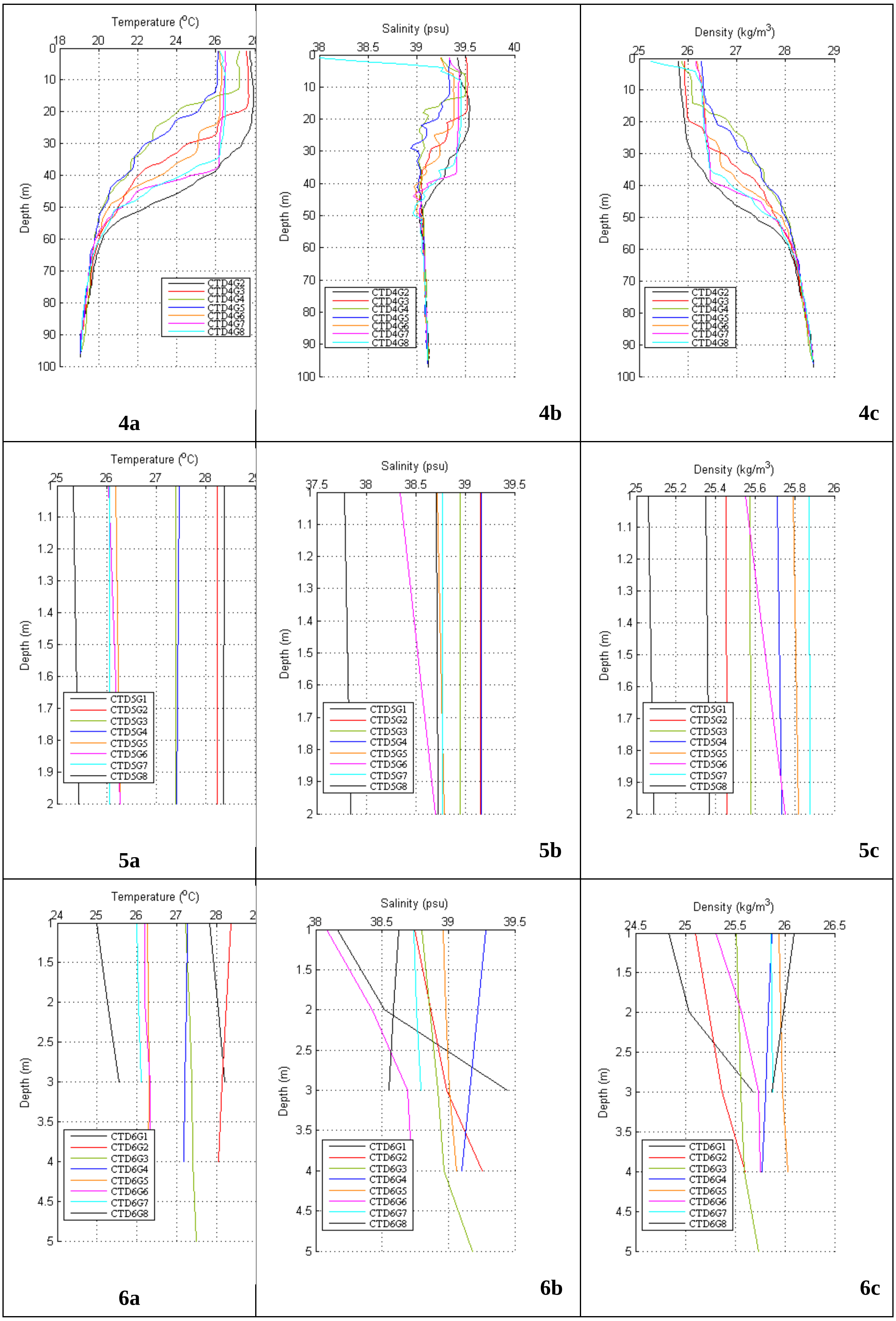

Figure 3.5 continues

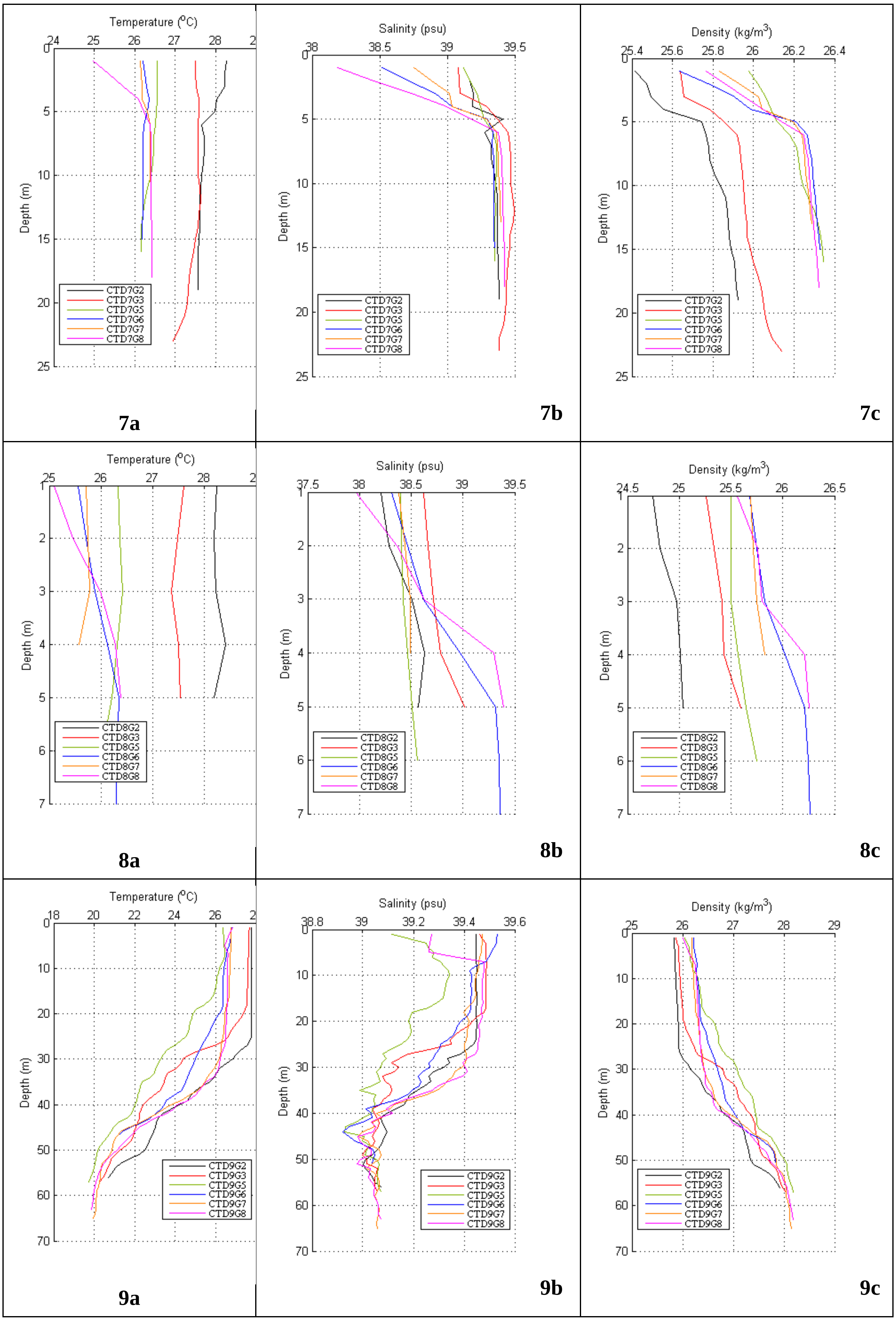

Figure 3.5 continues

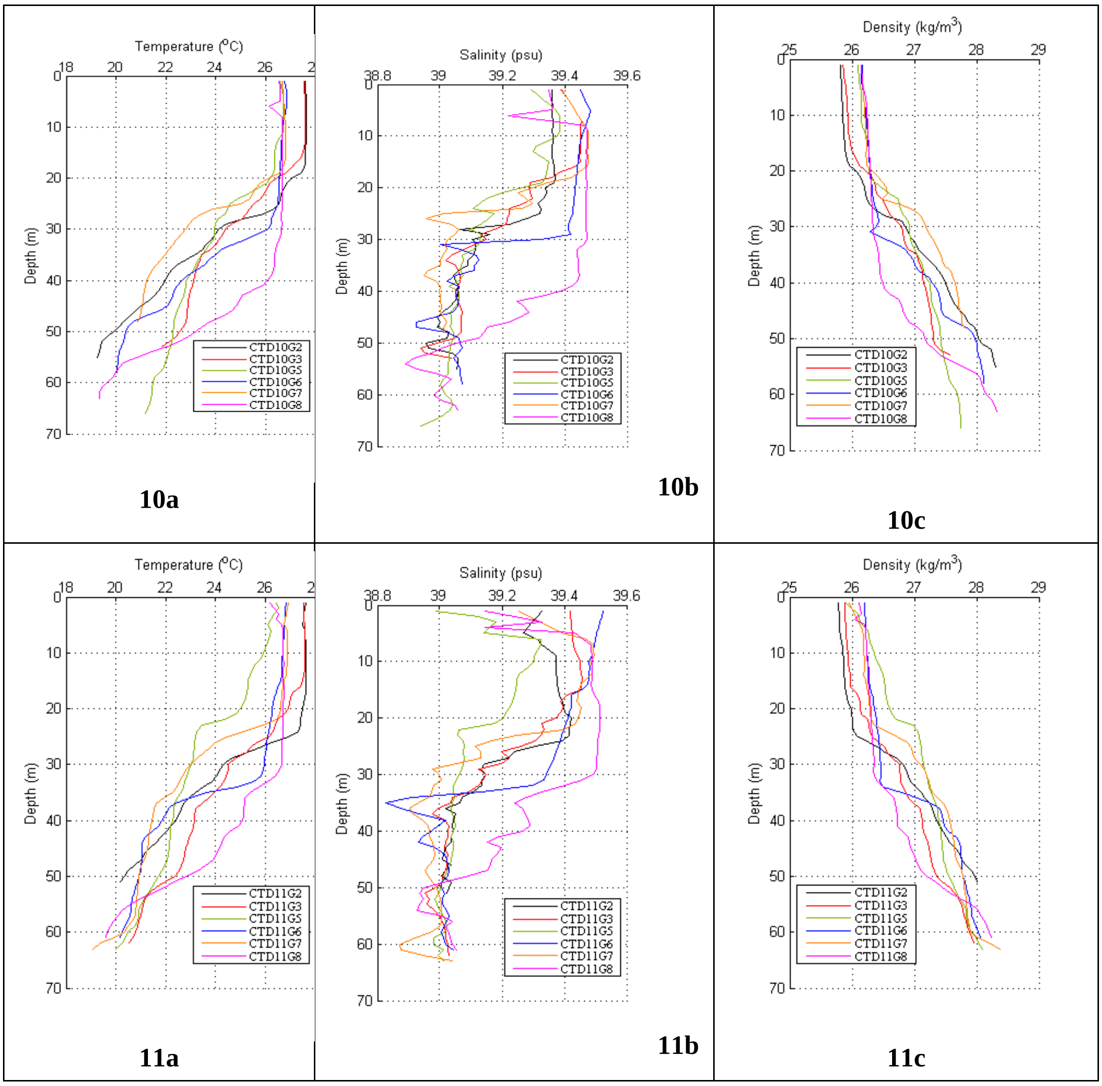

Figure 3.5 continues

Although the general weight of the more intensive rain categories are observed at about 5.3 % of the total rainy days, it is worth noting that they enable a rainfall of 72565 mm/m^2. Considering these amounts, paying attention to the fact of closed structure of the study area and the surface area of the surrounding region, it is clear how effective the rains can be over Üçağız and Ölüdeniz.

February 2011 CTD measurements reflect a typical winter formation in Figure 3.6. The lowest level of see water temperature and completion of winter specific vertical mixing process have been observed. The whole water column has gained a homogeneous structure based on the three parameters. It has been observed that, in all stations the temperature from surface to base remains between 17 – 18 ^{o}C. There is decrease in salinity and density at the first 10 m and in some stations up to 20 m of the surface part, due to fresh water entrance from rains, but at more depths it is seen

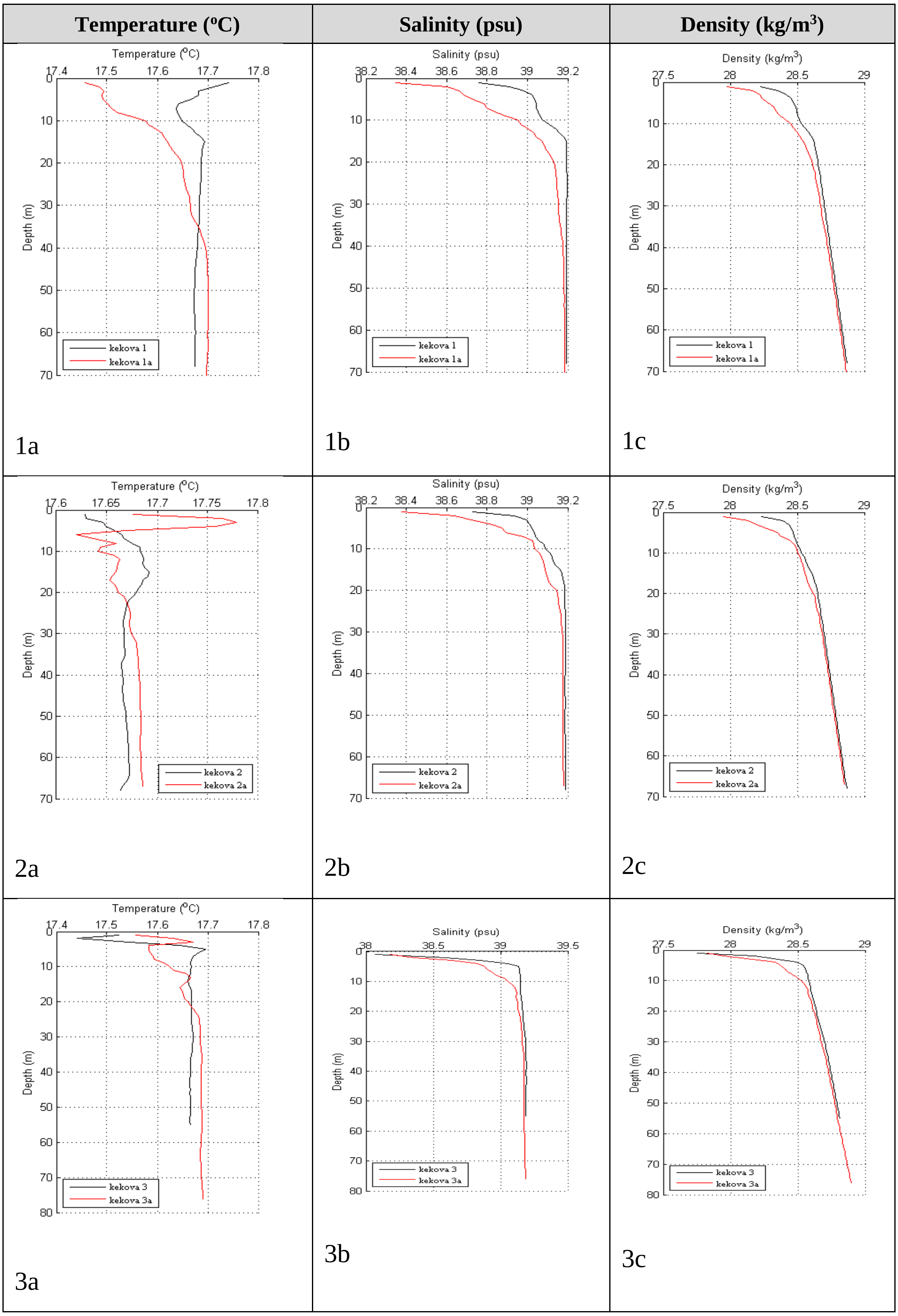

Figure 3.6 Station's vertical CTD profile in September and October in 2010.Numbers show station’s numbers.Letters indicate measurement parameters (a) Temperature, (b) Salinity and (c) Density

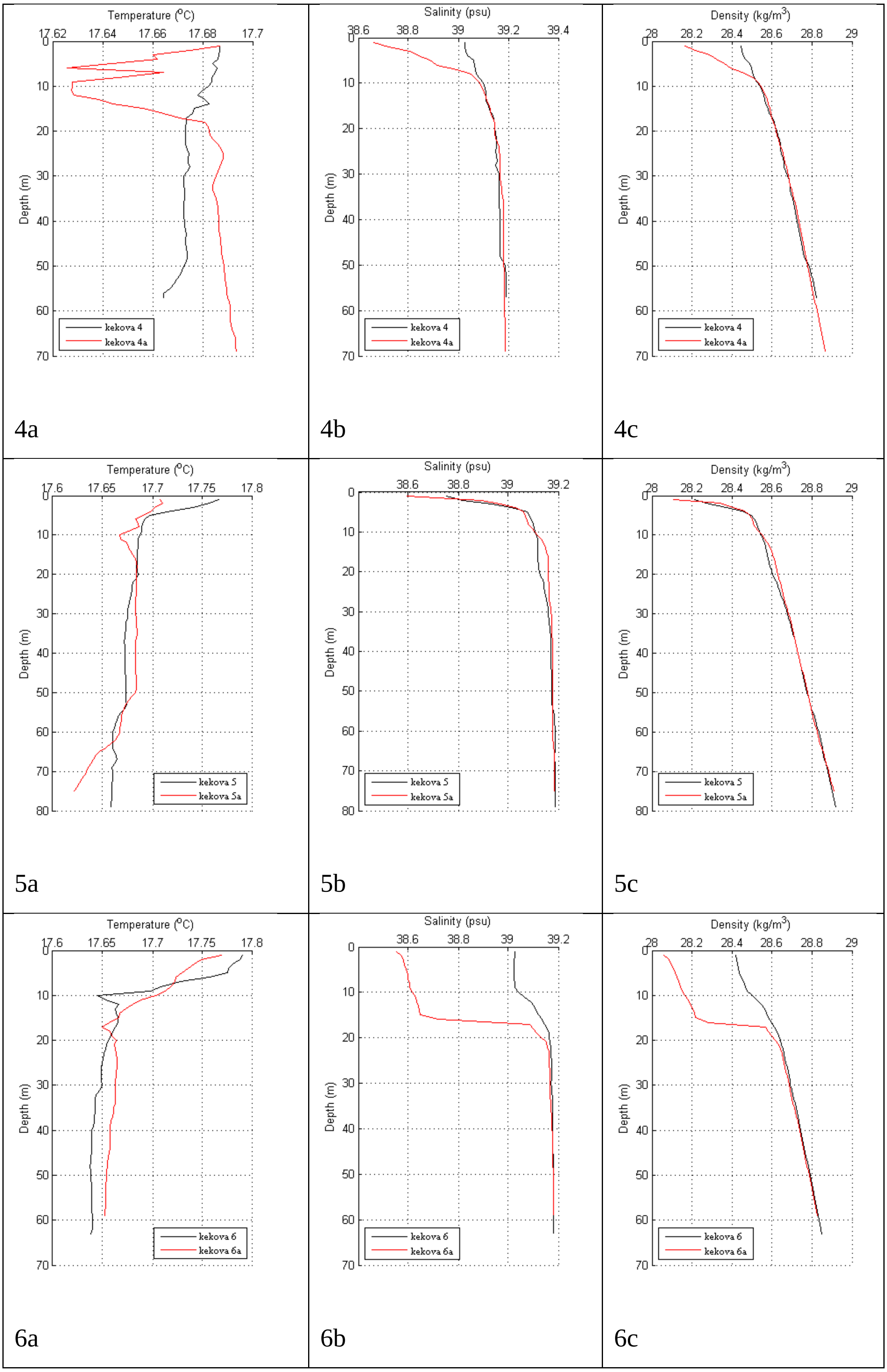

Figure 3.6 continues

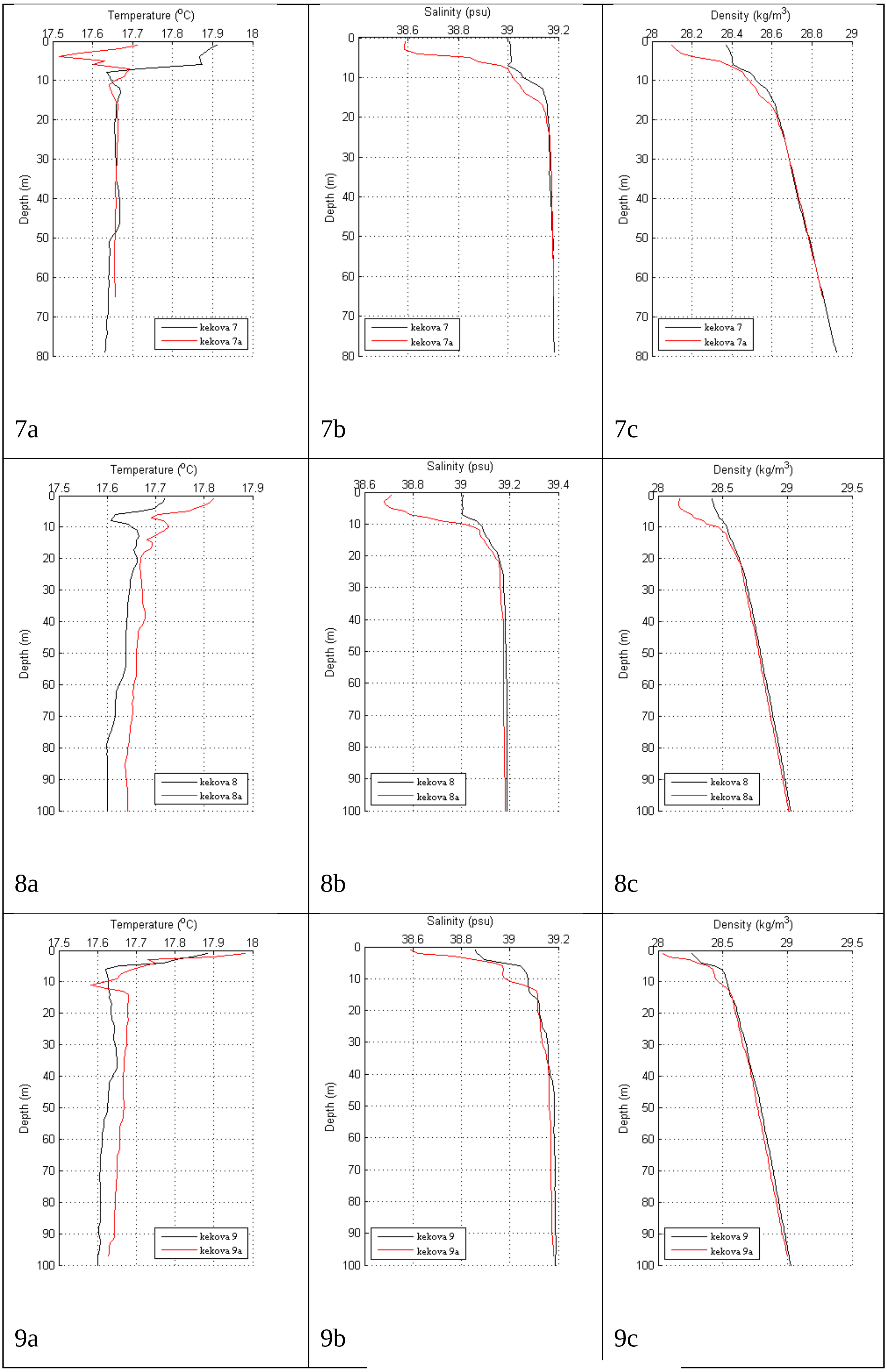

Figure 3.6 continues

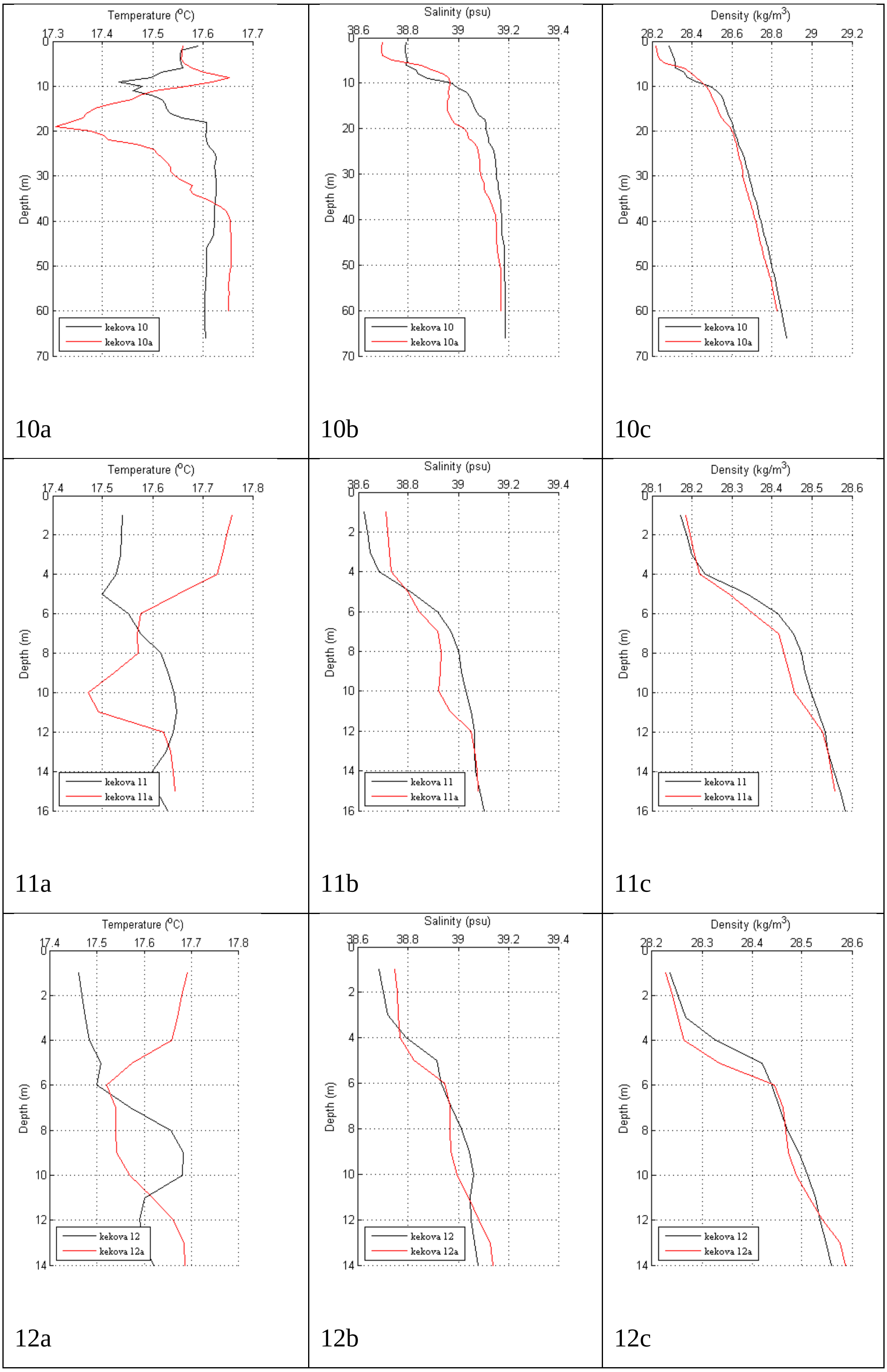

Figure 3.6 continues

that the salinity is fixed at the range 39,0-39,2 psu, and the density at28-29 kg/m3. According to the Secchi disc measurement results is shown in Figure 3.7 done about the clarity of water, the minimum value is observed at the most iner point of Sıçak Bay, while at all other stations a visibility beyond 10 m is recorded. The weakest carity, with about 1-3 m is the inner part of Üçağız Port.

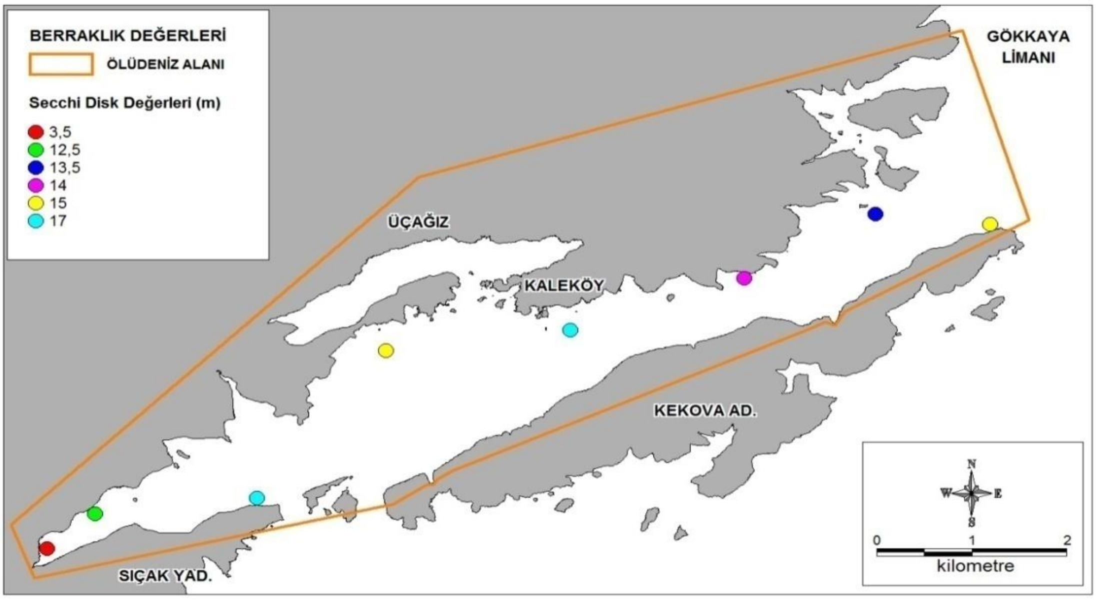

Figure 3.7 Secchi disk values measured at stations

3.4 Implementation of the ADCIRC ın the Kekova Bay

ADCIRC is a highly developed computer program for solving the equations of motion for a moving fluid on a rotating earth. These equations have been formulated using the traditional hydrostatic pressure and Boussinesq approximations and have been discretized in space using the finite element (FE) method and in time using the finite difference (FD) method.Elevation is obtained from the solution of the depth-integrated continuity equation in Generalized Wave-Continuity Equation (GWCE) form. Velocity is obtained from the solution of either the 2DDI or 3D momentum equations. All nonlinear terms have been retained in these equations. ADCIRC can be run using either a Cartesian or a spherical coordinate system.

The two dimensional,depth integrated version of the hydrodynamıc model ADCIRC was used the simulate tidal flow through Kekova Bay in Turkey, has been applied to two test cases, including: the wind induced flow in a laboratory basin and tidal flow in a model semi-circle bay.The primary objectives of this study is able to identify any potential limitations that ADCIRC-2DDI might hav efor modelling by Dynamics.

The agreement between the physical and numerical model results is highly encouraging. Model has been implemented to Kekova Bay located at the Mediterranean coast of Turkey to simulate tidal currents. M2 tide is the dominant tidal constituent for the area. There exist some field measurements performed on water salinity, water temperature and current pattern in Kekova Bay. Even though measurements provide only some preliminary data for the site, favorable results have been obtained from the application of the model to a real coastal water body.

A triangular finite element grid was generated using the THRIGRID package and is shown in Figure 3.8. Also shown is a contour plot of bottom bathymetry from the nodal water depth information in the finite element grid in Figure 3.9. Model presently requires the spefication of elevation boundary conditions on all open boundaries.

Model is run as a cold start by definition of IHOT = 0. This definition makes all variables in the initial condition is zero. The numerical results are then verified by testing the resulting predictions for independence of the grid size, time-step and other parameters. The grid size used for the solution was 3 m with a time step $\Delta t = 0.5$ s. The grid contained 35 nodes and the tidal forcing is only applied this node.Tide is used for boundary condition. Tide is entering into the open boundary nodes. For this reason, the tide information was given in fort 15 files for the open boundary nodes stated in fort.14 file. ‘Number of open boundaries’ value is one in our study.When you look at the file Fort.15, it is seen that 35 EMO EFA values exist under K1, O1, M2, S2 titles. These values are tidal amplitude and phase ones used for tidal forcing calculation in open boundary node. In this study, five tidal constituent is used and three argument, which are forcing frequency, nodal factor ve equilibrium argument, were given for the calculation of tidal force.

The model was run for bottom friction, $C_f = 0.003\ sn^{-1}$, also run using zero edyy viscosity and including all linear terms except the advective terms. Shortly, the change in water surface elevation because of tidal forcing is calculated in this 35 node (35 is number of nodes for the open boundary). Then, the numerical calculation of the model is began from this nodes to interior nodes by using the continuity and momentum equations and the pressure, velocity and other values are determined and are shown in Figure 3.10 - Figure 3.19.

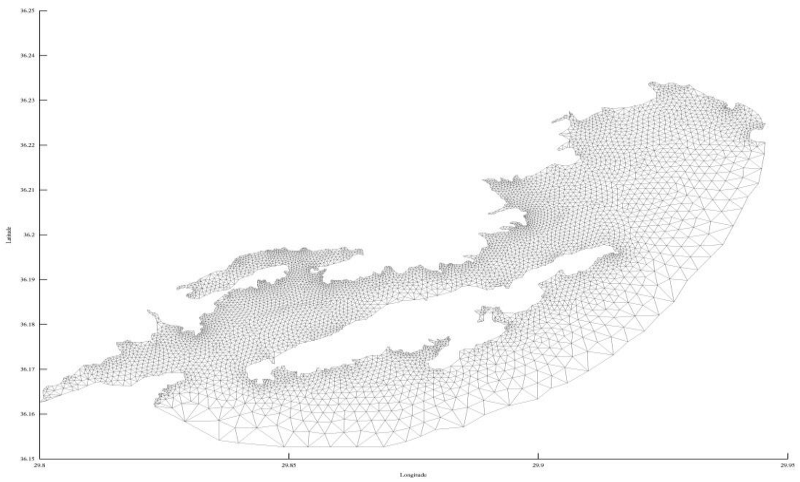

Figure 3.8 Finite element grid of Kekova Bay

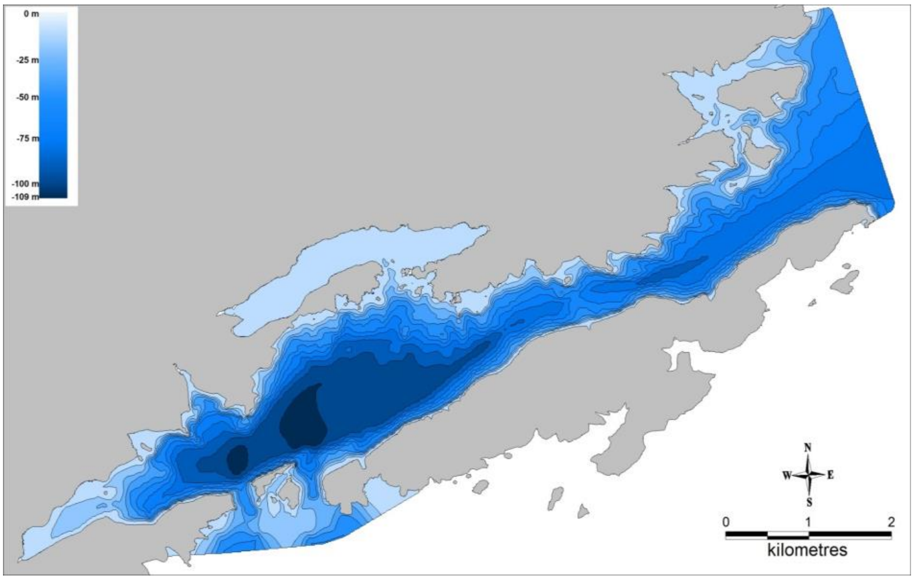

Figure 3.9 Finite element bathymetry of Kekova Bay

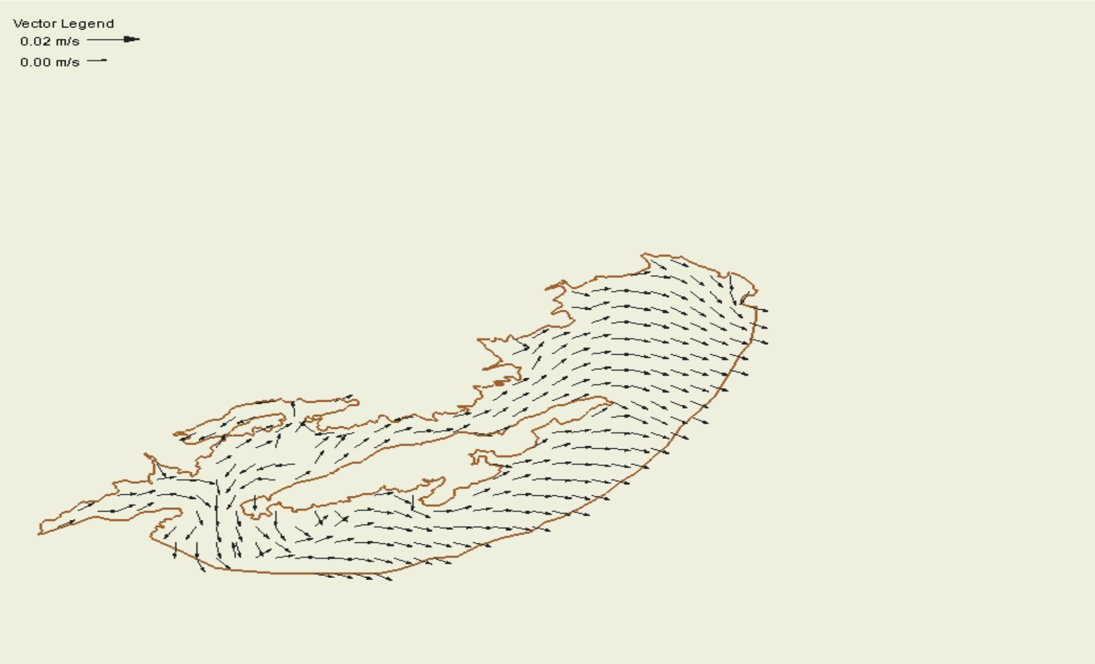

Figure 3.10 Simulated depth-averaged velocity using of $C_f = 0.003\ s^{-1}$ for every one hour on September 2010. Hour 7.00

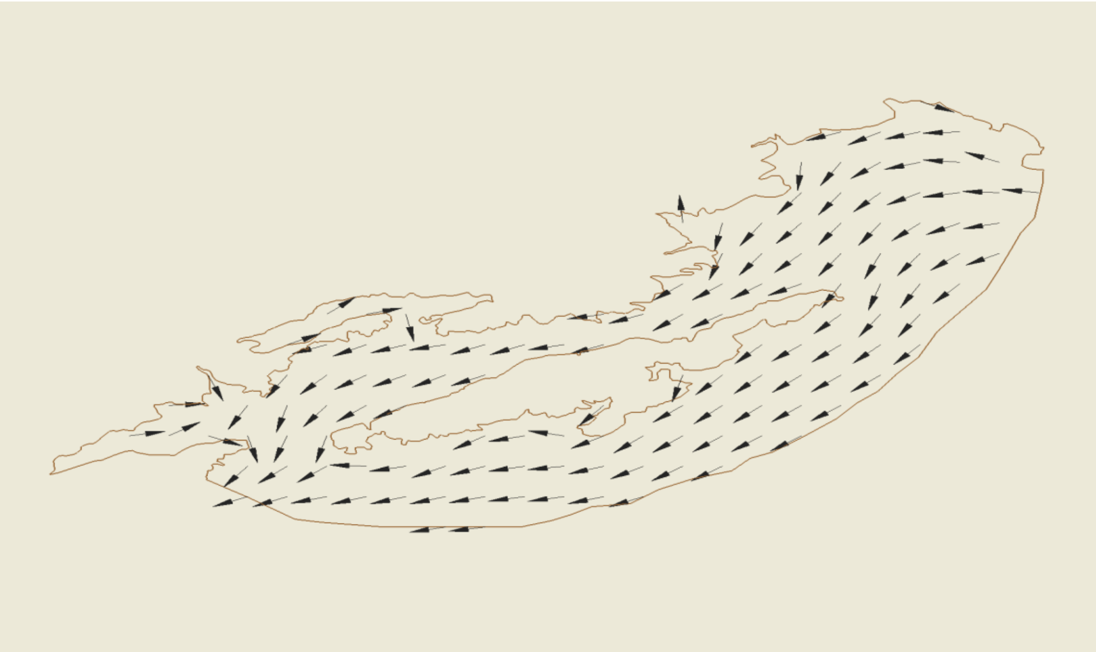

Figure 3.11 Simulated depth-averaged velocity using of $C_f = 0.003\ s^{-1}$ for every one hour on September 2010. Hour 8.00

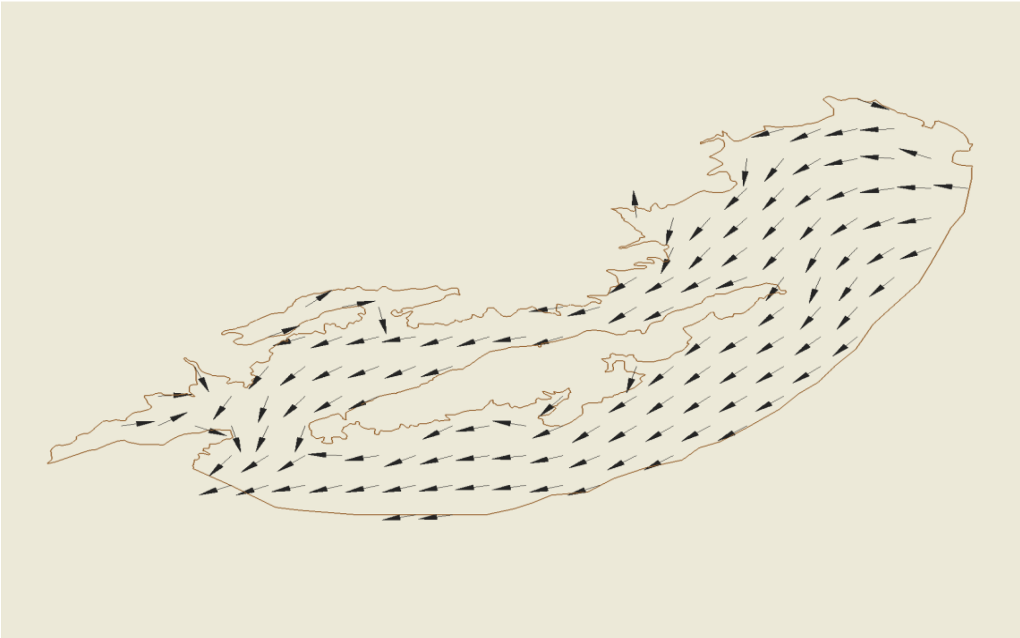

Figure 3.12 Simulated depth-averaged velocity using of $C_f = 0.003\ s^{-1}$ for every one hour on September 2010. Hour 9.00

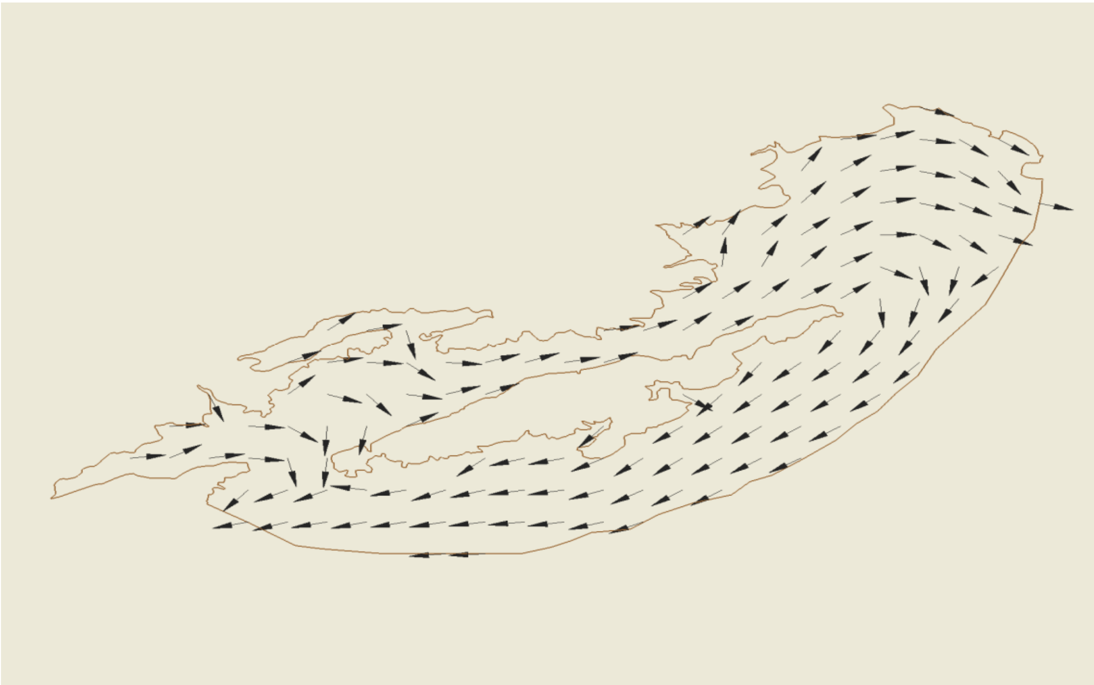

Figure 3.13 Simulated depth-averaged velocity using of $C_f = 0.003\ s^{-1}$ for every one hour on September 2010. Hour 10.00

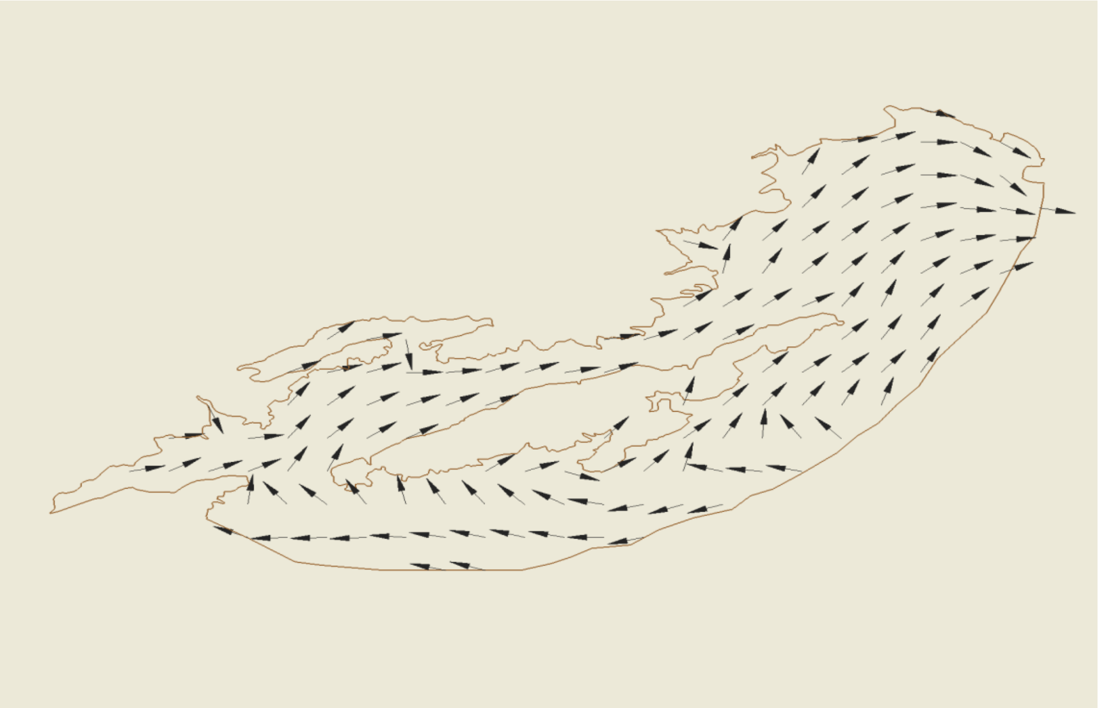

Figure 3.14 Simulated depth-averaged velocity using of $C_f = 0.003\ s^{-1}$ for every one hour on September 2010. Hour 11.00

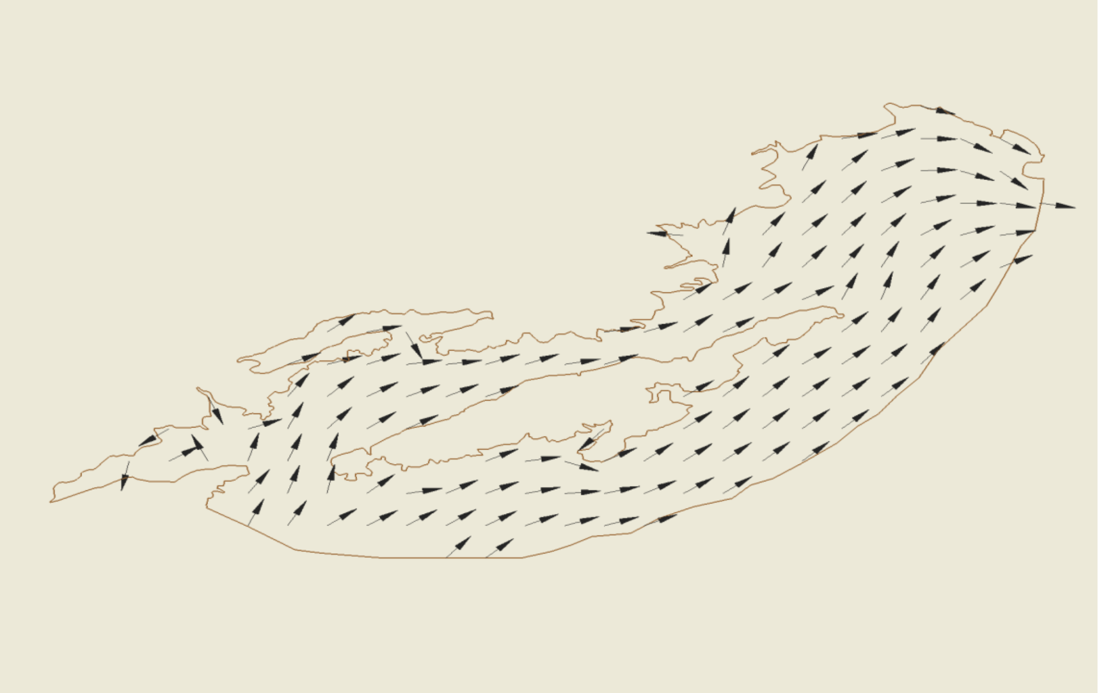

Figure 3.15 Simulated depth-averaged velocity using of $C_f = 0.003\ s^{-1}$ for every one hour on September 2010. Hour 12.00

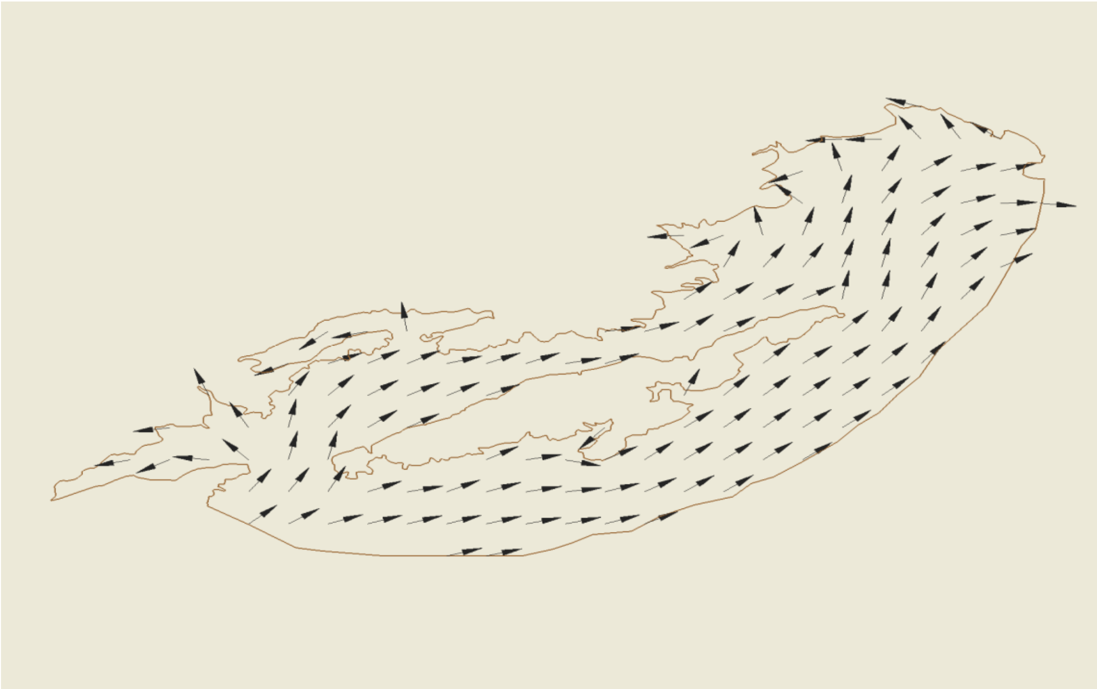

Figure 3.16 Simulated depth-averaged velocity using of $C_f = 0.003\ s^{-1}$ for every one hour on September 2010. Hour 14.00

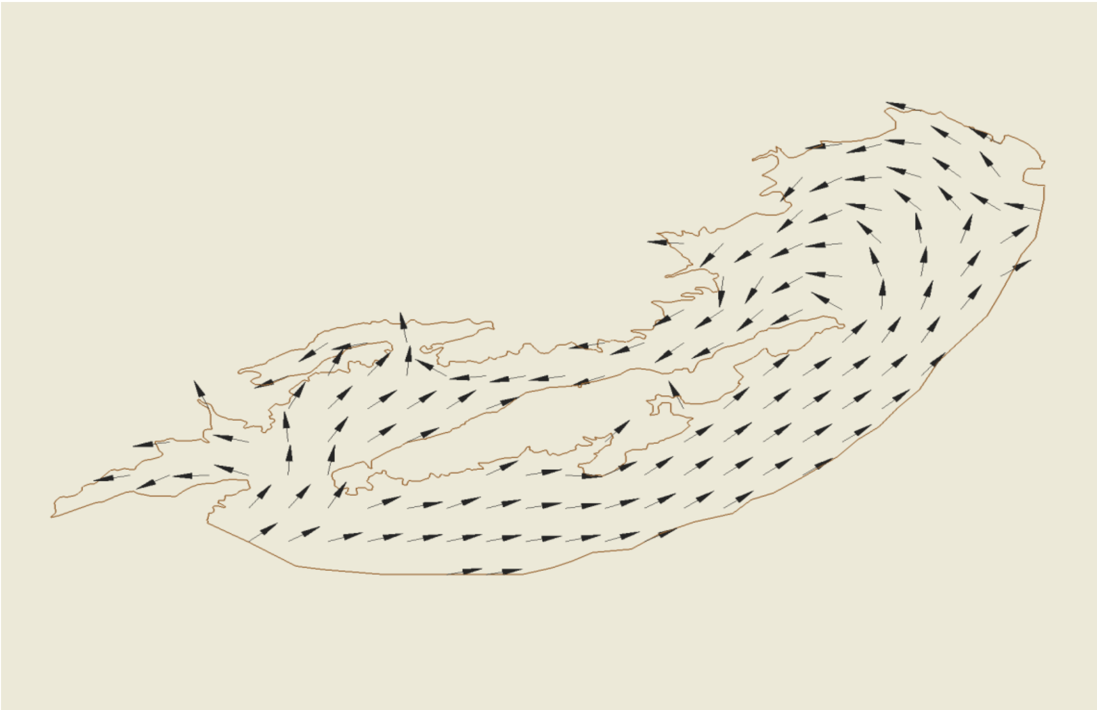

Figure 3.17 Simulated depth-averaged velocity using of $C_f = 0.003\ s^{-1}$ for every one hour on September 2010. Hour 15.00

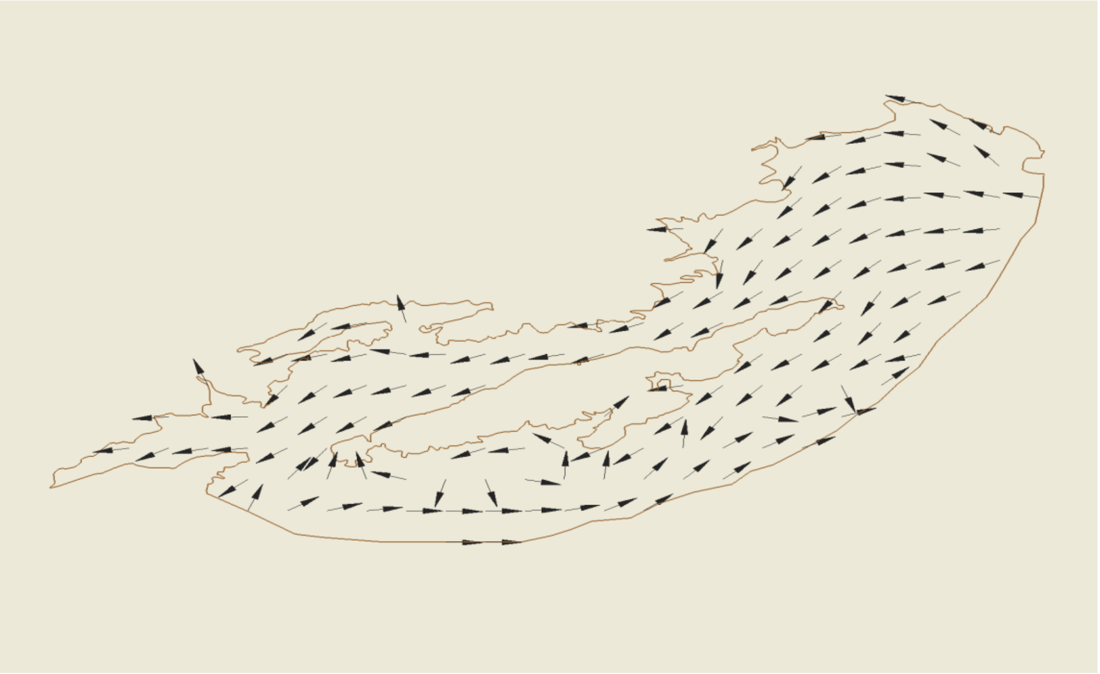

Figure 3.18 Simulated depth-averaged velocity using of $C_f = 0.003\ s^{-1}$ for every one hour on September 2010. Hour 16.00

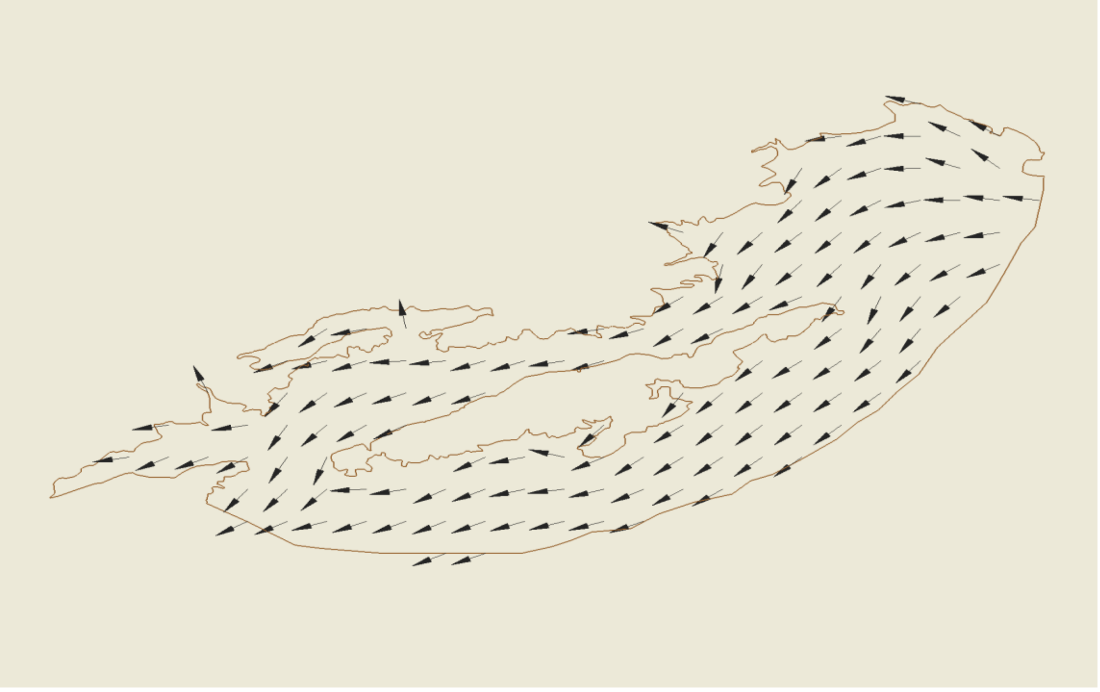

Figure 3.19 Simulated depth-averaged velocity using of $C_f = 0.003\ s^{-1}$ for every one hour on September 2010. Hour 17.00.

CHAPTER FOUR
CONCLUSION

4.1 Conclusion

For model purposes, a high horizontal as well as vertical resolution of model grid is required to resolve the mesocyle dynamics as well as the basin structured bottom topography and the complicated costline. By modelling of the Kekova bay is able to simulate most of the characteristic flow features. In order to understand the flow characteristic and water budget of the region, within the framework of 1. and 2. stage studies, every day for a week. The stations A2 and A3, which enable Ölüdeniz's connection with open see between the Kekova Island and Sıçak peninsula, are the points having the greatest average speeds. Station A6, located at the open area where the connection of the east end Ölüdeniz with the open see is situated, follows these stations. Stations at the strait connecting Sıçak bay (A1) and Üçağız to Ölüdeniz have almost the same flow rates. A4 station has been obtained no flow profile due to shallow depth of about 5 m in Üçağız.

Dominant direction represents the direction of motion of the water column, but Ölüdeniz's vector profiles gives the flow directions are highly variable in terms of both measurement days and hours and depth. The dominant directions can be seen that from station A6, there is incoming water into Ölüdeniz. Similarly, from both straits where stations A2 and A3 are locted, although effective much less, it is understood that there is incomng water to Ölüdeniz. The flow direction in station A1 located in Sıçak Bay show an east directed motion along Ölüdeniz.The dominant direction of A5 station located on the strait combinng Üçağız and Ölüdeniz indicate a flow from Üçağız to Ölüdeniz.

When the figures 3.4 are examined, it is seen that during the period of September-October 2010, the temperature at the surface reaches maximum values of 26-29 ^{o}C, at the see base of depth 70-100 m, even to values of 19-20 ^{o}C.

At stations with depths more than 50 m, the depth range where the termoklin layer is effective, it is a noteworthy detection that may change showing a vertical mobility in levels of time to time of 20-30 m at several measurment days. This situation reflects the dynamism of the flow system at Ölüdeniz during the study. As will be explained in greater detail at the section on flow system, the variations on dominant wind direction and magnitude may affect the water movements directly and very fast. The rate of this effect may be understood from the fact that water, in both horizontal and vertical planes, may move so fast as to create a temperature difference of about 3-4 ^{o}C day by day on surface waters. This situation may clearly be monitored at shallow stations despite the relative decreasing trend from surface to base. The same varation patterns are also observed in salinity and densty profiles.

REFERENCES

Al-Rabeh, A. H, Eunay, N., & Cekirge, H. M. (1990). A hydrodynamic model for wind driven and tidal circulation in the Arabian Gulf. *Applied Mathematical Modelling, 14*, 410-419.

Ayoub, N., Le Traon, P.Y., & De Mey, P. (1998). A description of the Mediterranean surface variable circulation from combined ERS-1 and TOPEX/POSEIDON altimetric data. *Journal of Marine Systems, 18,* 3–40.

Blain, C. A., Westerink, J. J., & Luettich, R. A. (1994). The influence of domain size on the response characteristics of a hurricane storm surge model. *Journal of Geophysical Research, 9,* 18467-18479.

Blain, C. A., & McManus, A. P (1998), *Insights into unstructured mesh generation for coastal ocean applications*. Mississippi: Naval Research Laboratory, Stennis Space Center.

Carey, G. F. (Ed.). (1995). *Finite element modeling of environmental problems*. New York: John Wiley and Sons.

Celia, M. A., & Gray, W. G. (1992). *Numerical methods for differential equations, fundamental concepts for scientific and engineering applications*. New Jersey: Prentice Hall.

Flather, R. A. (1988). A numerical model investigation of tides and diurnal-period continental shelf waves along Vancouver Island. *Journal of Physical Oceanography, 18*, 115-139.

Foreman, M. G. G. (1983). An analysis of the wave equation model for finite element tidal comparisons. *Journal of Computational Physics, 52*, 290-312.

Foreman, M. G. G. (1988). A Comparison of Tidal Models for the Southwest Coast of Vancouver Island. *Proceedings of the VII International Conference on Computational Methods in Water Resources*, *35*, 231-236.

Gray, W. G. (1982). Some inadequacies of finite element models as simulators of two-dimensional a circulation. *Advanced in Water Resources*, *5*, 171-177.

Gray, W. G., & Kinnmark, I. P. E. (1983). Quiet: a reduced noise finite element model for tidal circulation. *Advanced Engineering Software, 5*(3), 130-136.

Gray, W. G., Leijnse, T., Kolar, R. L., & Blain, C. A. (1993). *Mathematical tools for changing scales in the analysis of physical systems.* Florida: CRC Press.

Heaps, N. S. (Ed.). (1987). *A description of a three-dimensional coastal ocean circulation model in three-dimensional coastal ocean models*. Amsterdam: Coastal and Estuarine Sciences.

Heath, R. E., Johnson, B. H., & Kim, K. W. (1990). Grid-Induced errors in depth averaged flow fields. *Proceedings of the ASCE Hydraulics Division Specialty Conference*, San Diego, CA, ASCE, 767-772.

Hecht, A., Pinardi, N., & Robinson, A. (1989). Currents, water masses, eddies and jets in the Mediterranean Levantine Basin. *Journal of Physical Oceanography, 18*, 1320–1353.

Hendershott, M. C. (1981). *Long waves and ocean tide*. Evolution of physical oceanography, B. A. Warren and C. Wunsch (Eds.). MIT Press, Cambridge, MA, 292-341.

Herbich, J. (Ed.). (1990). *Waterlevel changes*. Handbook of Coastal and Ocean Engineering. Houston: Gulf Publishing.

Kincaid, B., & Cheney, W. (1991). *Numerical Analysis. Mathematics of Scientific Computing*. Canada: Brooks Cole Publication Cooperation.

Kinnmark, I. P. E. (1984*). The shallow water wave equations: formulation, analysis and application*. Ph.D. dissertation, Princeton University, Princeton.

Kinnmark, I. P. E., & Gray, W. G. (1984). A two-dimensional analysis of the wave equation model for the finite element tidal computations. *International of Journal of Numerical Methods, 20,* 369-383.

Kinnmark, I. P. E., & Gray, W. G. (1985). Stability and accuracy of spatial approximations for wave equation tidal models. *Journal of Computational Physics. 60*, 447-466.

Kolar, R. L. (1992). *Environmental conservation laws: formulation, numerical solution, and application*. Ph. D. dissertation, University of Notre Dame, France.

Kolar, R. L., Gray, W. G., Westerink, J. J., & Luettich, R. A. (1994a). Shallow water modeling in spherical coordinates: equation formulation, Numerical Implementation and Application. *Journal of Hydraulic Research, 32*, 3-24.

Kolar, R. L., Westerink, J. J, Cantekin, M. E., & C. A. Blain (1994b). Aspects of nonlinear simulations using shallow water models based on the wave-continuity equation. *Computers and Fluids, 23,* 523-538.

Kumlutaş, Y., Durmuş, S. H., & Ilgaz, Ç. (2011). Kaş-Kekova özel çevre koruma bölgesinin herpetofaunası. *Anadolu Doğa Bilimleri Dergisi, 2*(1), 28-33.

Lapidus, L., & Pinder, G. F. (Ed.). (1982). *Numerical solution of partial differential equations in science and engineering*. New York: John Wiley and Sons.

Le Mehaute, B. (Ed.). (1976). *An introduction to hydrodynamics and water waves*. New York: Springer-Verlag.

LeProvost, C., & Vincent, P. (1986). Some tests of precision for a finite element model of ocean tides. *Journal of Computational Physics, 65*, 273-291.

Luettich, R. A., & Westerink, J. J. (1995). Continental shelf scale convergence studies with a barotropic tidal model, in quantitative skill assessment for coastal ocean models. *Coastal and Estuarine Studies, 47*, 349-372.

Luettich, R. A. (2000). *ADCIRC: a parallel advanced circulation model for oceanic, coastal and estuarine waters*. (User Manuel). USA: Marine research Laboratory.

Lynch, D. R. (1983). Progress in hydrodynamic modeling, Review of U.S. Contributions 1979-1982. *Reviews of Geophysics and Space Physics, 21*(3), 741-754.

Lynch, D. R., & Gray, W. G. (1979). A wave equation model for finite element tidal computations. *Computational Fluids, 7*, 207-228.

Malanotte-Rizzoli P., Robinson, A.R. (Ed.) (1994). *Ocean processes in climate dynamics*. Dortrecht: Kluwer Academic Publishers.

Malanotte-Rizzoli, P., & Robinson, A. R. (Ed.). (1994). *Ocean processes in climate dynamics: global and mediterranean examples*. London: Kluwer Academic Publishers.

Ozsoy, E., Hecht, A., & Ünlüata, Ü. (1989). Circulation and hydrography of the Levantine Basin – results of POEM co-ordinated experiments. *Progress in Oceanography, 22*, 125–170.

Ozsoy, E., Ünlüata, Ü. & Top, Z. (1993b). The Mediterranean water evolution, material transport by double diffusive intrusions, and interior mixing in the Black Sea. *Progress in Oceanography, 31*, 275–320.

Platzman, G. W. (1981). Some response characteristics of finite element tidal models. *Journal of Computational Physics, 40*, 36-63.

Reid, R. O., & Whitaker R. E. (1981). *Numerical model for astronomical tides in the Gulf of Mexico*. Texas: Texas A & M University, Department of Oceanography.

Robinson, A. R., Theocharis, A., Lascaratos, A., & Leslie, W. G. (2001). Mediterranean Sea circulation and encyclopedia of ocean sciences. *Academic Press*, 5, 1689–1706.

Roether, W., Manca, B. B., Klein, B., Bregant, D., Georgopoulos, D., Beitzel, V., Kovačević, V., & Luchetta, A. (1996). Recent changes in Eastern Mediterranean deep waters. *Science, 271*, 333–335.

Schwiderski, E. W. (1980). On charting global ocean tides. *Journal of Geophysical Research, 18*, 243-268.

Stanley, D. J. (Ed.). (1972). *Geological evolution of the mediterranean basin*. Pennsylvania: Hutchinson & Ross.

Tchernia, P. (1980). *Descriptive regional oceanography*. New York:Pergamon Press.

Vincent, P., & LeProvost, C. (1989). Semidiurnal tides in the northeast Atlantic from a finite element numerical model. *Journal of Geophysical Research, 93,* 543-555.

Walters, R. A., & Carey, G. F. (1983). Analysis of spurious oscillation modes for the shallow water and navier stokes equation. *Computers and Fluids, 2*, 51-68.

Werner, F. E., & Lynch, D. R. (1989). Harmonic structure of English Channel southern bight tides from a wave equation simulation. *Advances in Water Resources, 12,* 121-142.

Westerink, J. J., Stolzenbach, K. D., & Connor, J. J. (1989). General spectral computations of the nonlinear shallow water tidal interactions within the bight of abaco. *Journal of Physical Oceanography, 19*, 1350-1373.

Westerink, J. J., & Gray, W. G. (1991). Progress in surface water modeling. *Revievs of Geophysics, 29*, 210-217.

Westerink, J. J., Luettich, R. A., Baptista, A. M., Scheffner, N. W., & Farrar, P. (1992a). Tide and storm surge predictions using a finite element model. *Journal of Hydraulic Engineering, 118*, 1373-1390.

.

Westerink, J. J., Luettich, R. A., Blain, A., & Scheffner, N. W. (1992b). *ADCIRC: an advanced three-dimensional circulation model for shelves, coast and estuaries, Report 2: ADCIRC-2DDI.* Technical Report of Department of the Army, User's Manual.

Westerink, J. J., Luettich, R. A., & Muccino, J. C. (1994a). Modeling tides in the western North Atlantic using unstructured graded grids. *Tellus, 46A*, 178-199.

Wüst, G. (1961). On the vertical circulation of the Mediterranean Sea. *Journal of Geophysical Research*, *66,* 3261–3271.

Zavatarelli, M., & Mellor, G. L. (1995). A numerical study of the Mediteranean-Sea circulation. *Journal of Physical Oceanography*, *25*, 1384–1414.